Universidade de Aveiro
2018
Departamento de Engenharia de Materiais e Cerâmica

Jéssica Alexandra de Sá Antunes

Fabrico de Microcápsulas Tridimensionais (3D) através da utilização de Biomateriais Multifuncionais

Manufacture of three-dimensional (3D) Microcapsules through the use of Multifunctional Biomaterials

Universidade de Aveiro
2018
Departamento de Engenharia de Materiais e Cerâmica

Jéssica Alexandra de Sá Antunes

Fabrico de Microcápsulas Tridimensionais (3D) através da utilização de Biomateriais Multifuncionais

Manufacture of three-dimensional (3D) Microcapsules through the use of Multifunctional Biomaterials

Dissertação apresentada à Universidade de Aveiro para cumprimento dos requisitos necessários à obtenção do grau de Mestre em Materiais e Dispositivos Biomédicos realizada sob a orientação científica do Doutor Vítor Gaspar e do Professor Doutor João Mano, Professor Catedrático do Departamento de Química da Universidade de Aveiro

o júri

presidente

Professor Doutor José Maria da Fonte Ferreira
Professor Associado c/ Agregação na Universidade de Aveiro

Professora Doutora Carmen de Lurdes Fonseca Jerónimo
Professora Associada c/ Agregação no Instituto de Clências Biomédicas de Abel Salazar da Universidade do Porto

Doutor Vítor Manuel Abreu Gaspar
Bolseiro de Pós-Doutoramento no Departamento de Química da Universidade de Aveiro

agradecimentos

Na realização desta dissertação de mestrado tive o privilégio de poder contar com importantes apoios e incentivos, pelo que, sem eles esta conquista não se teria tornado realidade, e aos quais estarei eternamente grata.

Em primeiro lugar, gostaria de expressar a minha gratidão para com o Professor Doutor João Mano, por me ter dado a oportunidade de trabalhar num grupo de investigação excecional. Um agradecimento também a todos os elementos do grupo COMPASS, em particular ao Luís Ferreira e Maria Monteiro pelo seu contributo em algum trabalho da minha tese.

Ao meu orientador, Doutor Vítor Gaspar, não só pela sua orientação, mas também pelo seu total apoio, colaboração e disponibilidade, por todas as palavras de incentivo, opiniões e críticas que foram fundamentais na concretização deste trabalho.

A todos os meus amigos, mas com especial relevância, à Rita Nunes e à Andreia Pereira que estiveram sempre do meu lado, quer nos momentos bons, quer na superação de todos os momentos baixos e de grande desespero. São amigas que eu vou levar comigo o resto da vida.

Um enorme Obrigada também à Dr. Emília Coutinho por tudo aquilo que tem feito por e para mim. Foi, sem dúvida, uma das fontes de motivação e força mais relevantes ao longo de toda a tese.

Ao meu afilhado, à minha tia Simone, à minha irmã e sobrinhas por toda a sua importância, mas porque fizeram a diferença em muitos dos meus dias.

Ao meu namorado, uma pessoa muito importante para mim, pelo amor, partilha, apoio incondicional, companheirismo, incentivo, (muita) paciência, ajuda e muita compreensão ao longo de todo este percurso.

Por fim, quero agradecer aos meus pais, por todo o esforço que fizeram para me proporcionarem mais um grau académico. São pessoas que eu admiro imenso, e as pessoas mais importantes da minha vida. Só por saber que estão sempre comigo, ainda que longe fisicamente, tudo isto se tornou mais simples e fácil, apesar de todos os obstáculos. Deram-me tudo o que precisei, material e emocionalmente falando. Obrigada por me ajudarem a ser um dos filhos mais felizes deste mundo. Obrigada por me ajudarem a ser mais e melhor. Obrigada pelos conselhos, e por todo o apoio. Obrigada por continuarem a ser os meus heróis. Porque os verdadeiros heróis não necessitam de capa ou máscara.

“Ninguém escapa ao sonho de voar, de ultrapassar os limites do espaço onde nasceu, de ver novos lugares e novas gentes. Mas saber ver em cada coisa, em cada pessoa, aquele algo que a define como especial, um objeto singular, um amigo,- é fundamental. Navegar é preciso, reconhecer o valor das coisas e das pessoas, é mais preciso ainda."

Antoine de Saint-Exupery

palavras-chave

Modelos tumorais 3D *in vitro*, Cancro da Próstata, Microcápsulas, Superfícies super-hidrofóbicas, Teste de fármacos anti-tumorais

resumo

O cancro da próstata é um dos cancros mais diagnosticados e uma das principais causas de morte entre os homens a nível mundial. Atualmente, apesar de muitos avanços na medicina, os tratamentos desta neoplasia em estágio avançado são bastante ineficazes. O desenvolvimento de modelos *in vitro* que recapitulam os tumores da próstata humanos podem ajudar na descoberta de novas terapias e fármacos contribuindo assim para um aumento da expectativa de vida do paciente. Até à data, as agências reguladoras recomendam que o teste da eficácia de fármacos anti-tumorais a nível pré-clínico deve ser efetuado em culturas celulares bidimensionais (2D), no entanto, esses modelos não imitam as principais características dos tumores *in vivo*, tais como a sua distribuição espacial, interações célula-célula e gradientes de nutrientes/oxigénio. Além deste facto as culturas 2D não replicam os componentes da matriz extracelular tumoral (ECM) e a heterogeneidade celular tumoral. Estas limitações são responsáveis pela baixa correlação de resultados entre as culturas 2D *in vitro* e os dados obtidos em ensaios clínicos.

Para superar essas questões, recentemente os modelos tumorais de cultura 3D *in vitro* têm sido investigados como alternativas valiosas. Estes modelos conseguem reproduzir vários aspetos do microambiente de tumores sólidos humanos, incluindo os seus padrões de expressão génica, interações 3D entre célula-célula, formação de núcleo necrótico e a intrínseca resistência aos fármacos.

O trabalho de investigação desenvolvido no âmbito desta dissertação descreve a produção de um novo modelo tumoral 3D *in vitro* do cancro da próstata que mimetiza a heterogeneidade celular na metástase óssea do cancro da próstata bem como o microambiente da matriz extracelular. O modelo criado é composto por células humanas do cancro da próstata (PC-3) e osteoblastos humanos, encapsuladas em micro-hidrogéis com forma quasi-esférica. Estas microcápsulas, foram produzidas numa superfície quase super-hidrofóbica onde uma mistura de ácido hialurónico metacrilado, gelatina metacrilada, células cancerígenas e osteoblastos foram depositadas e reticuladas com luz U.V. Os resultados demonstram que os microtumores formados são reprodutíveis em termos de morfologia, tamanho e número de células encapsuladas. As formulações de co-cultura HA-MA / Gel-MA apresentaram deposição de cálcio ao fim de 14 dias, quando comparadas às monoculturas, evidenciando assim a importância dos osteoblastos. A avaliação da citotoxicidade da cisplatina nas co-culturas heterotípicas demonstrou que os microgéis 2.5%HA-MA-5%Gel-MA têm maior resistência ao fármaco que os microgéis com 5%HA-MA-5%Gel-MA.

Em conclusão, os resultados indicam que as superfícies quase super-hidrofóbicas são úteis para a produção rápida, e sem solventes, de modelos 3D *in vitro* do cancro da próstata e podem vir a servir de plataforma de testes para a descoberta de novas terapias para o cancro da próstata.

keywords

3D *In vitro* Tumor Models, Prostate cancer, Microcapsules, Drug Screening, Superhydrophobic Surfaces

abstract

Prostate cancer is one of the most commonly diagnosed malignancy and a leading cause of death among men worldwide. Currently, despite many advances in medicine, the current treatments for this neoplasia are mostly ineffective. The development of advanced *in vitro* disease models that can recapitulate human prostate tumors may revert this scenario by accelerating the pre-clinical discovery of new therapies which can realistically impact patients' life span.

Up to now, regulatory agencies recommend that anti-tumor drug screening should be performed in two-dimensional (2D) cell cultures for gathering preliminary pre-clinical data. However, these models fail to mimic key characteristics of *in vivo* human tumors including their spatial distribution, cell-cell contacts and nutrients/oxygen gradients. Moreover, these 2D models utterly fail to replicate tumors extracellular matrix (ECM) and cellular heterogeneity. These intrinsic limitations cause a number of false positive/negative results and provide a poor correlation with clinical trials data.

To overcome these issues, *in vitro* 3D tumor models were proposed as valuable alternatives. Such platforms are able to reproduce various aspects of human solid tumors microenvironment, including gene expression patterns, 3D cell-cell interactions, necrotic core formation and drug resistance phenotypes.

The research work developed within the scope of this dissertation describes the production of a novel 3D prostate cancer *in vitro* tumor model that mimics prostate cancer bone metastasis cellular heterogeneity and ECM microenvironment. The model is comprised of human prostate cancer cells (PC-3) and human osteoblasts, encapsulated in spheroidal-shaped hydrogel microparticles. Such cell-laden spheroidal microcapsules were assembled on a quasi-superhydrophobic surface by unitary droplet dispensing through U.V. mediated photocrosslinking of methacrylated hyaluronic acid and methacrylated gelatin blends.

The obtained results show that spheroidal microtumors were reproducible in terms of morphology, size and number of encapsulated cells. The selected HA-MA/GelMA formulations present the deposition of calcium after 14 days, when compared to the monocultures, thus evidencing the importance of osteoblasts inclusion. The evaluation of cisplatin cytotoxicity in heterotypic co-cultures showed that 2.5% HA-MA-5% GelMA microgels have higher drug resistance than 5% HA-MA-5% GelMA

Overall, the findings indicate that quasi SH are suitable for rapid, and solvent-free, manufacture of 3D prostate tumor *in vitro* models that may serve as testing platforms for the discovery of new therapies for prostate cancer.

Contents

List of Figures

Section 1. Introduction

List of Abbreviations and Acronyms

2D	Two-Dimensional
3D	Three-Dimensionally
3D-CRT	Three-Dimensional Conformal Radiation Therapy
ADT	Androgen-Deprivation Therapy
AR	Androgen Receptor
ATB	Antibiotic
BM	Bone-Marrow
BMP	Bone Morphogenetic Protein
BPH	Benign Prostatic Hyperplasia
CA	Contact Angle
CRPCa	Castration-Resistant Prostate Cancer
CXCL12	C-X-C motif chemokine ligand 12
CXCR4	C-X-C chemokine receptor type 4
DHT	Dihydrotestosterone
DMF	N,N-dimethylformamide
DoF	Degree of functionalization
DRE	Digital Rectal Examination
EBRT	External Beam Radiation Therapies
ECM	Extracellular Matrix
ET1	Endothelin-1
FDA	Food and Drug Administration
FGF	Fibroblast Growth Factor
FTIR	Fourier Transformed Infrared spectroscopy
HA	Hyaluronic Acid
HIFU	High Intensity Ultrasound
hOB	Human Osteoblasts
HTS	High Throughput Studies
IGF	Insulin-like Growth Factor
IMRT	Intensity Modulated Radiation Therapy
LHRH	Luteinizing Hormone-Releasing Hormone
LNCaP	Lymph node Neoplasm of the Prostate Cancer

MCS	Multicellular Spheroid
MCTS	Multicellular Tumor Spheroids
miRNA	MicroRNA
MMP	Matrix Metalloproteinase
MPCa	Mucinous Prostate cancer
MRI	Magnetic Resonance Imaging
NMR	Nuclear Magnetic Resonance
OPG	Osteoprotegerin
PCa	Prostate Cancer
PDGF	Platelet-Derived Growth Factor
PLGA	Poly Lactic-co-Glycolic Acid
PS	Polystyrene
PSA	Prostate Specific Antigen
RANKL	Receptor Activator of Nuclear factor-κB Ligand
RT	Room Temperature
SBRT	Stereotactic Body Radiation Therapy
SH	Superhydrophobic
SL	Superhydrophilic
TEA	Triethylamine
TEB	Tissue Engineered Bone
TGFβ	Transforming Growth Factor-β
TME	Tumor Microenvironment
TRUS	Transrectal Ultrasound
uPA	Urokinase-type Plasminogen Activator
VEGF	Vascular Endothelial Growth Factor

List of Publications

I- Mini review article: *"Hydrophobized Platforms for Spheroidal 3D In vitro Tumor Models Assembly-Advances and Prospects"* Page **30**

II- Article: *"In-air production of 3D Co-culture Tumor Spheroids for Expedite In vitro Drug Screening".* Manuscript in preparation. Page **66**

1. Introduction

1. Introduction

Statistically, cancer kills one out of eight people in the world [1]. Cancer can be caused by numerous environmental and epidemiological factors, and it is characterized by an unbridled proliferation of cells that have the ability to invade healthy tissues in a process known as metastization. Tumor development is a dynamic process in which cancer cells differentiate, proliferate and move to diverse sites interacting three-dimensionally (3D) with each other and with the surrounding extracellular matrix (ECM). This process is identical to those involved in the formation of the first tissues during embryonic developmental stages because such cells have specific genetic information to grow and spread [2]. Prostate cancer (PCa) has long been identified from ancient times, first described by ancient Egyptians and Prostate removal has started more than 100 years ago [3].

Among, all cancers, prostate cancer is one of the most frequently diagnosed non-cutaneous malignancies in men. Despite significant advances in this treatment, prostate cancer is one of the leading causes of cancer death in men, representing 19 % of all cases, nearly 1 in 5 new diagnostics [4]–[6]. In Portugal, prostate cancer represents about 3.5 % of all deaths in the country and more than 10 % of cancer-related deaths, recorded in 2010 according to the Portuguese Urology Association [7]. Inheritance, advanced age, and ethnic origin are some examples that may influence the development of prostate cancer. Alcohol consumption, exposure to ultraviolet radiation, sexual behavior and exogenous factors may also be involved in the development of prostate cancer (PCa), however its direct link to the development of the disease is lesser important than those formerly described. Recent prostate cancer development studies performed on healthy men from age 20 to 40 revealed the presence of histological foci of prostate cancer, suggesting its beginning at a relatively early age, although prostate cancer is a disease mainly associated with older men [8]. Statistically, one in six men will develop some form of prostate cancer during their lifetime and, curiously, almost 50 % of men, after autopsies, have tumors inside the prostate. Although most cases are clinically indolent, a variable proportion of patients develops castration-resistant PCa (CRPCa), an aggressive and deadly form of the disease, associated with metastasis formation [6]. This indicates that prostate cancer is a slow-growing cancer that may not lead directly to morbidity, but there are aggressive forms of the disease that, when detected at late stages, lead to fatal outcomes [6], [9]. Another important example of an aggressive PCa is mucinous (or colloidal) prostate

cancer (MPCa). This sub-type is an adenocarcinoma characterized by approximately 25 % of extracellular mucin and reported to have a more aggressive evolution in some cases [10].

Dysregulation of microRNA (miRNA) expression has also recently been implicated as a possible mechanism in PCa development and disease progression (Figure 1).

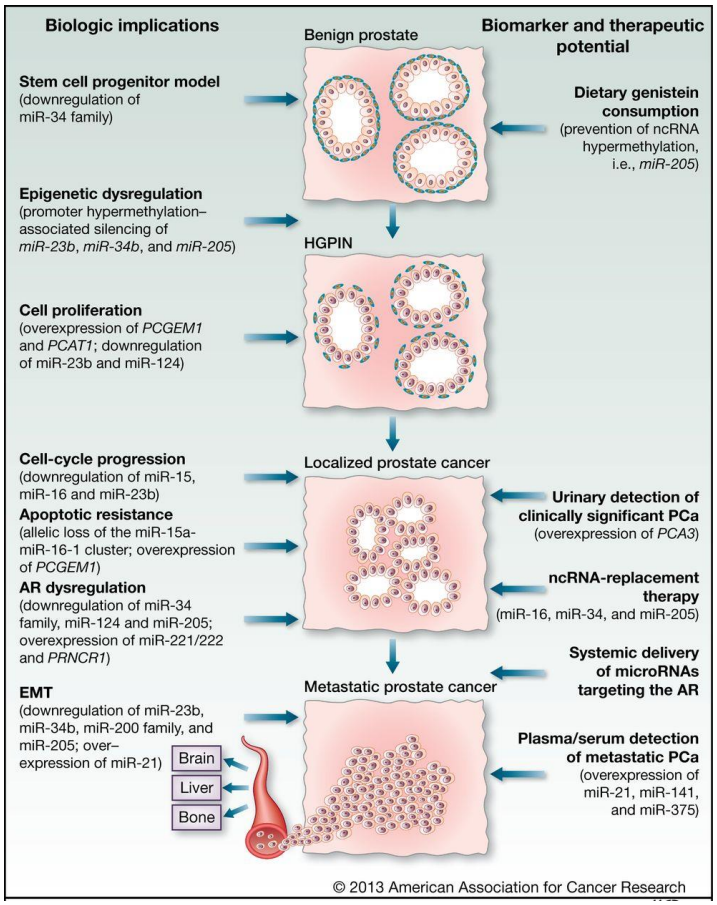

Figure 1. Most important RNA classes responsible for the molecular pathogenesis of prostate cancer onset and evolution. Adapted from [10].

In the prostate several neoplastic transformation events can occur because PCa is a multifocal disease. The outermost peripheral zone of the prostate gland is the largest part of this organ and is the location to where most prostate carcinomas spread. On the contrary, benign prostatic hyperplasia (BPH), a non-malignant condition, commonly found in older men, arises generally at the transition zone [8]. Both of these conditions are remarkably challenging to detect at an early stage and currently there is a high demand for the discovery of novel disease biomarkers.

Androgen signaling plays a critical role in the normal development, proliferation, and differentiation prostate, as well as the onset of prostate cancer through their interactions with

the androgen receptor (AR). The AR is a protein that is able to bind to androgens and act a transcription factor to regulate a diverse array of genes. Testosterone is the most common androgen [8], [11].

Genetic and epigenetic changes contribute to the onset of PCa, but almost all prostate cancers begin with androgen dependence, but prostate cancer cells often escape from primary hormonal control, so when androgen deprivation therapy is given, the prognosis of the disease improves. Despite this, some cancer cells can survive and grow during this treatment, originating prostate cancer independent of androgen. When this happens, the disease is fatal because there are no therapies yet capable of solving the problem [6], [9], [12]. The main methods of diagnosis the PCa are a digital rectal examination (DRE), prostate-specific antigen test (PSA) and transrectal ultrasound (TRUS) biopsy. Prostate epithelial cells, in the normal secretions of the prostate, produce a serine protease named PSA. This unique biomolecule was discovered about 20 years ago and has lately become the leading and only tumor marker for diagnosis, monitoring, and prognosis of prostatic carcinoma accepted by the US Food and Drug Administration (FDA) with the purpose of diagnosing premature prostatic carcinoma. When there is rupture of the normal architecture of the prostate this serine protease is released into the bloodstream, being present in relatively large concentrations [8], [13]. Patients who present positive PSA tests undergo a prostate biopsy, where the prostate tissue is analyzed to determine whether the cancer is present or not [13]–[15].

After the biopsy, the prostate tissue is evaluated by the Gleason scale, classifying the tumor from 1 to 5 (depending on its differentiation), evaluates the patient in the condition of his primary tumor, presence and percentage of distant metastases [13]. Figure 2 shows the treatment that each patient will make according to the results of the biopsy.

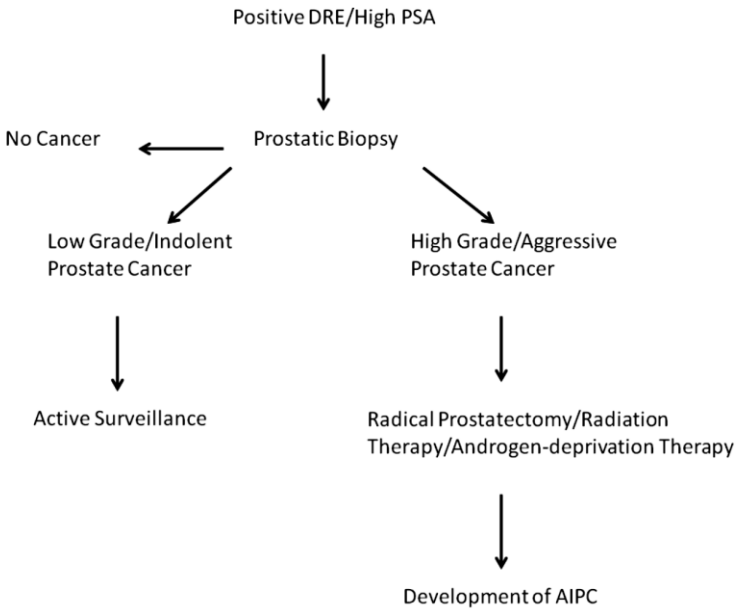

Figure 2. Decision diagram of prostate cancer diagnosis and treatment. Adapted from [9].

Cancers with assessments equal or lower than 6 are monitored only, without requiring treatment whereas cancers with higher scores are treated with radical prostatectomy and androgen deprivation therapy [9].

If PSA analysis, which usually provides information about the location of the disease, indicates that the cancer is located inside the prostate, the patient will undergo radical prostectomy. This treatment method has an effectiveness of almost 40 %, and is the most usual in this type of cases. The reminiscent tumor tissue is not cured because it is impossible to remove the entire tumor mass (these patients are thought to have residual disease after surgery). However, there are cases where patients are apparently cured, but they return having the disease later. The PSA test in post-prostatectomy patients is of paramount importance in deciding who has residual disease, who relapsed (and when) and who can be considered cured. Conventional treatments are: surgical excision of the prostate (radical prostatectomy) external beam radiation therapy or internal radiation therapy (brachytherapy); however, radiation resistance has become a practical deterrent to prostate cancer radiotherapy. In the case of advanced cancer, these regimens are usually followed or replaced by androgen deprivation therapy, which will initially reduce the tumor load and / or the circulation of PSA to low or undetectable levels, but ultimately the disease will recur in most cases [4], [6], [16]. All of these medical decisions and biomarkers research are

intimately related with the complexity of the disease and ultimately of its unique tumor microenvironment.

1.1. The tumor microenvironment: from prostate cancer to bone metastatic niche

Most prostate cancers begin when there are interactions between the epithelial cells and the surrounding stroma (Figure 3). These interactions define the progression and invasiveness of tumor cells. This unique niche is known as the tumor microenvironment (TME) and is the cellular environment in which the tumor exists. TME is composed of different cell types, including both cancerous and non-cancerous cells, which are embedded in a tumor-specific ECM [17]. Non-malignant cells (stromal cells) and the specific composition of the extracellular matrix (ECM) in the TME both contribute to the malignancy and behavior of cancer cells [18].

The complex tumor microenvironment controls: (i) the initiation, (ii) growth and proliferation, (iii) metastasis and (iv) therapeutic resistance of cancer cells; both during disease progression and treatment. The extracellular matrix that surrounds human tumors is characterized by higher than normal levels of some ECM components, such as collagens (I, II, III, V and IX) and proteoglycans including hyaluronic acid (HA). As the tumor progresses the tumor ECM will become more rigid than normal tissue ECM, causing metastases [19], [20].

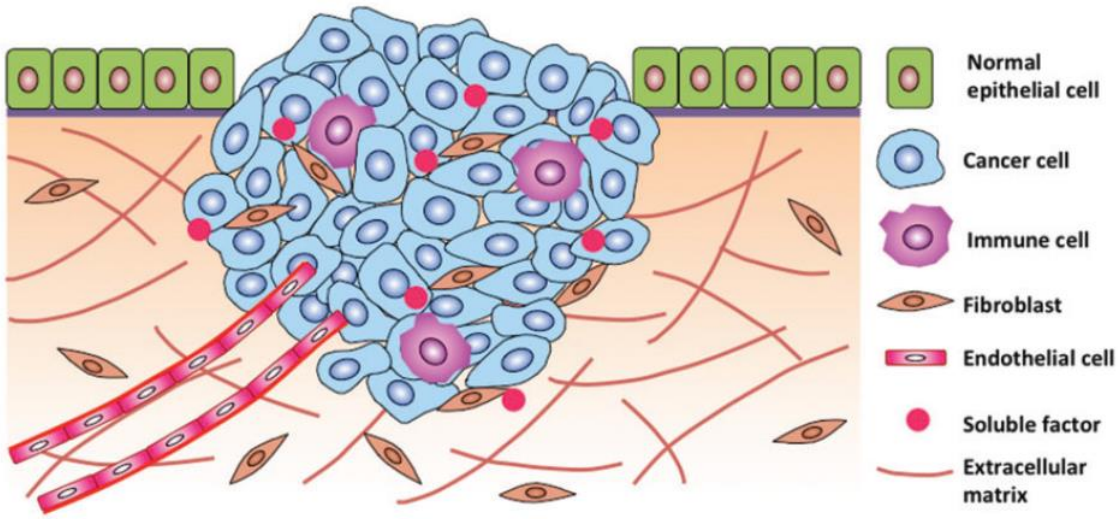

Figure 3. Tumor is a complex heterocellular microenvironment where cancer cells are in constant communications with the stromal cells, the extracellular matrix, and biochemical signaling molecules. Tumor

stroma plays a major role in regulating functions of cancer cells and their responses to therapeutic compounds. Adapted from [21].

In the process of developing a malignant disease, cancer cells acquire resistance to apoptotic signals, leading to the uncontrolled proliferation of cancerous cells with invasive potential, where the formation of a supporting stroma and the development of the vasculature occur [18]. The ECM is comprised by fibrous proteins (e.g., collagen, laminin and fibronectin) and glycosaminoglycans, and it has a three-dimensional (3D) structure that provides biochemical and physical support to the surrounding cells [18], [22]. The ECM changes during tumor development and progression, so modifications in ECM structure would be the main contribution in shaping the surrounding tumor stroma [18]. Interestingly, prostate tumor microenvironment and its complex stromal cellular and acellular components change in metastatic foci.

Prostate cancer (PCa), during the advanced stage of the disease, is highly likely to form bone metastases, which is why secondary tumors form, contributing to its high level of fatality. Several studies have reported that about 90% of patients with advanced prostate cancer will develop bone metastases [18], [23], [24]. Metastasis from prostate cancer cells to the bone is a process involving several steps: 1) cancerous cells are released from the primary site; 2) the displacement of cells into the blood or lymph and 3) fixation of tumor cells to bone tissue and development of a tumor at the site of bone metastasis [23]. Bone-metastatic cancer cells interact with bone-marrow (BM) cells that promote their proliferation, chemoresistance, and evolution. Understanding the role of these bone cells (osteoblasts, osteocytes, osteoclasts, hematopoietic cells, mesenchymal cells, and immune cells) and how they interact with tumor cells, is an important aspect for the development of therapies for the metastasis [23]. Throughout the whole process from the primary tumor to the metastasis, it is widely accepted that non-malignant cells actively influence the fate of cancer cells [18]. Factors secreted by prostate cancer cells alter the balance between the activity of osteoblasts (bone forming cells) and osteoclasts (bone lysis cells). Both are involved in the progression of prostate cancer metastases because they inhibit these factors and determine the phenotype of bone lesions. Prostate cancer metastases cause osteoblasts (excessive bone formation), osteolytic (bone lysis), or mixed bone response (Figure 4) [24], [25]. X-ray analysis of bone metastases of prostate cancer shows the joining of many osteoblasts to prostate cancer cells, whereas in normal bone or bone metastases of other

cancers this does not occur, or occurs in small amounts, for this reason we can associate the increased activity of osteoblasts to the metastasis of prostate cancer to the bone [25].

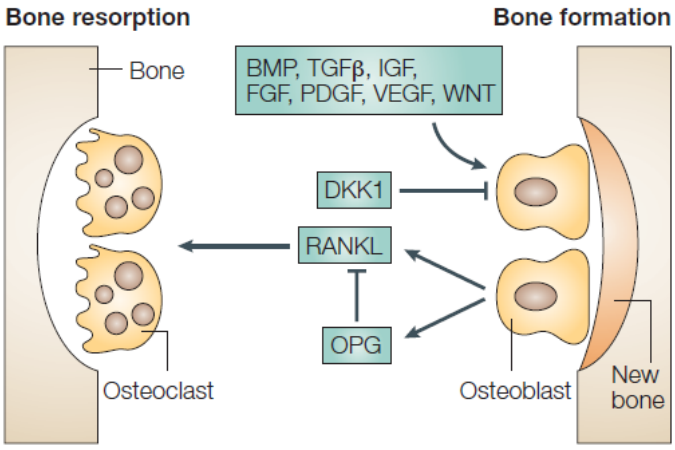

Figure 4. Role of osteoblasts and osteoclasts in bone remodelling. Bone mass is maintained by a balance between the activity of osteoblasts (right), which form bone, and osteoclasts (left), which break it down. Normally, bone formation and bone resorption are closely coupled processes involved in the normal remodelling of bone. Osteoblasts make bone by producing a matrix that then becomes mineralized. Osteoblasts also regulate osteoclast activity through expression of cytokines such as receptor activator of nuclear factor-κB ligand (RANKL), which activates osteoclast differentiation, and osteoprotegerin (OPG), which inhibits RANKL. Factors that are known to stimulate osteoblast proliferation or differentiation are boné morphogenetic protein (BMP), transforming growth factor-β (TGFβ), insulin-like growth factor (IGF), fibroblast growth factor (FGF), platelet-derived growth factor (PDGF), vascular endothelial growth factor (VEGF) and WNT. The WNT antagonist DKK blocks osteoblast proliferation. Osteoclasts are large multinucleate cells that break down bone and are responsible for bone resorption. Adapted from [25].

In addition, several other factors such as bone morphogenetic proteins (BMPs), transforming growth factor-β1 (TGF-β1) and TGF-β2, insulin-like growth factor 1 (IGF-1) and IGF-2, fibroblast growth factor (FGF); platelet-derived growth factor (PDGF) and WNT are endocrine and paracrine factors involved in bone formation and resorption that regulation of osteoblast proliferation and differentiation and also increase the invasion, proliferation, and survival of prostate cells in bone tissue. Vascular endothelial growth factor (VEGF) modifies the bone microenvironment and affect osteoblast function indirectly (Figure 5) [25], [26].

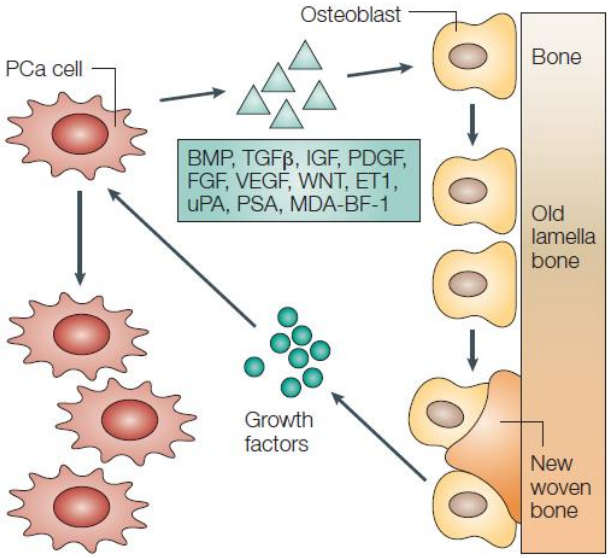

Figure 5. Biological interplay between prostate cancer cells and osteoblasts in the metastatic niche. PCa cells influence bone homeostasis by secreting paracrine factors that regulate osteoblast proliferation or differentiation. These factors include BMP, TGFβ, IGF, PDGF, VEGF, endothelin-1 (ET1), MDA-BF-1, urokinase-type plasminogen activator (uPA) and PSA. These factors (BMP, TGF-β, IGF, PDGF, VEGF, ET1, MDA-BF-1) have been shown to support osteoblast proliferation by exerting direct effects on osteoblasts or influence osteoblast proliferation by modifying growth factors present in the bone microenvironment (uPA and PSA). In addition, these growth factors modulate osteoblast function to promote deposition of new bone matrix. The newly formed bone has features of immature bone (woven bone) with collagen fibres arranged in irregular random arrays. Woven bone is eventually converted into lamellar bone, which is mature bone with collagen fibres arranged in lamellae. Osteoblasts also produce factors that stimulate proliferation of prostate cancer cells (green circles); these bone-derived factors have not yet been identified. Adapted from [25].

1.2. Current Treatments for prostate cancer

Despite significant advances in treatment prostate cancer and its metastatic niche, particularities such as hormone dependence or the slow progression of the disease, can limit the medical decision for the best therapeutic approach to be applied, and sometimes there are several valid treatment options for the same case [27].

The European Association of Urology, recommends that in patients with localized PCa, cryotherapy and focused high intensity ultrasound (HIFU) should be used as a treatment. However, there are more ablative approaches for the treatment of PCa, such as: laser ablation therapy, radiofrequency ablation, irreversible electroporation and photodynamic therapy [28], [29].

Because prostate cancer often grows very slowly, some men (especially those who are older or have other serious health problems) might never need treatment for their prostate cancer. Instead, their doctors may recommend approaches known as watchful waiting or active surveillance.

1.2.1. Watchful waiting or active surveillance

Active surveillance is often used to mean monitoring the cancer closely. Usually this approach includes a doctor visit with a prostate-specific antigen (PSA) blood test and digital rectal exam (DRE) about every 6 months. Prostate biopsies may be done every year as well. Watchful waiting (observation) is sometimes used to describe a less intensive type of follow-up that may mean fewer tests and relying more on changes in a man's symptoms to decide if treatment is needed. These treatments are used when there is no symptom; the cancer is expected to grow slowly (based on the Gleason scale); is small; is just located in the prostate [30].

1.2.2. Surgery for Prostate Cancer

Prostate cancer surgery is a common choice to try to cure prostate cancer if it is not thought to have spread outside the prostate gland. The main type of surgery for prostate cancer is a radical prostatectomy. In this operation, the surgeon removes the entire prostate gland plus some of the tissue around it, including the seminal vesicles. The major possible side effects of radical prostatectomy are urinary incontinence (being unable to control urine) and erectile dysfunction (impotence; problems getting or keeping erections). These side effects can also occur with other forms of prostate cancer treatment [31], [32].

1.2.3. Radiation Therapy for Prostate Cancer

Radiation therapy uses high-energy rays or particles to kill cancer cells and may be used as the first treatment for cancer that is still just in the prostate gland and is low grade. This approach can also be used as a part of the first treatment (along with hormone therapy) for cancers that have grown outside the prostate gland and into nearby tissues, in order to help keep the cancer under control for as long as possible and to help prevent or relieve symptoms.

The 2 main types of radiation therapy used for prostate cancer are: External beam radiation and Brachytherapy (internal radiation). External beam radiation therapies (EBRT), is based on the use of radiation beams (emitted from a machine outside the body), that are focused on the prostate gland. This type of radiation can be used overcome early stage cancers, or to help relieve symptoms such as bone pain if the cancer has spread to a specific area of the bone, but its use to treat advanced diseases is limited [33], [34].

- Three-dimensional conformal radiation therapy (3D-CRT), use special computers to precisely map the location of your prostate. Radiation beams are then shaped and aimed at the prostate from several directions, which makes it less likely to damage normal tissues.
- Intensity modulated radiation therapy (IMRT) an advanced form of 3D therapy, is the most common type of EBRT for prostate cancer. It uses a computer-driven machine that moves around the patient as it delivers radiation. Along with shaping the beams and aiming them at the prostate from several angles, the intensity (strength) of the beams can be adjusted to limit the doses reaching nearby normal tissues. This lets doctors deliver an even higher dose to the cancer.
- Stereotactic body radiation therapy (SBRT) this technique uses advanced image guided techniques to deliver large doses of radiation to a certain precise area, such as the prostate. Because there are large doses of radiation in each dose, the entire course of treatment is given over just a few days.
- Proton beam radiation therapy focuses beams of protons instead of x-rays on the cancer. Unlike x-rays, which release energy both before and after they hit their target, protons cause little damage to tissues they pass through and release their energy only after traveling a certain distance. This means that proton beam radiation can, in theory, deliver more radiation to the prostate while doing less damage to nearby normal tissues.

Possible side effects of EBRT are bowel, urinary and erection problems, feeling tired and lymphedema.

Brachytherapy (internal radiation therapy) also called seed implantation or interstitial radiation therapy) uses small radioactive pellets, or “seeds,” each about the size of a grain of rice. These pellets are placed directly into prostate. Brachytherapy alone is generally used only in men with early-stage prostate cancer that is relatively slow growing (low-grade), combined with external radiation is sometimes an option for men who have a higher risk of the cancer growing outside the prostate. Imaging tests such as transrectal ultrasound or MRI are used to help guide the placement of the radioactive pellets. Special computer programs calculate the exact dose of radiation according to the tumor mass. Possible side effects of brachytherapy treatments are bowel, urinary and erection problems [33].

1.2.4. Cryotherapy for Prostate Cancer

Cryosurgery or cryotherapy is the use of very cold temperatures to freeze and kill prostate cancer cells. Despite it sometimes being called cryosurgery, it is not actually a type of surgery. Cryotherapy is sometimes used to treat early-stage prostate cancer. Most doctors do not use cryotherapy as the first treatment for prostate cancer, but it is sometimes an option if the cancer has come back after radiation therapy. This type of procedure requires spinal or epidural anesthesia or general anesthesia.

The doctor uses transrectal ultrasound (TRUS) to guide several hollow probes (needles) through the skin between the anus and scrotum and into the prostate. Very cold gases are then passed through the needles to freeze and destroy the prostate. To be sure the prostate is destroyed without too much damage to nearby tissues, the doctor carefully watches the ultrasound during the procedure. Warm saltwater is circulated through a catheter in the urethra during the procedure to keep it from freezing. Cryotherapy doesn't appear to be as good as radiation for more advanced prostate tumors [35].

1.2.5. Hormone therapy

Prostate cancer therapy involving hormones is also called androgen deprivation therapy (ADT) or androgen suppression therapy. The goal is to reduce levels of male hormones, called androgens, in the body, or to stop them from affecting prostate cancer cells. Androgens stimulate prostate cancer cells to grow. The main androgens in the body are testosterone and dihydrotestosterone (DHT). Lowering androgen levels or stopping them from getting into prostate cancer cells often makes prostate cancers shrink or grow more slowly for a time. But hormone therapy alone does not cure prostate cancer.

Currently there are various types of hormone therapy that can be applied both based on surgical or pharmacological-based strategies:

- Orchiectomy (surgical castration), even though this is a type of surgery, its main effect is as a form of hormone therapy. In this operation, the surgeon removes the testicles, where most of the androgens (testosterone and DHT) are made. This causes most prostate cancers to stop growing or shrink for a time.

- LHRH agonists: Luteinizing hormone-releasing hormone (LHRH) agonists (also called LHRH analogs or GnRH agonists) are drugs that lower the amount of testosterone made by the testicles. Treatment with these drugs is sometimes called chemical castration or medical castration because they lower androgen levels just as well as orchiectomy. Even though LHRH agonists cost more than orchiectomy and require more frequent doctor visits.
- Pharmaceutical LHRH antagonist: Degarelix (FIRMAGON®) [36] is an LHRH antagonist. It works like the LHRH agonists, but it lowers testosterone levels more quickly and doesn't cause tumor flare like the LHRH agonists do. Treatment with this drug can also be considered a form of medical castration. This drug is used to treat advanced prostate cancer. It is given as a monthly injection under the skin. The most common side effects are problems at the injection site (pain, redness, and swelling).
- CYP17 inhibitor: LHRH agonists and antagonists can stop the testicles from making androgens, but other cells in the body, including prostate cancer cells themselves, can still make small amounts, which can fuel cancer growth. Abiraterone (ZYTIGA®) [37] blocks an enzyme called CYP17, which helps stop these cells from making androgens. Abiraterone can be used in men with advanced castrate-resistant prostate cancer (cancer that is still growing despite low testosterone levels from an LHRH agonist, LHRH antagonist, or orchiectomy).

Drugs that stop androgens from working are anti-androgens. Androgens have to bind to a protein in the prostate cell called an androgen receptor to work. Anti-androgens are drugs that bind to these receptors, so the androgens won't be able to do so. Flutamide (EUXELIN®) [38]; Bicalutamide (CASODEX®) [39] and Nilutamide (NILANDRON® [40]) are drugs of this type. Enzalutamide (XTANDI®) [41] is a newer type of anti-androgen. Enzalutamide can be used in men with metastatic prostate cancer before chemotherapy [42]. Normally when androgens bind to their receptor, the receptor sends a signal to the cell's control center, telling it to grow and divide. Can often be helpful in men with castration-resistant prostate cancer [43].

1.2.6. Chemotherapy-based prostate cancer therapy

Chemotherapy-based approaches are based on the systemic injection, or oral administration of anti-cancer drugs. These drugs enter the bloodstream and go throughout the body, making this treatment potentially useful for cancers that have spread (metastasized) to distant organs. Chemotherapy is sometimes used if prostate cancer has spread outside the prostate gland and in cases where hormone therapy does not promote the desired therapeutic outcome. Recent research has also shown that chemotherapy might be helpful if administered in combination with hormone therapy. Chemotherapy is not a standard treatment for early prostate cancer, but some studies are looking to see if it could be helpful if given for a short time after surgery. Some of the anti-cancer drugs used to treat PCa include: Docetaxel (Taxotere®) [44]; Cabazitaxel (JETVANA®) [45]; Mitoxantrone (Novantrone®) [46] and Estramustine (Emcyt®) [42].

Chemotherapy drugs main target is prostate cells that are rapidly dividing. But other cells in the body, such as those in the bone marrow (where new blood cells are made), the lining of the mouth and intestines, and the hair follicles, also divide quickly. These cells can therefore be affected by chemotherapy as well, which can lead to deleterious side effects in healthy organs. The side effects of chemotherapy depend on the type of pharmaceutical, administered dose and the administration regime. Some common side effects associated with these treatments are: Hair loss, mouth sores, loss of appetite, nausea and vomiting, diarrhea, increased chance of infections (from having too few white blood cells), easy bruising or bleeding (from having too few blood platelets) and fatigue (from having too few red blood cells).

From these former examples of currently applied therapies for PCa, it becomes clear that all of them elicit, to a certain extent, deleterious side effects. Adding to this, most of these approaches are not sufficient to completely eradicate the disease or even to prolong patient survival rates beyond 5-years past diagnosis. Such scenario evidences the necessity to actively investigate new, and more advanced, PCa therapies [47].

In recent decades, researchers have actively sought to capture the complexity of human prostate cancer and of its metastasis by developing various types of disease models that could help in understanding the pathophysiology and biological hallmarks of PCa, as well as discover more effective treatments than those currently applied.

However, the pre-clinical discovery of new anti-cancer therapeutics using laboratory animal models, involves high costs and ethical issues associated with the use of rodents, and has demonstrated a very low correlation with the data that is obtained in clinical trials [48].

To overcome these issues 3D *in vitro* tumor models have been researched in the last two decades as potential alternative preclinical testing platforms to screen for new anti-cancer therapeutics or therapeutics combinations (Figure 6).

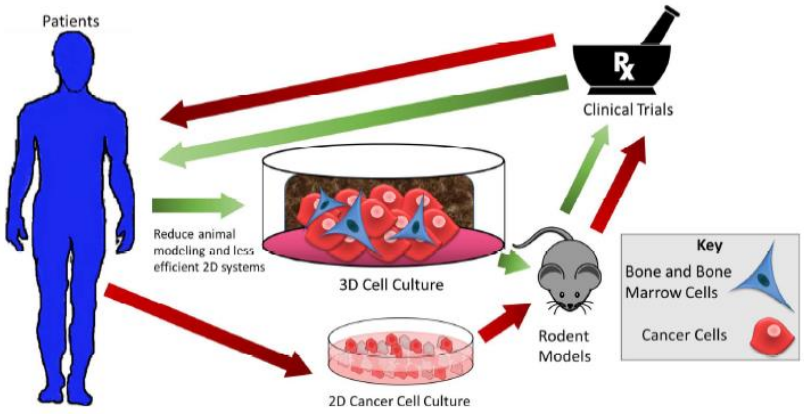

Figure 6. Traditional workflow of designing and testing anti-cancer therapeutics. General methods utilize 2D cell cultures and then laboratory animal models at pre-clinical stages, and finally clinical trials in human patients (longer red pathway). By taking advantage of 3D cell cultures (green pathway) scientists are able to bypass the main limitations of 2D flat *in vitro* cell culture models, minimize large-scale and expensive animal models, decrease false positives, and improve clinical research by identifying promising candidates in a more expedite approach. Adapted from [23].

1.3. *In vitro* 3D tumor models for new Prostate Cancer therapies discovery

The development of improved *in vitro* models for tumor biology is very important since they can expedite the discovery of new treatments or treatment combinations. To date, regulatory agencies recommend that pre-clinical drug screening must be based on two-dimensional (2D) models to study the efficacy of anti-tumor drugs. These models have been proposed under the assumption that the cell monolayers reflect the main characteristics of *in vivo* tumors. Adding to this, in the pharmaceutics pre-clinical discovery process it is clear that 2D *in vitro* cultures do not represent the 3D spatial environment of a human tumor, do not recapitulate ECM or stromal cellular components, [2], [48] nor are able to mimic the resistance to multiple drugs (dysregulation of cellular metabolism, apoptosis, among other

factors). In fact, in 2D flat culture systems, cells are grown under non-physiological and limited conditions. In 2D cultures, cells become attached to rigid and flat substrates, which forces them to polarize and increase their area of exchange for culture media, causing excessive nutrition and oxygenation [49], [50]. Ultimately, this reductionist model which lacks cell–cell and cell–matrix interactions do not replicate the *in vivo* response. Two-dimensional systems cannot provide a complex and dynamic 3D microenvironment for cells, and thus lead to poorly in vitro/in vivo correlative findings. In fact, various studies have shown that 2D *in vitro* cell culture cannot replicate real microenvironment and cell actions *in vivo* because of lack of cell–cell and cell–matrix interactions and loss of tissue-specific architecture, mechanical and chemical cues, which are vital for unique functions of real tissues in the human body. Therefore, in order to advance the development of new treatments for cancer, it is of extreme importance to recapitulate the complex cellular microenvironment into a simpler system, since only in this way can one perceive the mechanisms involving tumor initiation and progression [49]–[52]. For instance, b1-integrin inhibits the growth of 3D multicellular spheroid (MCS) formation of PC-3 prostate adenocarcinoma cells, but in the 2D culture the same results are not observed [53].

To reduce these contradictory results, multicellular spheroids were developed, which passed the biology of cancer into the third dimension (3D), giving rise to models of a greater complexity [54], [55]. However, they have important limitations since they are grown as independent cellular aggregates and also show reduced interactions with the extracellular matrix (ECM) [56], [57]. To minimize this effect, and considering that the tumor microenvironment controls tumorigenesis, tumor-ECM mimics (e.g., hydrogels) were introduced as cell culture systems in order to incorporate cells in a ECM mimetic 3D matrix. The major difficulty with this approach is the appropriate modulation of physical, chemical and mechanical cues of human tumors ECM.

Sutherland and co-workers, in 1971, were the first to propose the multicellular tumor spheroids (MCTS) as 3D models, which are very interesting in the simulation of small non-vascularized solid tumors [49]. 3D spheroids form only when cell-cell interactions are stronger than those between cells and the substrate, and cell's nucleus adopts a glycolytic metabolic activity. Generally, 3D spheroids are not vascularized, the dispersion of oxygen and nutrients is therefore limited, increasing the pH outside the cell, as in the regions of tumor hypoxia and acidity between the nucleus and tumor blood vessels [20], [58]–[61].

As an example [21], Ham et al., produced spheroids of cancer cells, stromal fibroblasts and immune cells, so as to mimic the multi-cellular components of the tumor microenvironment [21]. Despite achieving interesting results regarding the formation of a necrotic core and hypoxia gradients these models still fail to recapitulate the tumor ECM (Figure 7).

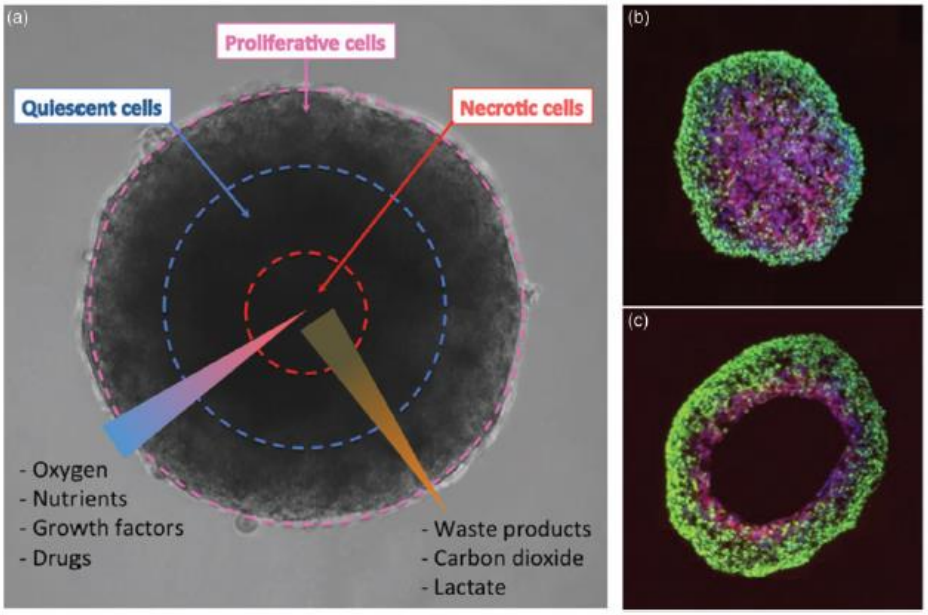

Figure 7. a) Concentration gradients of oxygen, nutrients, and metabolites generate distinct concentric zones in spheroids: An outer zone containing proliferative cells, a middle zone with quiescent cells, and an inner zone containing necrotic cells. Abundance of oxygen and glucose at the outer zone and efficient removal of waste products facilitate cell proliferation, whereas low oxygen levels and a buildup of toxic metabolites such as carbon dioxide and lactate generate a necrotic core. (b,c) Development of hypoxia and anoxia is shown in spheroids. Adapted from [21].

Given their tumor-like features, *in vitro* multicellular 3D spheroids have been particularly useful for studying the efficacy of novel chemotherapeutic agents or drug delivery systems. Significant differences in drug responses have been observed for numerous cancer types in spheroid culture, but increased chemical resistance appears to depend upon the type of cancer cells and the specific treatment under study [62]. Therefore, MCSs have emerged as a powerful tool to reduce the gap between the *in vitro* and *in vivo* model. Producing MCS of homogeneous size is essential for the conduct and functions of cells [50].

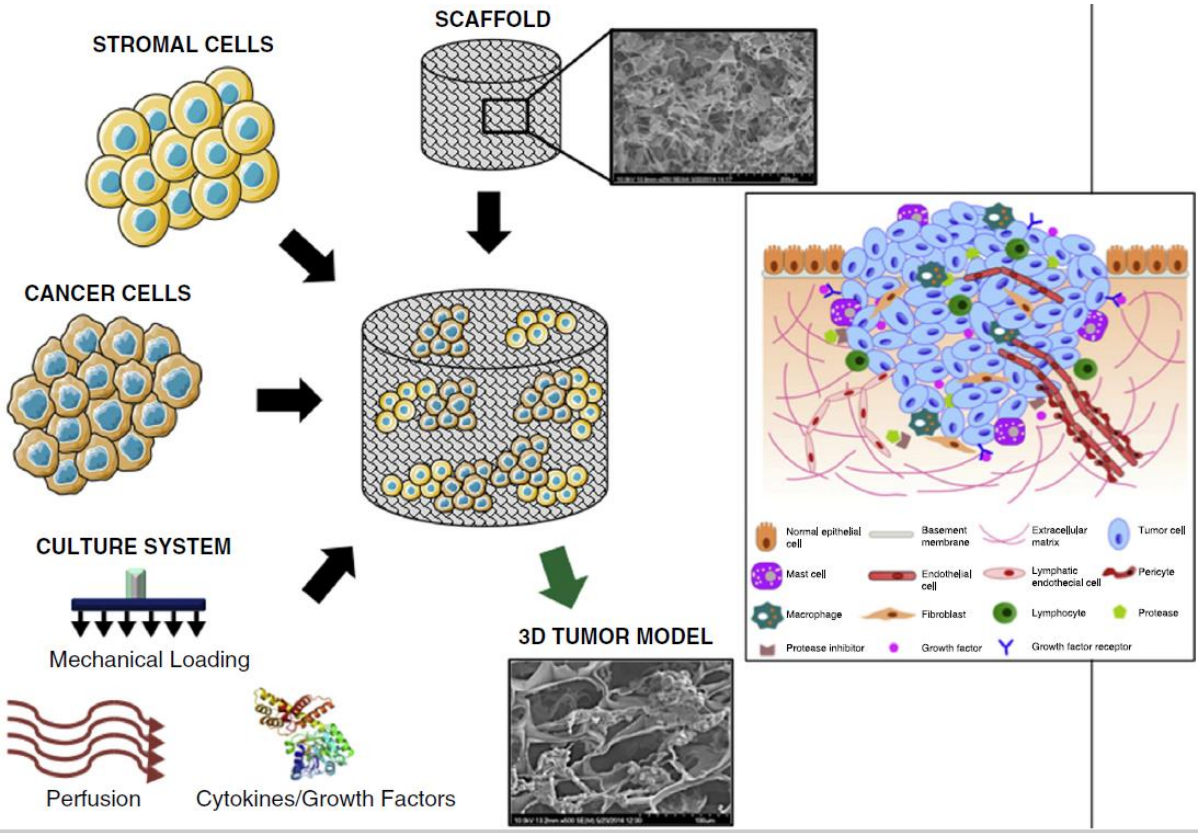

Figure 8. Various steps to generate a scaffold-based three-dimensional tumor model. Adapted from [19].

In the manufacture of 3D-MCTS, polymeric hydrogels can function as tumor-ECM mimics and serve to recapitulate cell-matrix interactions. In order for the microenvironment of 3D-MCTSs and cell responses to be as close to reality as possible, it is possible to adjust the scaffold structure, morphology, stiffness, and its biomimetic components during synthesis [63]. The synthesized polymeric hydrogels can be chemically modified to have the desired ECM characteristics (E.g., integrins, matrix metalloproteinases, collagen, fibrinogen) promote cell aggregation and maintain tissue functionality to simulate the *in vivo* environment *in vitro*. In addition, synthesized polymers have high reproducibility and improved handling characters. 3D-MCTSs from breast, prostate and Lewis lung cancer cells were successfully produced in a poly (lactic-co-glycolic acid) (PLGA) scaffold [19].

1.4. Prostate cancer 3D *in vitro* tumor models

3D culture systems can be subdivided into: (i) scaffold-free or (ii) scaffold-based platforms. Scaffold-free 3D cancer models are best exemplified by tumor spheroids. Scaffold

materials can be synthetic or natural in origin. Biomaterials are broadly for mimicking tumors extracellular matrix (ECM), due to their advantageous features, such as biocompatibility, biodegradability, and bioavailability, and also the capability to interact with cells. From the different types of biomaterials, natural polymers are particularly valuable since they can be engineered and their properties tuned to obtain desirable mechanical and physical characteristics, such as those found in tumors ECM [17], [64]–[66]. Recent studies related to prostate cancer migration to bone (which has a porous collagen-rich matrix), have reported that these cells proliferate at the same rate regardless of the rigidity of the matrix [67].

1.4.1. Scaffold-free 3D Prostate cancer models

1.4.1.1. 3D Prostate cancer spheroids

Mosaad and co-workers,[68] described the use of non-adherent microwells with a nylon netting (named microwell-mesh) that allows the manufacture of microtumors by promoting cells aggregation. The authors analyzed the response of 3D tumor spheroids and 2D cell cultures to Docetaxel and Abiraterone Acetate drugs, and concluded that 3D micro-tumors are not hypersensitive, unlike 2D microtumors (Figure 9 and 10).

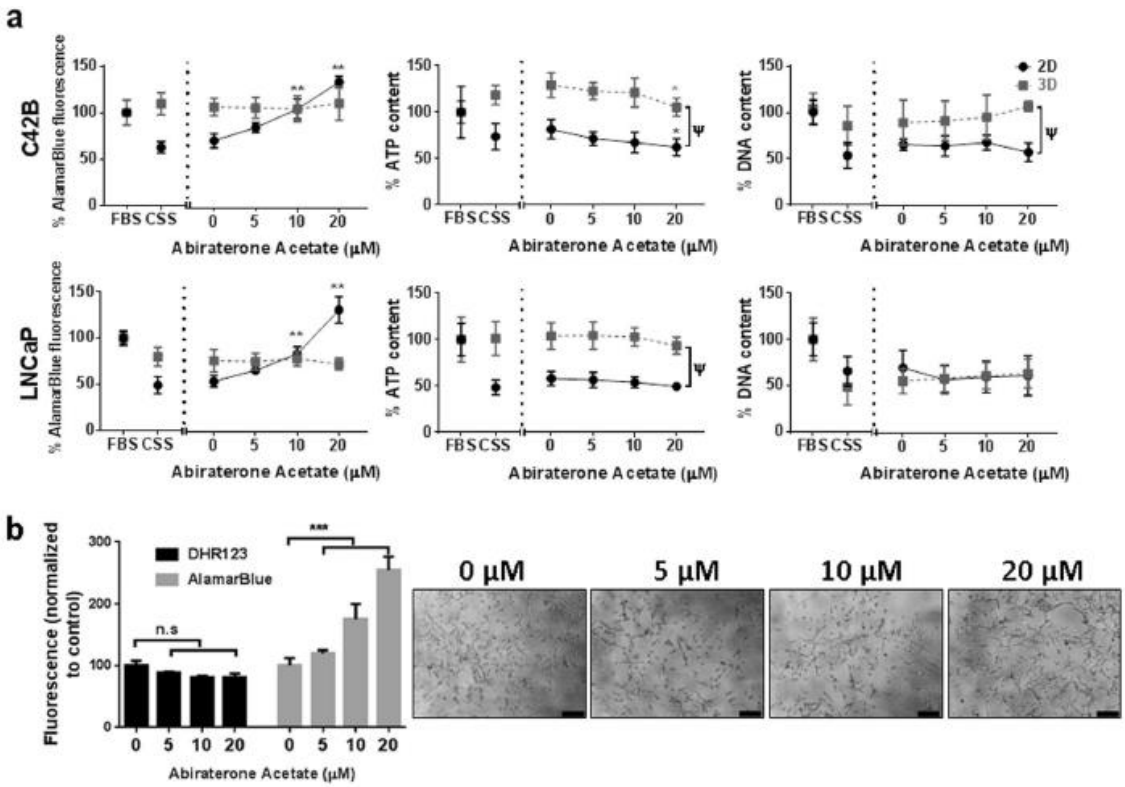

Figure 9. Monolayer and micro-tumor behavior of C42B and LNCaP cell lines in androgen deprived conditions. (**a**) C42B (Top) and LNCaP (Bottom) cells were seeded in expansion culture medium for 24 hours

followed by medium exchange to androgen-depleted medium (CSS) for a further 48 hours. Abiraterone Acetate was then added to the culture medium at the indicated concentrations for an additional 48 hours. AlamarBlue®, Cell Titer-Glo 3D Cell Viability and PicoGreen assays were then performed to assess metabolic activity, ATP quantity, and DNA quantity, respectively. All results are represented as a percentage of the FBS-containing culture medium control values. (**b**) Metabolic activity (AlamarBlue® assay) and DHR123 staining of LNCaP monolayers at specified Abiraterone Acetate concentrations. Results represented as the mean fluorescence values of four individual samples normalized to control culture values. Adapted from [68].

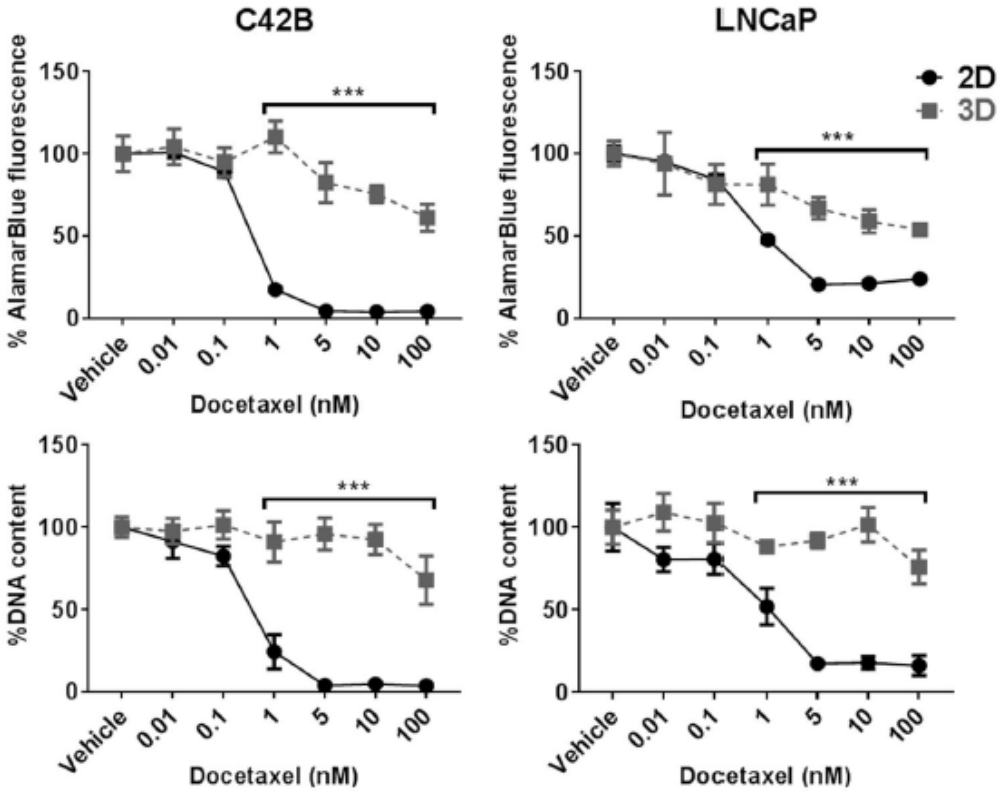

Figure 10. C42Band LNCaP Docetaxel drug response. C42B and LNCaP cells in 2D and 3D cultures were treated with Docetaxel in the indicated concentrations for 72 hours followed by metabolic activity and DNA content measurements. All results are represented as a percentage of the vehicle control values. Adapted from [68].

1.4.1.2. Prostate cancer modeling in Hydrogel-based models

The efficacy of three new anticancer drugs (Camptothecin, Docetaxel and Rapamycin) for the treatment of metastatic bone prostate cancer was evaluated by *Gursky* and co-workers by using an hydrogel-based 3D drug screening platform. In this study, hydrogels derived from hyaluronic acid (HA) have been used to develop a lymph node neoplasm of the prostate (LNCaP) and to understand drugs mechanisms of action, to find new targets or to address efficacy, toxicity of these chemotherapeutics. [69]

To evaluate the efficacy of the three drugs it is necessary to have an adequate microenvironment. The inclusion of HA allowed the cells to grow in the hydrogel matrix and to form distinct clustered structures reminiscent of real tumors [69] (Figure 11).

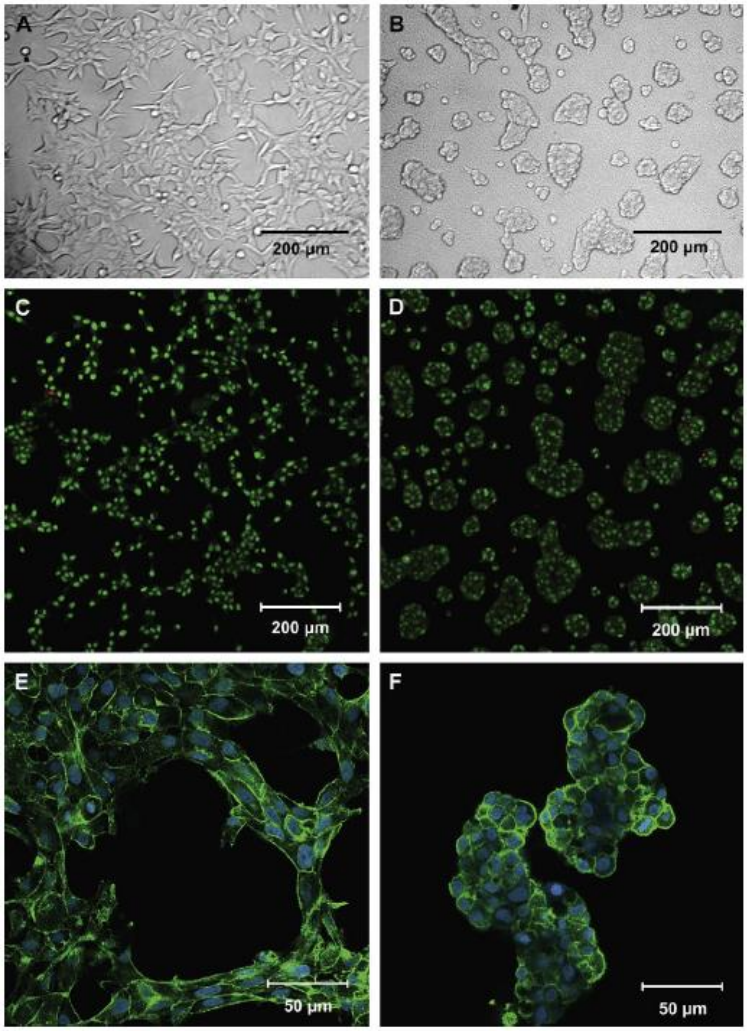

Figure 11. C4-2B cells form clusters in HA hydrogels but not on plastic. Phase-contrast images of cells cultured on plastic (A) or in HA hydrogel (B) for 2 days. Confocal images of live/ dead stained cells cultured on plastic (C) or HA hydrogel (D) for 2 days. Cells were stained with Syto-13 (green) for live cells and PI (red) for dead cells. Confocal images of cells cultured on plastic (E) or HA hydrogel (F) for 2 days stained for F-actin with phalloidin (green) and Draq5 for nucleic (blue). Adapted from [69].

Lu and colleagues, [70] produced microparticles based on the electrospay technique, encapsulated different cell types (MDA-MB-231, RFP and MCF-10A) to produce multilayer spherical hydrogel microparticles, and demonstrated that distinct cells could be encapsulated at various sites of the same particles (Figure 12). They have also been shown that ECM-containing microparticles are excellent for creating controlled-size tumor micro-tissues. They developed microcapsules of co-culture with MDA-MB-231 breast cancer cells, normal

mammary epithelial cells MCF-10A and normal human pulmonary fibroblasts, and were also able to produce microcapsules capable of mimicking the hypoxic conditions of an avascular tumor *in vivo* [70].

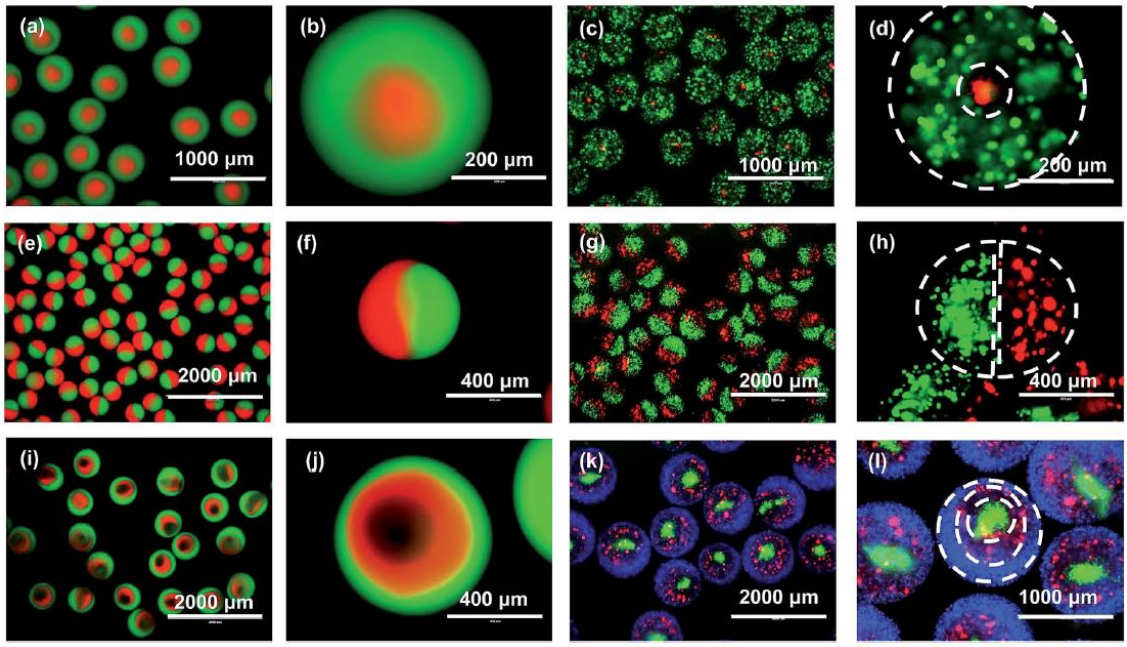

Figure 12. Hydrogel microparticle designs and their applications for cell encapsulation. (a and b) Double-layer hydrogel microparticles made of fluorescently labeled alginate (red: alginate labeled with Alexa Fluor® 594 dye; green: alginate labeled with Alexa Fluor® 488 dye). (c and d) Double-layer alginate microparticles encapsulating different types of cells (green cells: MDA-MB-231 expressing GFP; red cells: normal human lung fibroblasts expressing RFP). (e and f) Side-by-side alginate hydrogel microparticles. (g and h) Cell encapsulation using side-by-side microparticles. (i and j) Triple-layer hydrogel microparticles (the inner most layer in i and j was unlabeled alginate). (k and l) Cell encapsulation using triple-layer particles (the blue cells in k and l were MCF-10A stained with Hoechst). Adapted from [70].

1.4.1.3. 3D tumor models of prostate cancer-bone metastasis

Metastasis is one of the most complex processes in cancer, one of the most difficult to study and mimic using in vitro models therefore, it is crucial to understand the molecular and cellular phenomena involved in the metastatic cascade [71], [72]. Invasion of cancer cells through the basal membrane into a blood or lymphatic vessel (intravasion) followed by entrance into other tissue and / or organs (extravasion) are critical steps [73], [74].

There are few studies addressing the development of metastases in 3D models, but an in vitro 3D microfluidic model of the tumor–vascular interface was designed to integrate live imaging, precise control of microenvironmental factors, and endothelial barrier measurement [73]. Bone metastasis is the most difficult case to control, in prostate cancer.

As such, there some studies that explored the development of 3D tumor models to represent these cases.

In one case, *Sieh* and co-workers developed tissue engineered bone (TEB) constructs from alveolar osteoblasts (hOB-human osteoblasts) and bone marrow stromal cells by using a cell sheet-based technique, then inserted PCa (PC3 and LNCaP) cells within TEB. It was verified that PC-3 and LNCaP cells formed clusters within the bone matrix. From hOB-PC-3 and hOB-LNCaP co-cultures, cell density of PC-3 cells within the TEB construct was lower compared to LNCaP cells, perhaps indicating a difference in affinity between the two cell types towards the bone matrix. LNCaP cells showed greater integration into the bone matrix and formed clusters of cells, however, that appearance was not present in the hOB-PC3 co-culture (Figure 13)[75].

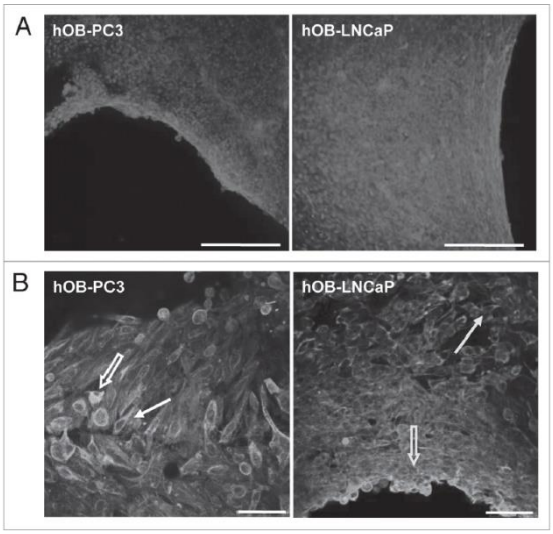

Figure 13- Fluorescence images of direct co-cultures of hOBs and CaP cells within TEB. Adapted from [75].

Fitzgeralnd and co-workers developed a collagen-based scaffold with 3D bone metastases from prostate cancer (PC3 and LNCaP) to assess the potential of the model in gene therapy designed for bone metastases. Metastatic cells were cultured in 2D and compared to the growth of 3D cells in 3 different collagen scaffolds (Figure 14). In the 3D model, cell proliferation, prostate specific antigen secretion (PSA), viability and matrix metalloproteinase enzyme (MMP) were observed (Figure 15). The evaluation of chemosensitivity was evaluated between 2D and 3D cultures through the use of the drug

Docetaxel. Both cultures were found to actively integrate and proliferate in the scaffolds, and were also more resistant to treatment with Docetaxel (Figure 16).

In summary, a 3D cell culture model of prostate cancer bone metastasis was developed in which for the first time there was success in the delivery of gene therapy in a 3D model *in vitro* [76].

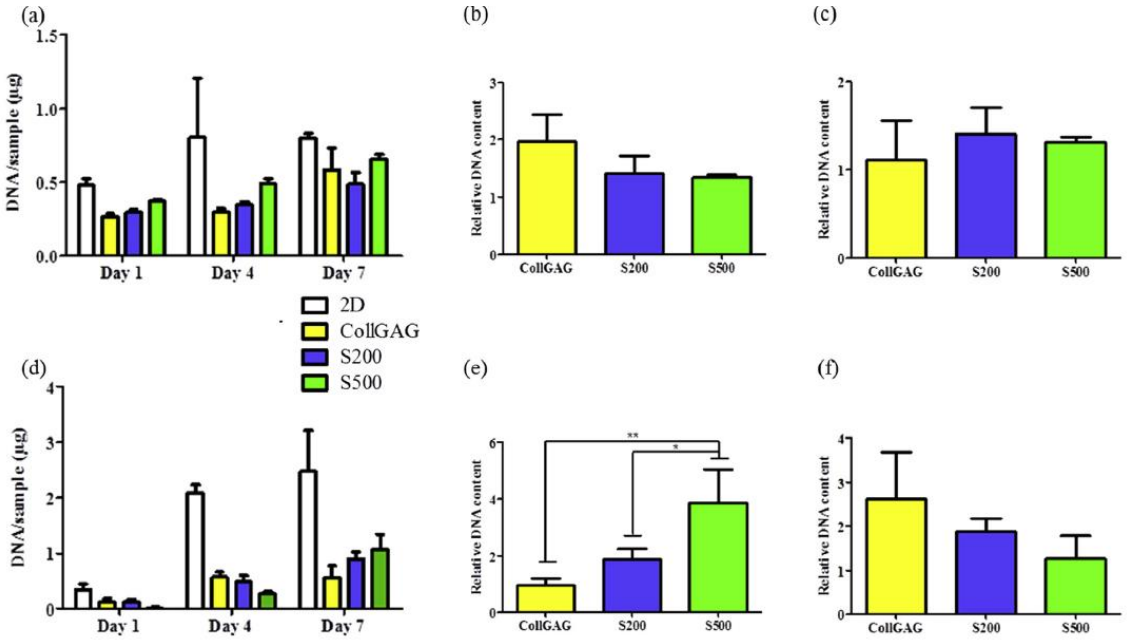

Figure 14. Proliferation of PC3 and LNCaP prostate cancer cells in 2D vs 3D on three different collagen-based scaffolds. Proliferation rate of PC3 cells on days 1, 4 and 7 (a) and relative PC3 cell DNA content on scaffolds on day 7 vs day 4 (b) and day 11 vs day 7 (c). Proliferation rate of LNCaP cells on days 1, 4 and 7 (d) and relative LNCaP cell DNA content on scaffolds on day 7 vs day 4 (e) and day 11 vs day 7 (f). Cells were cultured in 2D on tissue culture plates and in 3D using three collagen-based scaffolds (CollGAG, S200 and S500). Adapted from [76].

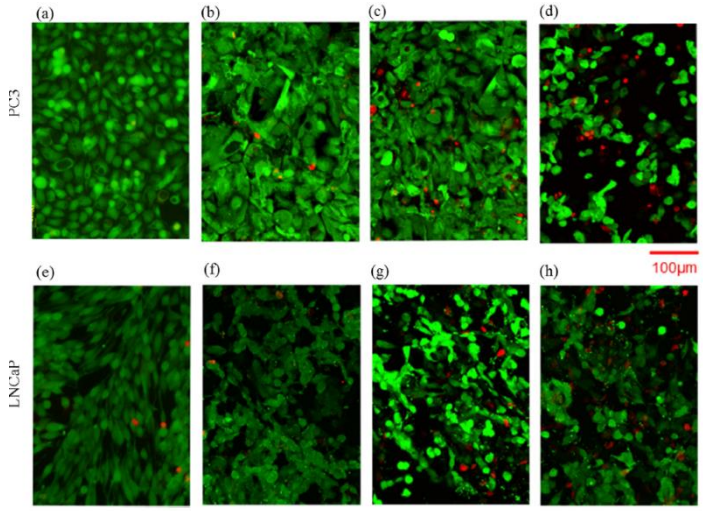

Figure 15. Live/dead staining of PC3 and LNCaP cells grown in 2D and on collagen-based scaffolds 7 days after cell seeding. PC3 cells in 2D (a), on CollGAG (b), S200 (c) and S500 (d) scaffolds. LNCaP cells

in 2D (e), on CollGAG (f), S200 (g) and S500 (h) scaffolds. Live cells are represented in green and dead cells are shown in red. Adapted from [76].

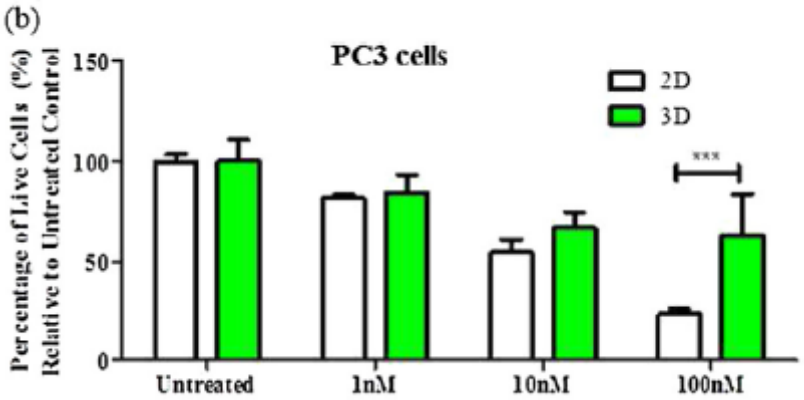

Figure 16. (b) PC-3 cell numbers in 2D and 3D models, normalized to untreated control after Docetaxel treatment. Adapted from [76].

The use of super-hydrophobic surfaces has lately been used to produce 3D models of disease. In the following sub-chapter is presented a mini-review on super-hydrophobic surfaces, since it is the method used in my work to develop a 3D model of prostate cancer.

References

[1] M. R. Stratton, P. J. Campbell, and P. A. Futreal, "The cancer genome," *Nature*, vol. 458, no. 7239, pp. 719–724, 2009.

[2] M. Alemany-Ribes and C. E. Semino, "Bioengineering 3D environments for cancer models," *Adv. Drug Deliv. Rev.*, vol. 79, pp. 40–49, 2014.

[3] L. L. Capasso, "Antiquity of cancer," *Int. J. Cancer*, vol. 113, no. 1, pp. 2–13, 2005.

[4] S. Jayakumar, A. Kunwar, S. K. Sandur, B. N. Pandey, and R. C. Chaubey, "Differential response of DU145 and PC3 prostate cancer cells to ionizing radiation: Role of reactive oxygen species, GSH and Nrf2 in radiosensitivity," *Biochim. Biophys. Acta - Gen. Subj.*, vol. 1840, no. 1, pp. 485–494, 2014.

[5] R. Siegel, "Cáncer Statistics," *Ca Cáncer J.*, vol. 67, no. 1, pp. 7–30, 2017.

[6] E. J. Sousa *et al.*, "Enoxacin inhibits growth of prostate cancer cells and effectively restores microRNA processing," *Epigenetics*, vol. 8, no. 5, pp. 548–558, 2013.

[7] A. P. de Urulogia, "No Title." [Online]. Available: http://www.apurologia.pt/frameset.htm?http://www.apurologia.pt/doencas.htm.

[8] M. Shen and C. Abate-Shen, "Molecular genetics of prostate cancer: new prospects for old challenges," *Genes Dev.*, no. 212, pp. 1967–2000, 2010.

[9] P. Saraon, A. P. Drabovich, K. A. Jarvi, and E. P. Diamandis, "Mechanisms of Androgen-Independent Prostate Cancer.," *Ejifcc*, vol. 25, no. 1, pp. 42–54, 2014.

[10] A. C. Westphalen, F. V. Coakley, J. Kurhanewicz, G. Reed, Z. J. Wang, and J. P. Simko, "Mucinous adenocarcinoma of the prostate: MRI and MR spectroscopy features," *Am. J. Roentgenol.*, vol. 193, no. 3, pp. 238–243, 2009.

[11] F. Alimirah, J. Chen, Z. Basrawala, H. Xin, and D. Choubey, "DU-145 and PC-3 human prostate cancer cell lines express androgen receptor: Implications for the androgen receptor functions and regulation," *FEBS Lett.*, vol. 580, no. 9, pp. 2294–2300, 2006.

[12] A. Takagi *et al.*, "Three-dimensional cellular spheroid formation provides human prostate tumor cells with tissue-like features," *Anticancer Res.*, vol. 27, no. 1 A, pp. 45–54, 2007.

[13] E. P. Diamandis, "Prostate specific antigen- its usefulness in clinical medicine," *Trends Endocrinol Metab.*, vol. 9, no. 8, pp. 310–316, 1998.

[14] G. Sardana, B. Dowell, and E. P. Diamandis, "Emerging biomarkers for the diagnosis and prognosis of prostate cancer," *Clin. Chem.*, vol. 54, no. 12, pp. 1951–1960, 2008.

[15] A. Heidenreich *et al.*, "EAU guidelines on prostate cancer. Part 1: Screening, diagnosis, and local treatment with curative intent - Update 2013," *Eur. Urol.*, vol. 65, no. 1, pp. 124–137, 2014.

[16] B. G. Timms, "Prostate development: A historical perspective," *Differentiation*, vol. 76, no. 6, pp. 565–577, 2008.

[17] A. Nyga, U. Cheema, and M. Loizidou, "3D tumour models: Novel in vitro approaches to cancer studies," *J. Cell Commun. Signal.*, vol. 5, no. 3, pp. 239–248, 2011.

[18] Z. Erlangung *et al.*, "The prostatic tumour stroma : Design and validation of a 3D in vitro angiogenesis co-culture model." 2016.

[19] Z. Liu and G. Vunjak-Novakovic, "Modeling tumor microenvironments using custom-designed biomaterial scaffolds," *Curr. Opin. Chem. Eng.*, vol. 11, pp. 94–105, 2016.

[20] Y. Liang *et al.*, "A cell-instructive hydrogel to regulate malignancy of 3D tumor spheroids with matrix rigidity," *Biomaterials*, vol. 32, no. 35, pp. 9308–9315, 2011.
[21] S. L. Ham, R. Joshi, P. S. Thakuri, and H. Tavana, "Liquid-based three-dimensional tumor models for cancer research and drug discovery," *Exp. Biol. Med.*, vol. 241, no. 9, pp. 939–954, 2016.
[22] J. Urosevic and R. R. Gomis, "Organ-specific metastases," *Nat. Biomed. Eng.*, vol. 2, no. 6, pp. 347–348, 2018.
[23] A. M. Sitarski, H. Fairfield, C. Falank, and M. R. Reagan, "3D Tissue Engineered in Vitro Models of Cancer in Bone," *ACS Biomater. Sci. Eng.*, p. acsbiomaterials.7b00097, 2017.
[24] A. Shiirevnyamba *et al.*, "Enhancement of osteoclastogenic activity in osteolytic prostate cancer cells by physical contact with osteoblasts," *Br. J. Cancer*, vol. 104, no. 3, pp. 505–513, 2011.
[25] C. J. Logothetis and S. H. Lin, "Osteoblasts in prostate cancer metastasis to bone," *Nat. Rev. Cancer*, vol. 5, no. 1, pp. 21–28, 2005.
[26] H. Skogseth, M. Dybwad, A. Flatberg, and J. Halgunset, "Mature Bone-Producing Osteoblasts Alter Gene Expression of Metastasis Related Genes in Prostate Cancer Cells," *J. Carcinog. Mutagen.*, vol. 01, no. 03, pp. 1–7, 2010.
[27] "alamar blue." [Online]. Available: https://www.thermofisher.com/za/en/home/references/protocols/cell-and-tissue-analysis/cell-profilteration-assay-protocols/cell-viability-with-alamarblue.html.
[28] W. Van Den Bos *et al.*, "Focal therapy in prostate cancer: International multidisciplinary consensus on trial design," *Eur. Urol.*, vol. 65, no. 6, pp. 1078–1083, 2014.
[29] C. G. Jespersen, M. Nørgaard, and M. Borre, "Androgen-deprivation therapy in treatment of prostate cancer and risk of myocardial infarction and stroke: A nationwide danish population-based cohort study," *Eur. Urol.*, vol. 65, no. 4, pp. 704–709, 2014.
[30] A. cancer Society, "watchful watting or active surveillence." [Online]. Available: https://www.cancer.org/cancer/prostate-cancer/treating/watchful-waiting.html.
[31] M. a Dall'Era *et al.*, "Active surveillance for prostate cancer: a systematic review of the literature," *Eur Urol*, vol. 62, no. 6, pp. 976–983, 2012.
[32] A. cancer Society, "Surgery for prostate cancer." [Online]. Available: https://www.cancer.org/cancer/prostate-cancer/treating/surgery.html.
[33] A. cancer Society, "Radiation therapy for prostate cancer." [Online]. Available: https://www.cancer.org/cancer/prostate-cancer/treating/hormone-therapy.html.
[34] C. Rae and R. J. Mairs, "Evaluation of the radiosensitizing potency of chemotherapeutic agents in prostate cancer cells," *Int. J. Radiat. Biol.*, vol. 93, no. 2, pp. 194–203, 2017.
[35] A. cancer Society, "Cryotherapy for prostate cancer." [Online]. Available: https://www.cancer.org/cancer/prostate-cancer/treating/cryosurgery.html.
[36] "Firmagon." [Online]. Available: https://firmagon.com/.
[37] "Zytiga." [Online]. Available: https://www.zytiga.com/.
[38] "Euxelin." [Online]. Available: https://www.rxlist.com/eulexin-drug.htm.
[39] "Casodex." [Online]. Available: https://www.rxlist.com/casodex-drug.htm.
[40] "Nilandron." [Online]. Available: https://www.rxlist.com/nilandron-drug.htm.
[41] "Xtandi." [Online]. Available: https://www.xtandi.com/.
[42] "Estramustine."

[43] A. cancer Society, “Hormonal therapy for prostate cancer.”
[44] “Docetaxel.” [Online]. Available: https://www.macmillan.org.uk/cancerinformation/cancertreatment/treatmenttypes/chemotherapy/individualdrugs/docetaxel.aspx.
[45] “Jetvana.” [Online]. Available: http://www.jevtana.com/.
[46] “Novantrone.”
[47] A. cancer Society, “Chemotherapy for prostate cancer.”
[48] M. R. Carvalho, D. Lima, R. L. Reis, V. M. Correlo, and J. M. Oliveira, “Evaluating Biomaterial- and Microfluidic-Based 3D Tumor Models,” *Trends Biotechnol.*, vol. 33, no. 11, pp. 667–678, 2015.
[49] R. Akasov *et al.*, “3D in vitro co-culture models based on normal cells and tumor spheroids formed by cyclic RGD-peptide induced cell self-assembly,” *Biotechnol. Lett.*, vol. 39, no. 1, pp. 45–53, 2017.
[50] X. Cui, Y. Hartanto, and H. Zhang, “Advances in multicellular spheroids formation,” *J. R. Soc. Interface*, vol. 14, no. 127, p. 20160877, 2017.
[51] F. Pampaloni, E. G. Reynaud, and E. H. K. Stelzer, “The third dimension bridges the gap between cell culture and live tissue,” *Nat. Rev. Mol. Cell Biol.*, vol. 8, no. 10, pp. 839–845, 2007.
[52] K. S. M. SMALLEY, M. LIONI, and M. HERLYN, “Life Isn’T Flat: Taking Cancer Biology To the Next Dimension,” *Vitr. Cell. Dev. Biol. - Anim.*, vol. 42, no. 8, p. 242, 2006.
[53] T. A. Mahmood, R. De Jong, J. Riesle, R. Langer, and C. A. Van Blitterswijk, “Adhesion-mediated signal transduction in human articular chondrocytes: The influence of biomaterial chemistry and tenascin-C,” *Exp. Cell Res.*, vol. 301, no. 2, pp. 179–188, 2004.
[54] R. M. Sutherland and J. A. Mccredie, “Growth of Multicell Spheroids in Tissue Culture as a Model of Nodular Carcinomas<xref ref-type="fn" rid="FN2">2</xref>,” *JNCI J. Natl. Cancer Inst.*, pp. 113–120, 1971.
[55] R. M. Sutherland, B. Sordat, J. Bamat, H. Gabbert, B. Bourrat, and W. Mueller-Klieser, “Oxygenation and Differentiation in Multicellular Spheroids of Human Colon Carcinoma,” *Cancer Res.*, vol. 46, no. 10, pp. 5320–5329, 1986.
[56] D. Loessner, K. S. Stok, M. P. Lutolf, D. W. Hutmacher, J. A. Clements, and S. C. Rizzi, “Bioengineered 3D platform to explore cell-ECM interactions and drug resistance of epithelial ovarian cancer cells,” *Biomaterials*, vol. 31, no. 32, pp. 8494–8506, 2010.
[57] D. W. Hutmacher *et al.*, “Translating tissue engineering technology platforms into cancer research,” *J. Cell. Mol. Med.*, vol. 13, no. 8 A, pp. 1417–1427, 2009.
[58] D. R. Grimes, C. Kelly, K. Bloch, and M. Partridge, “A method for estimating the oxygen consumption rate in multicellular tumour spheroids,” *J. R. Soc. Interface*, vol. 11, no. 92, pp. 20131124–20131124, 2014.
[59] R. A. Gatenby *et al.*, “Cellular adaptations to hypoxia and acidosis during somatic evolution of breast cancer,” *Br. J. Cancer*, vol. 97, no. 5, pp. 646–653, 2007.
[60] N. Kazmi, M. A. Hossain, R. M. Phillips, M. A. Al-Mamun, and R. Bass, “Avascular tumour growth dynamics and the constraints of protein binding for drug transportation,” *J. Theor. Biol.*, vol. 313, pp. 142–152, 2012.
[61] O. Trédan, C. M. Galmarini, K. Patel, and I. F. Tannock, “Drug resistance and the solid tumor microenvironment,” *J. Natl. Cancer Inst.*, vol. 99, no. 19, pp. 1441–1454, 2007.

[62] P. Orlandi *et al.*, "Idarubicin and idarubicinol effects on breast cancer multicellular spheroids.," *J. Chemother.*, vol. 17, no. 6, pp. 663–667, 2005.
[63] F. Ruedinger, A. Lavrentieva, C. Blume, I. Pepelanova, and T. Scheper, "Hydrogels for 3D mammalian cell culture: a starting guide for laboratory practice," *Appl. Microbiol. Biotechnol.*, vol. 99, no. 2, pp. 623–636, 2014.
[64] M. Rimann and U. Graf-Hausner, "Synthetic 3D multicellular systems for drug development," *Curr. Opin. Biotechnol.*, vol. 23, no. 5, pp. 803–809, 2012.
[65] Y. Peck and D.-A. Wang, "Three-dimensionally engineered biomimetic tissue models for *in vitro* drug evaluation: delivery, efficacy and toxicity," *Expert Opin. Drug Deliv.*, vol. 10, no. 3, pp. 369–383, 2013.
[66] J. F. Mano, "Designing biomaterials for tissue engineering based on the deconstruction of the native cellular environment," *Mater. Lett.*, vol. 141, pp. 198–202, 2015.
[67] P. K. Chaudhuri, B. C. Low, and C. T. Lim, "Mechanobiology of Tumor Growth," *Chem. Rev.*, vol. 118, no. 14, pp. 6499–6515, 2018.
[68] E. O. Mosaad, K. F. Chambers, K. Futrega, J. A. Clements, and M. R. Doran, "The Microwell-mesh: A high-throughput 3D prostate cancer spheroid and drug-testing platform," *Sci. Rep.*, vol. 8, no. 1, pp. 1–12, 2018.
[69] L. A. Gurski, A. K. Jha, C. Zhang, X. Jia, and M. C. Farach-Carson, "Hyaluronic acid-based hydrogels as 3D matrices for in vitro evaluation of chemotherapeutic drugs using poorly adherent prostate cancer cells," *Biomaterials*, vol. 30, no. 30, pp. 6076–6085, 2009.
[70] Y.-C. Lu *et al.*, "Designing compartmentalized hydrogel microparticles for cell encapsulation and scalable 3D cell culture," *J. Mater. Chem. B*, vol. 3, no. 3, pp. 353–360, 2015.
[71] A. Shablak, R. E. Hawkins, D. G. Rothwell, and E. Elkord, "T cell-based immunotherapy of metastatic renal cell carcinoma: Modest success and future perspective," *Clin. Cancer Res.*, vol. 15, no. 21, pp. 6503–6510, 2009.
[72] S. Valastyan and R. A. Weinberg, "Tumor metastasis: Molecular insights and evolving paradigms," *Cell*, vol. 147, no. 2, pp. 275–292, 2011.
[73] I. K. Zervantonakis, S. K. Hughes-Alford, J. L. Charest, J. S. Condeelis, F. B. Gertler, and R. D. Kamm, "Three-dimensional microfluidic model for tumor cell intravasation and endothelial barrier function," *Proc. Natl. Acad. Sci.*, vol. 109, no. 34, pp. 13515–13520, 2012.
[74] S. Bersini *et al.*, "A microfluidic 3D invitro model for specificity of breast cancer metastasis to bone," *Biomaterials*, vol. 35, no. 8, pp. 2454–2461, 2014.
[75] S. Sieh, A. A. Lubik, J. A. Clements, C. C. Nelson, and D. W. Hutmacher, "Interactions between human osteoblasts and prostate cancer cells in a novel 3D in vitro model," *Organogenesis*, vol. 6, no. 3, pp. 181–188, 2010.
[76] K. A. Fitzgerald *et al.*, "The use of collagen-based scaffolds to simulate prostate cancer bone metastases with potential for evaluating delivery of nanoparticulate gene therapeutics," *Biomaterials*, vol. 66, pp. 53–66, 2015.

1.5. Hydrophobized Platforms for Spheroidal 3D *In vitro* Tumor Models Assembly – Advances and Prospects

Subchapter 1.5.

This subchapter is based on the mini-review entitled

"Hydrophobized Platforms for Spheroidal 3D *In vitro* Tumor Models Assembly *Platforms – Advances and Prospects"*

Manuscript in preparation

Hydrophobized Platforms for Spheroidal 3D *In vitro* Tumor Models Assembly – Advances and Prospects

Jéssica Antunes, Vítor M. Gaspar[#], João F. Mano[#]

Department of Chemistry, CICECO, University of Aveiro, Campus Universitário de Santiago, 3810-193, Aveiro, Portugal

[#]Corresponding authors:
Professor Dr. João F. Mano
Department of Chemistry, CICECO – Aveiro Institute of Materials
University of Aveiro, Campus Universitário de Santiago
3810-193, Aveiro, Portugal
E-mail: jmano@ua.pt
Telephone: +351 234370733

Dr. Vítor Gaspar
Department of Chemistry, CICECO – Aveiro Institute of Materials
University of Aveiro, Campus Universitário de Santiago
3810-193, Aveiro, Portugal
E-mail: vm.gaspar@ua.pt
Telephone: +351 234370733

Abstract

The development of hydrophobized platforms to buildup tailored 3D multicellular *in vitro* microtumors for therapeutics preclinical screening is currently gaining a remarkable momentum. Such focus is related to the unique water and protein repellent properties of hydrophobic surfaces which rapidly promote cells self-assembly into dense 3D heterotypic agglomerates that recapitulate major hallmarks of solid tumors *in vitro*. Considering this, herein we showcase the recent technological advances on precision engineered hydrophobized surfaces and discuss their use for establishing reproducible 3D microphisiological tumor models with potential for rapid scalability toward high-throughput/high-content imaging platforms. In addition, an in dept overview of disruptive studies employing static multi-array surfaces or dynamic non-wettable microfluidic chips for 3D multicellular spheroids fabrication and preclinical anti-cancer therapeutics screening is provided and critically discussed considering envisioned future advances.

Keywords: 3D *in vitro* tumor models; Anti-cancer Therapies, Hydrophobized surfaces; Microphysiological systems; Therapeutics Screening.

1. Introduction

Presently 2D flat cell culture *in vitro* testing platforms are increasingly recognized as simplistic preclinical models due to their unnatural culture environment when compared to the *in vivo* setting they aim to mimic. This disadvantage is particularly evident in the area of cancer *in vitro* modeling since 2D cell monolayers are utterly unable to recapitulate key cell-cell and cell-tumor extracellular matrix (ECM) interactions. Moreover, 2D flat cultures do not reproduce malignant cells gene expression patterns, nor mimic the complex 3D compact architectures of *in vivo* solid human tumors [2], [3], [8]–[10]. To bridge this gap, in the last decade *in vitro* 3D culture models have been developed as valuable microphysiological models of human tumors [11]–[13].

Up-to-date various types of 3D assemblies have been reported including 3D multicellular tumor spheroids, cancer cell laden tumor-ECM like hydrogels, or tumor organoids [1]. Among these, multicellular 3D spheroids (3D MCTS) have received a particular focus as *in vitro* malignant microtissues due to their ease of self-assembly, cost effectiveness, controllable morphology and potential to be used as large scale high-throughput/high-content imaging models. Multicellular spheroids generally display a spherical morphology and have been widely used for recapitulating the cancer microenvironment of solid tumors due to their highly compact structure. Due to their density 3D MCTS represent better *in vitro* the cellular heterogeneity, spatial distribution, gene expression patterns and also nutrient, oxygen and pH gradients of solid human tumors in comparison to their 2D and 3D hydrogel counterparts [2], [3], [14]. The establishment of such gradients leads to the formation of multiple milieus within the microtumor mass including: (i) an outer layer of highly proliferative cells, (ii) an intermediate layer comprised of quiescent cells, and (iii) an hypoxic and acidic necrotic core, similar to that found in human solid tumors [15]–[17]. There is also a growing body of evidence that cells within 3D spheroids volume produce extracellular matrix (ECM) constituents such as collagen I/IV, laminin and fibronectin, key components of tumors ECM that ultimately play a role in cell proliferation and resistance to chemo- or radiotherapeutics [18], [19]. Since spheroids are able to recapitulate these tumor hallmarks, the overall drug response rates provide a more realistic *in vitro/in vivo* correlation with human tumors when compared to their 2D monolayer counterparts [5], [20]. Owing to this noteworthy potential, there is currently a high demand from pharmaceutical companies for multicellular 3D spheroids testing

platforms production through scalable and robust methodologies that can assure the highest rate of microtumor-to-microtumor reproducibility and *in vivo* mimicry.

To date, various methodologies have been developed for the production of monotypic or heterotypic 3D spheroids, mainly through the use of: (i) centrifugal pelleting apparatus, (ii) spinner flasks gyratory rotation systems/rotating wall vessels that promote cells aggregation, (iii) hydrophobized multi-well/multi-array non-adhesive substrates, (iv) on-chip hydrophobized microfluidic platforms, (v) porous 3D synthetic polymer scaffolds and 3D synthetic/natural-origin hydrogels, as well as (vii) external force cell agglomeration systems (electric, acoustic, or magnetic), [3], [21]–[23]. Conventional methods for producing 3D tumor spheroids have however various disadvantages such as the formation of aggregates with irregular shapes and sizes, the inability to be used for high throughput drug screening (HTS) [3], have low yields and are time consuming. On the other hand hydrophobized surfaces have shown potential to overcome most of these limitations [17], [21], [24].

Hydrophobized platforms for 3D *in vitro* tumor spheroids assembly can be classified in: (i) static (e.g., non-adherent surfaces) or (ii) dynamic flow multi-arrays (e.g., lab-on-a-chip microfluidics). These two classes represent the most cost-effective hydrophobic technologies to rapidly generate a significant number of 3D multicellular tumor spheroids. Such production and testing platforms allow to establish heterotypic multicellular co-cultures of various cell lines (e.g., normal or malignant) or patient-specific tumor explants, offer the possibility to obtain a reproducible spherical morphology and to fabricate size tailored 3D microtumors via precise control over key parameters (e.g., droplet size, flow rate, cell number, etc.) [21], [25]. Moreover, these platforms may allow the simultaneous production of 3D microtumors and evaluation of new drug candidates anti-cancer performance in the same spot/compartment.

Considering the relevance of this technology for 3D tumor *in vitro* microphisiological models' generation, this review offers an overview of hydrophobized surfaces manufacturing techniques and provides an up-to-date exhibit of impactful studies that employ this technology both for 3D tumor spheroids production and for expedite drug screening. It is envisioned that the widespread use of cost-effective hydrophobized surfaces will accelerate the development of more *in vivo*-like 3D tumor spheroids.

2. Hydrophobized Platforms Design and Manufacturing

To date the development of hydrophobized surfaces has been highly inspired by nature, for example through the mimicry of lotus leaf and rose petal surfaces which repel water by entraining particles. Currently the manipulation of surfaces water-response properties can be easily achieved through chemical modification but the advancement of lithographic techniques for patterned controlled surface functionalization is one of the most important factors that contributed for the widespread development of surfaces with extreme wettability (super-hydrophobic) and low surface energy. In fact, hydrophobicity is generally a consequence of both surface chemistry and the presence of a unique hierarchic topography comprised of nano to micro organization, both of which are crucial for the development of anti-corrosive coatings, in the prevention of bacterial surface spreading, and also for the fabrication of tailored biomaterial-based scaffolds and microgels/microcapsules [1], [3], [26]–[29].

Inspired by natural structures, Barthlott and Neinhuis studied thousands of lotus leaves and concluded that leaf's hydrophobicity was attributed to the existence of micrometric papillae (5-9 mm in diameter) on rough surfaces and wax, showing that the orientation, shape, density, size and roughness, influence surfaces hydrophobicity. These studies indicate that a rough structure is not only a crucial factor in achieving wettability but is also closely related to water bonding properties [30]. Overall, several studies indicate that both chemical composition and appropriate surface topography are fundamental for obtaining water-repellent behavior on diverse surfaces [31], [32]. In addition, surface properties are also important in various biomedical applications because they utterly define biomaterials biological performance *in vivo* as well as the efficiency of the material to interact with cells and proteins. The type of biomaterials-cells interactions that are established depends on various surface properties, such as wettability, topography and roughness, surface loading and chemical [27], [33]. In addition to solid-liquid interactions, icephobicity, low protein adsorption and anti-bacterial properties on hydrophobized and super-hydrophobic surfaces have been investigated and demonstrated [31].

The mechanism of water repulsion begins when a drop of water is delivered to the surface, at this time the liquid-solid interface tends to reach an equilibrium configuration with a characteristic angle called the static contact angle (CA). Depending on the value of

this angle, the surfaces are considered hydrophobic or hydrophilic. For angles between $0 \leq \theta \leq 90°$ the surface is considered hydrophilic, whereas for angles between $90° \leq \theta \leq 150°$ the surfaces are considered hydrophobic, as shown in Figure 1, and may promote cells self-agglomeration into a 3D tumor microtissue. Moreover, surfaces with angles greater than 150° are considered super-hydrophobic [26]. By definition, super-hydrophobic surfaces must have two requirements: 1) a contact angle (AC) greater than 150°, i.e., the liquid is totally repelled by the solid surface; 2) the liquid has low adhesion to the solid substrate and therefore can be released spontaneously [34]–[37]. The second characteristic is related to the very low contact angle hysteresis (CAH), which is the difference between the advancing and receding CAs [37], as can be seen in Figure 1F. Normally CAH of super-hydrophobic surfaces is less than 10° [38].

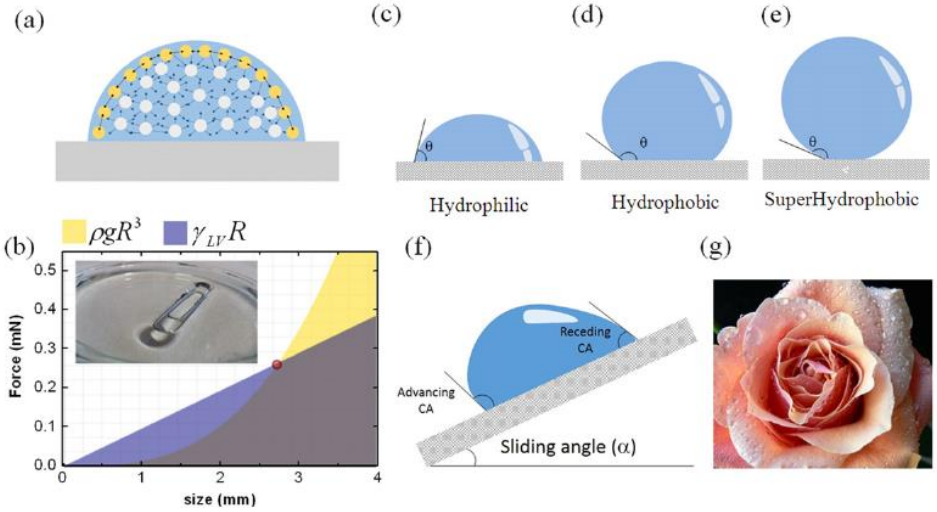

Figure 1. (a) Schematics of the interactions between neighboring atoms in a water droplet resting on an ideal flat surface (figure not drawn to scale). (b) Surface tension plotted against gravity for a water droplet on earth. The red spot indicates the crossover between the gravitational-driven and the surface-driven regime. This crossover gives rise to many counterintuitive phenomena, such as paperclip floating (inset). Schematic drawings of a droplet resting on (c) a hydrophilic flat surface, (d) a hydrophobic surface and (e) a super-hydrophobic surface. (f) Schematic representation of the advancing and receding angles. (g) Photograph of a rose: sticky droplets can be observed on the rose petals. Adapted from [26].

The contact angle can be generally determined by the measurement of the tangential angle of the liquid-vapor interface at the three-phase limit (Figure 2). On a smooth surface, the contact angle is generally described by the Young equation:

$\text{Cos}(\theta) = \frac{\gamma SV - \gamma SL}{\gamma LV}$, where γSV relates to the interfacial tension between liquid and vapor, γSL is the interfacial tension between solid and liquid, and γLV is the interfacial tension between solid and vapor [38].

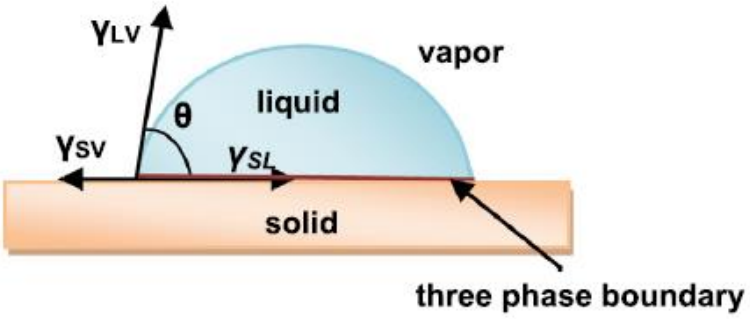

Figure 2. Diagram showing the forces at the three-phase contact line of a liquid droplet on a solid. Adapted from [38].

While hydrophobic surfaces found in nature (e.g., on plant leaves or insect wings) [28], [35] do not change throughout their useful life, due to their continuous regeneration, artificial hydrophobized surfaces degrade over time [35]. The hydrophobicity of these surfaces changes essentially due to two factors: (i) the mechanical wear or loss of roughness, increases water-surface contact, and (ii) the contamination or degradation of the hydrophobic surface coating [35].

Hydrophobized and super-hydrophobic surfaces have numerous biomedical applications (Figure 3), having been used for the fabrication of cell laden hydrogels that serve as cell deliver platforms [39], for biosensing applications [40], to study bioactive molecules release profile [39], or to function as detection/capture systems for rare cells such as tumor circulating cells [21].

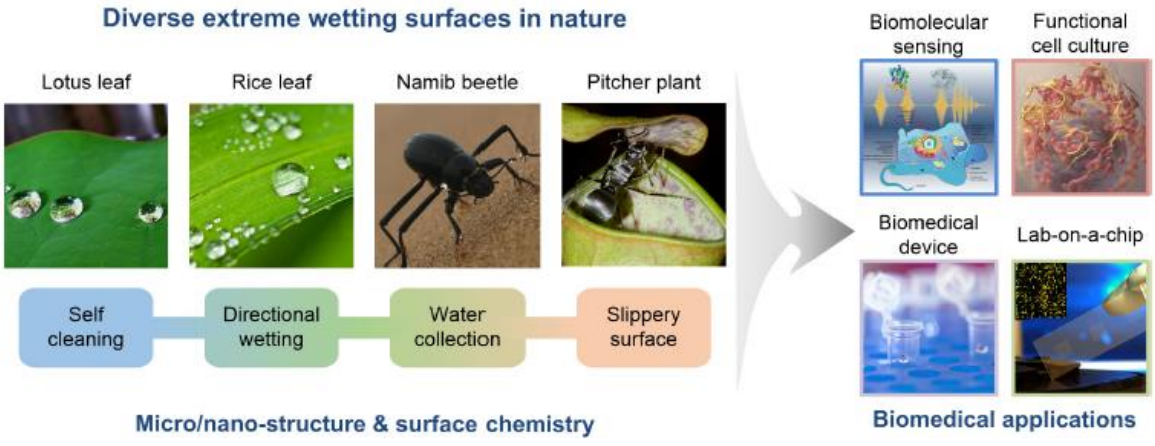

Figure 3. Various natural extreme wetting surfaces and their potential biomedical applications. Lotus leaf (image by Tanakawho, reproduced under Creative Commons Attribution (CC BY) license); Namib beetle (image by James Anderson, reproduced under Creative Commons Attribution Non-commercial Share-alike (CC BY-NC-SA) license); Pitcher plant (image by Bauer, reproduced under CC BY); Biomedical device (image from the School of Natural Resources & Environment, University of Michigan, reproduced under CC BY license); Lab-on-a-chip (image from Argonne National Laboratory, reproduced under CC BY-NC-SA license); and others (public domain photo and images). Adapted from [28].

In addition to the former applications, hydrophobized surfaces have also been recently employed for the generation of *in vitro* 3D microtumor tissues and as drug screening (HTS)/high content imaging (HCI) platforms. [1], [5], [21], [26], [34], [41], [42].

Hydrophobized surfaces may be engineered as static multi-array platforms with micropatterned spots (e.g., via lithographic patterning), or as chemically hydrophobized microchannels included in lab-on-a-chip microfluidic devices (Figure 4). Both these systems have been used for fabrication of tumor-ECM mimicking biomaterial scaffolds and for creating spheroidal microtissues under highly reproducible and scalable experimental settings.

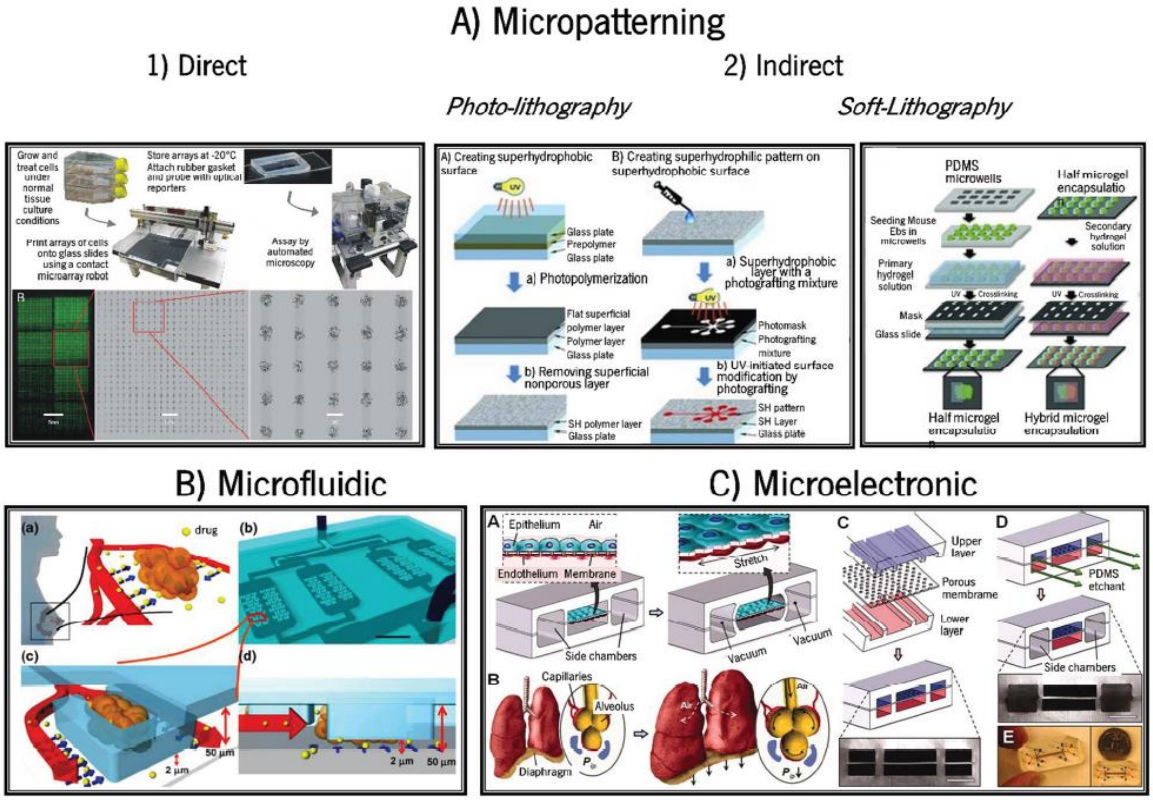

Figure 4. Examples of current microfabrication approaches to process supports for large scale 3D tumor spheroids production. A) Micropatterning approaches are based on direct (A1) or indirect photocuring technologies (A2). By using a direct surface depositing technology based on robotic microarray spotting device (A1), cells are printed onto streptavidin slides, to obtain high-density cellular arrays. Using an indirect technology based, Super-hydrophobic porous polymer films on a glass can be produced by UV-initiated photolithography. Individual embryo bodies were successively encapsulated in PEG and GelMA microgel by photolithography. B) Microfluidic technology was used to generate spheroid culture array: the spheroid culture chamber was formed by bonding the PDMS device to a glass slide. In each chamber, there are U-shape traps arrayed in the density of 7,500 traps per square centimeter. C) Using microelectronic approaches, a human breathing lung-on-a-chip microdevice was developed. The micro-fabricated lung mimic device uses microchannels coated with PDMS membrane and ECM to form an alveolar-capillary barrier, recreating physiological breathing movements by applying vacuum to the side chambers. Adapted from [1].

2.1. Static Hydrophobized Platforms

In comparison to standard 2D monolayer cultures and other dynamic 3D cell culture platforms (e.g., magnetic or microgravitational agitation-based systems), hydrophobized surfaces for 3D tumor spheroids high throughput manufacture and drug screening has several advantages including the higher reproducibility and control over cell number and 3D spheroids size/morphology, their ease of manufacture, cost-effectiveness, as well as the absence of mechanical forces for promoting cells assembly (e.g., *via* forced floating, hanging drop-based methods). Static hydrophobized surfaces can be engineered for 3D spheroids assembly as: (i) non-patterned systems (standard hydrophobized surfaces and non-adherent cell culture plates), (ii) as multi-array patterned hydrophobic/super-hydrophobic platforms [3] and (iii) as hydrophobic/super-hydrophobic – hydrophilic micropatterned platforms [43].

In a recent study, Salgado and co-workers used the lithographic method, more precisely photolithography, to produce a static super-hydrophobic substrate for establishing 3D *in vitro* microtissues. In particular, UV / ozone radiation was used to obtain patterned hydrophilic regions in a hydrophobic polystyrene substrate via a photomask. The engineered platform was then employed to evaluate the effect of different alginate combinations with various natural biopolymers (Chitosan, Collagen, Hyaluronic acid and Gelatin), and their outcome in cells bioactivity upon entrapment in the combinatory hydrogels' matrix (L929 fibroblasts and MC3T3-E1 pre-osteoblast cells). The different biomaterial-cell combinations were achieved with the aid of a digital micropipette, that deposited 1 μL sample volumes in the hydrophilic regions [44]. The authors then performed destructive and non-destructive assays to evaluate cell viability (Figure 5). Overall, the results showed that this methodology allows not only the rapid establishment of 3D microtissues laden in ECM mimicking components, but also permitted a rapid and non-destructive on-chip analysis of ECM-like materials cytotoxicity [44].

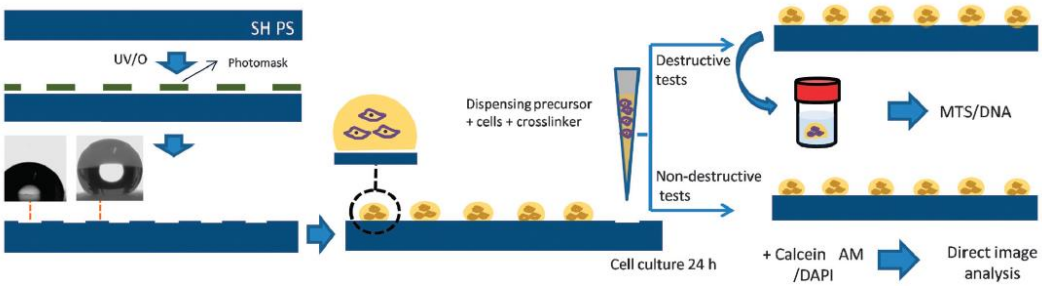

Figure 5. Schematic representation of the process used to create hydrophilic spots in the initially superhydrophobic substrate using a hollow mask to imprint wet table spots by the action of UV irradiation. Images of the contours of water droplets in the original (super-hydrophobic) and surface modified (hydrophilic) substrates are included. The characterization of each construct can be carried out by individual destructive tests or using colorimetric/image analysis during which cell-laden biomaterials maintain in the chip. Adapted from [44].

This example evidences the versatility of static micropatterned platforms in the sense that they can be employed both for rapid generation of scaffold-free, or scaffold-based 3D microtissues, and simultaneously for on-spot recovery/downstream analysis of the formed microphysiological models. Despite these benefits, the use of microfluidic chips further simplifies liquid handling procedures by offering "in-line" micro-compartmentalization and mass fabrication of 3D microsystems (> 1000 droplets/min) [17]. The following chapter will focus on these dynamic platforms.

2.2. Dynamic Flow Hydrophobized Microfluidic Chips

Current developments in microfluidics and microarray-like platforms decrease 3D microtumors cost and increase the amount of simultaneously generated 3D models in a high throughput mode. Moreover, microfluidic platforms can be used for high content imaging generally offering the possibility to generate and analyze 3D tumor models in the same platform [28], [38], [45] and also with the possibility of producing complex spherical particles with controllable sizes and shapes [1], [24], [27], [39], [46].

In addition to these features, hydrophobized microfluidic platforms can be used to process spheroidal 3D tumor models that are comprised not only by cancer cells but also by tumor ECM-mimicking biomaterials (e.g., Gelatin, collagen, Matrigel, etc.). Despite these being relevant advantages, the most important chip microfluidics feature is their ability to modulate the dynamic physiological cancer microenvironments concerning 3D flow conditions (e.g., shear stress, nutrient gradients) and to offer the possibility to evaluate cell movement and metastasis under flow [47].

Due to significant advances in microfluidics engineering techniques obtained in the past decade, currently microfluidic chips can be fabricated with numerous microchannels and compartment designs that are valuable for 3D multicellular spheroids manufacture and for high throughput drug screening. To date various chemical approaches have been used to hydrophobize microfluidic chips, either those comprised by elastomers (e.g., PDMS) or by other types of materials (e.g., Quartz, Dolomite®). The most common hydrophobization methodology involves the use of Aquapel™ (PPG industries, USA), with some studies reporting the posterior use of albumin coatin to prevent on-chip cell adhesion to microchannels [17]. Microfluidic channels hydrophobization for development of droplet-based microfluidics is particularly valuable since a large number of cells can be rapidly compartmentalized in each drop, that will lead to the formation of a 3D spheroid, as recently demonstrated by Kwak and co-workers [17].

In the following chapters pertinent examples using this and other technologies for 3D spheroids generation and drug screening in hydrophobized platforms are presented and discussed in light of their advantages and envisioned improvements.

3. 3D microtumors assembly in Patterned hydrophobized static surfaces

The assembly of 3D tumor models in cell-repellent surfaces has been receiving a significant focus and various 3D cell culture platforms currently being marketed take advantage of this approach. One such example of commercially available plates for researchers to establish 3D cell cultures in hydrophobic surfaces are round-bottom, ultra-low adhesion (Corning® ULA) and cell-repellent (Greiner Bio-one® CELLSTAR®) 96/384 well culture plates that have been shown to promote the establishment of spherically-shaped and reproducible 3D tumor spheroids [48]. Although these present interesting characteristics, the plates are highly expensive. In this context, our group has previously described the development of a biomimetic super-hydrophobic polystyrene (PS) surface with a unique topographic roughness at the micro/nanoscale and microindentations where quasi-spherical liquid droplets were deposited and self-fixed (Figure 6a). Droplets stability and adhesion to the patterned surface allowed the inversion of the platform by 180° and 3D cell clusters generation *via* the hanging drop method (Figure 6a). This device was used both as a micro-

reactor to evaluate 3D spheroids growth and as a platform for drug screening. In this context, cytotoxicity tests using Doxorubicin as anti-cancer model drug were performed in mouse fibroblasts (L929) and the obtained results demonstrated a direct dose/cytotoxicity correlation. Moreover, the platforms were also employed to study more fundamental 3D spheroid properties such as necrotic core formation and establishment of acidic pH conditions in spheroids volume, an important aspect of solid tumors as previously discussed [45].

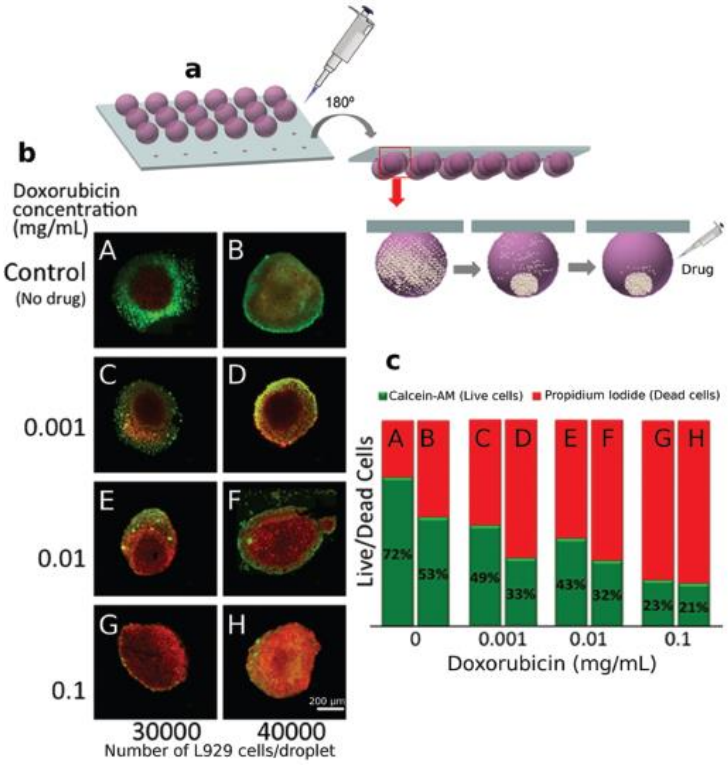

Figure 6. Manufacture of patterned super-hydrophobic surface for establishing self-aggregated 3D *in vitro* tumor models. a) Scheme of patterned super-hydrophobic surfaces with micro-indentations able to suspend arrays of droplets containing cells after upon 24 h spheroids are formed, and drug-screening tests may be performed on the individual droplets. b) Confocal laser scanning imaging of L929 3D spheroids obtained 24 h following the administration of different Doxorubicin doses. c) Percentage of live (green)/dead (red) cells per spot in the different conditions tested. Adapted from [45].

In a follow up study, our group also manufactured alginate hydrogels for cells encapsulation using the discontinuous dewetting effect in an SH-SL (microarray superhydrophobic (SH) and super-hydrophilic (SL)) combined with the sandwich method to obtain simultaneous droplets generation/gelation. In a first step, we produced alginate droplets with HeLa cells (Human cervical tumor cells) on the SH slide, and $CaCl_2$ droplets were then dispensed in the SL slide. The precise junction of the two slides allowed the formation of calcium crosslinked alginate hydrogels. Figure 7 shows the entire

manufacturing process, from obtaining the slides to the production of hydrogels and fluorescence microscopy images of the cellular encapsulation [43].

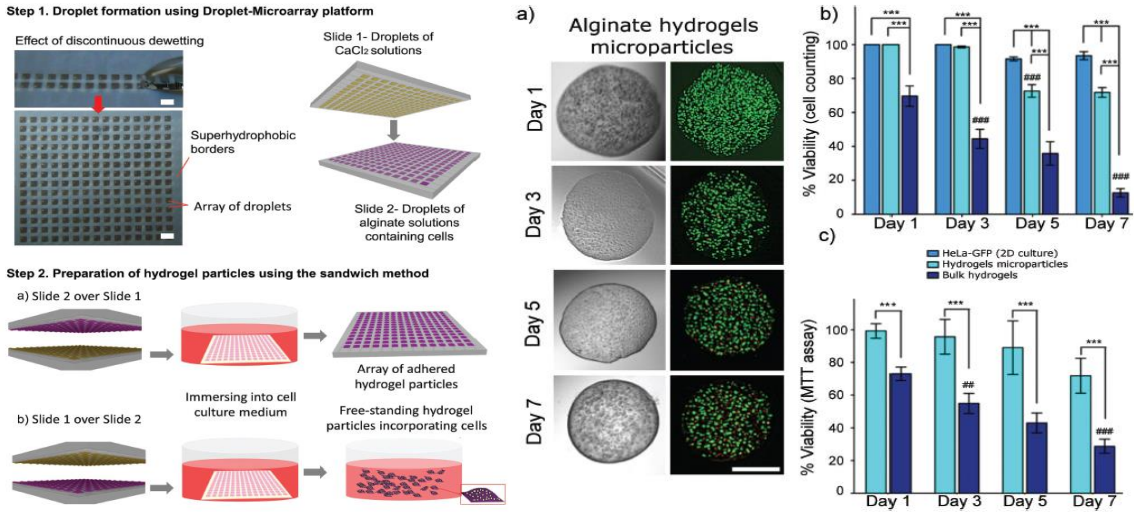

Figure 7. Schematic representation of the droplet microarray platform and workflow for the high-throughput fabrication of hydrogel particles via the sandwiching method. *Step 1:* Formation of an array of droplets of a hydrogel precursor on a super-hydrophobic/super-hydrophilic array. *Step 2:* Crosslinking of alginate droplets by parallel addition of $CaCl_2$ solutions into the individual droplets *via* the sandwiching method. By changing the position of $CaCl_2$ containing droplets of slide 1 (bottom vs top), it is possible to form either an array of fixed hydrogel particles (Step 2a) or to detach hydrogel particles to form free-floating hydrogel particles (Step 2b). Scale bar: 2 mm. a) Representative brightfield and corresponding fluorescence images of free-standing hydrogels encapsulating HeLa-GFP cells for up to 7 d of culturing time. Dead cells are visualized using PI staining. Scale bar: 1 mm. b) Percentage of live cells obtained using image-based analysis and c) MTT colorimetric assay. Statistical differences by time point analysis were marked with (*), (**), (***), which stand for *p*-values < 0.05; $p < 0.01$; $p < 0.001$, respectively. Statistical differences related to the previous time points are indicated by ## ($p < 0.01$) or ### ($p < 0.001$). Adapted from [43].

As the results demonstrate, this approach led to the rapid formation of 3D spherical alginate cellular aggregates that showed higher cell viability at day 7 when compared to their bulk hydrogel counterparts. Interestingly, this sandwich-like technology made possible to either maintain the 3D spherical microtumor tissues on the chip, or to retrieve them immediately for further downstream processing and drug screening (Figure 7, left panel). This is a major advantage when compared to 3D spheroids manufactured in compartmentalized microfluidic recesses since key downstream analysis techniques such as gene expression and histomorphological analysis require the extraction and processing of the formed microtissue.

In line with this approach, Li and co-workers employed indirect ice-based soft-lithography (Figure 8A) to develop quasi-spherical microwells for breast cancer (MCF-7) 3D spheroids generation. For this purpose, initially water droplets were deposited on template

superhydrophobic PDMS surfaces with different water contact angle (Figure 8B) and frozen. By manipulating the initial water volume and by tailoring the superhydrophobicity of the PDMS substrate the researchers were able to control the morphology and dimensions of the formed microwells [49]. The phenotypic and morphological changes associated with 3D spheroids epithelial to mesenchymal transition (EMT) were then compared with their 2D culture counterparts by visualization of key mesenchymal markers, such as E-cadherin, vimentin and cytokeratin (Figure 8C, D and E). A direct comparison of 2D vs 3D cultures showed no alteration in cytokeratin or vimentin markers, however in the 3D spheroids there was an emergence of heterogeneous populations with decreased E-cadherin expression [49], a known EMT biomarker that is also involved in the process of metastization.

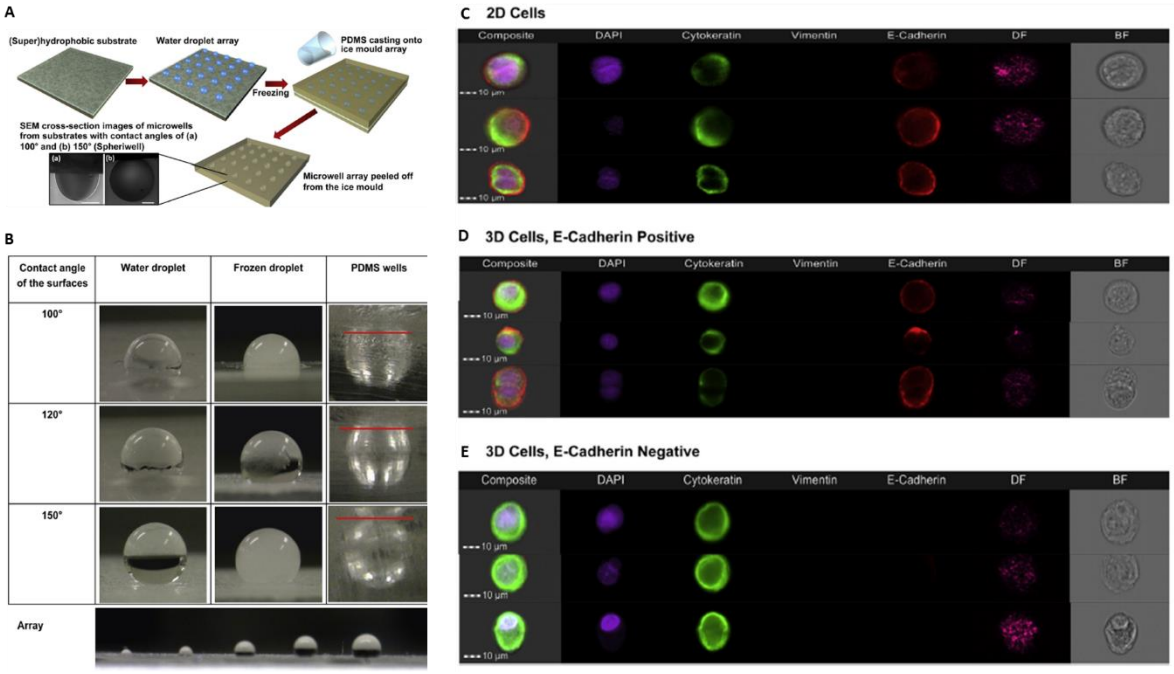

Figure 8. (A) Schematic representation of the fabrication of concave microwells by ice lithography. Water droplets were printed on (super-hydrophobic substrates then frozen and used as molds to prepare the microwells. Microwells prepared from superhydrophobic substrates have a quasi-spherical shape (spheriwells) which entrap multicellular spheroids once formed. (B) Photographs of water droplets, ice molds and the resulting PDMS microwells obtained using substrates with different hydrophobicity. The shape of the droplets as defined by the hydrophobicity of the substrate is maintained. Water droplets of various volumes can be easily printed with good spatial resolution using a non-contact spotting system. (C, D and E) Images of individual cells and their fluorescence profile (left to right) from imaging flow cytometry. As labelled left to right the composite image (incorporates a bright-field, cytokeratin, vimentin, E-cadherin and DAPI image), DAPI, Cytokeratin, Vimentin, E-cadherin, Dark-field (DF) and Bright-field (BF). C: Immunostained MCF-7 cells grown in 2D monolayers. D and E: Immunostained cells from dissociated Spheroids grown in spheriwells with (D) and without E-cadherin expression (E).Adapted from [49].

In order to complete the study, the team tested 2D and 3D cultures with different concentrations of a model anti-cancer drug, Paclitaxel. The obtained IC50 for 2D monolayer models was 3 μM , whereas the IC 50 of the MCF-7 cells cultured in a 3D environment was significantly higher, 297 μM [49]. The results obtained are in accordance with several studies published in the literature because as expected, cells in 3D environments are more resistant to drugs than those cultured as 2D flat monolayers. Since cells in living organisms are in a three-dimensional arrangement, it makes sense that drug screening is performed under these conditions, otherwise a poor *in vitro/in vivo* correlation is obtained.

In addition, our group recently reported the development of a micropatterned super-hydrophobic polystyrene platform with hydrophilic regions (SH-SL) where heterotypic cultures of fibroblasts (L929) and osteosarcoma (SaOs-2) cells were established (Figure 9. Similar to past studies by simple 180° plate inversion heterotypic 3D were assembled by the hanging drop technique. After the formation of 3D cell spheroids, we evaluated the effect of Doxorubicin on co-culture models [4].

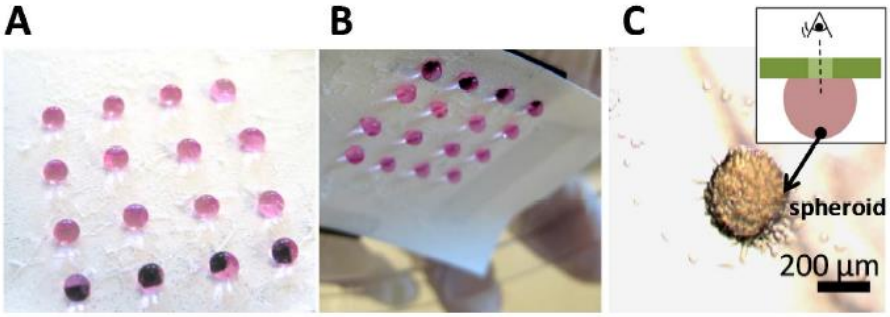

Figure 9. Micrographs of superhydrophobic platfors with the cell suspensions turned (A) upside and (B) tilted down. (C) Transmitted light microscopy micrograf of a heterotypic 3D tumors spheroid, observed from the top of the chip, through the transparent spot (as indicated in the schematic representation). Adapted from [4].

Even with a 106-fold higher concentration of Doxorubicin, L929 cells died less than SaOs-2 cells (Figure 10). In both types of cells, spheroids with higher cell density presented lower viability, a factor that can be explained by the fact that, in general, the larger the number of cells, the larger the cell aggregates and, consequently, the greater the compaction of the spheroid and therefore, the diffusion of oxygen and nutrients to the center of the cellular mass will be more difficult [4]. This platform has proved to be quite versatile, and it is possible to work with many cell varieties, drug solutions and stainings.

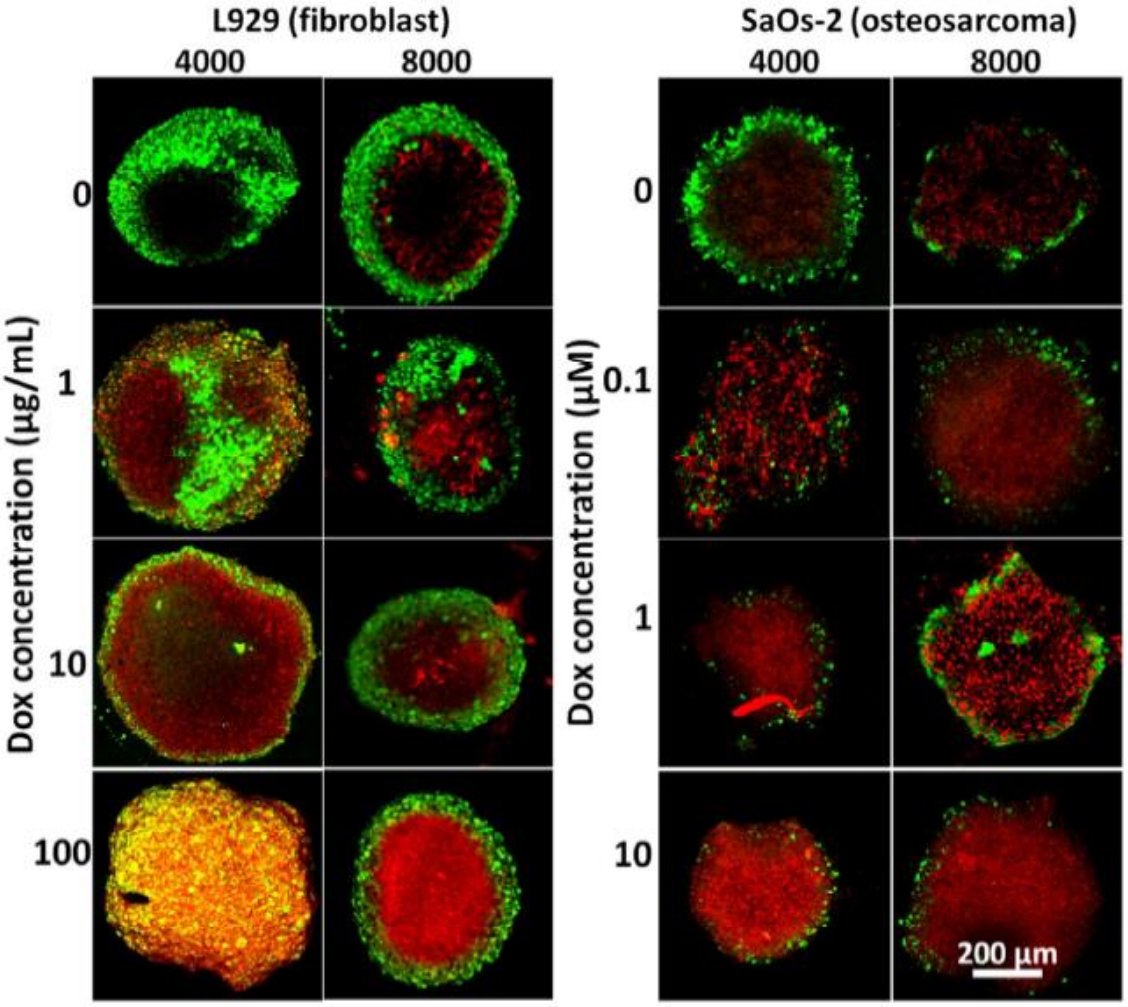

Figure 10. Confocal microscopy assembled images of the cell spheroids formed by L929 and SaOs-2 cells, with live (green)/dead (red) staining (calcein AM/propidium iodide). Adapted from [4].

3.1 Hydrophobized platforms for Heterotypic 3D Co-culture Tumor Models

As previously demonstrated, there is a significant body of studies that employ super-hydrophobic or hydrophobized substrates for 3D models' assembly, however, their majority involves only the establishment of monotypic (one cell type) 3D microtumors. Such models are therefore a simplistic reproduction of the complex tumor microenvironment and of its heterogenic cellular components. Spherical co-culture models are considered very important to increase the knowledge of cancer biology and the development and discovery of novel anti-cancer drugs. For example, studying the interactions between different cells can be applied in cell-based anti-cancer immunotherapies [21].

In this context, Michael and co-workers recently described the use of paper for tumor models assembly [50]. Paper has widely explored in the biomedical, electronic and chemical industries, and has even been used for manufacture of point-of-care diagnostic platforms. In this particular study researchers used BSA to form a protein corona on normal paper and then used hydrophilic cellulose fibers become hydrophobic when exposed to UV light, as shown in Figure 11. Then breast cancer (MCF-7) and CCD 1058Sk breast skin fibroblasts were used to produce 3D heterotypic tumor spheroids via the hanging drop technique. In addition the authors manufactured micropatterned paper spots with different channel width to mimic the different diameter of blood vessels surrounding the main tumor (Figure 11C). The model anti-cancer drug 5-Fluoroacil (2000 μM) was then administered on these spots [50].

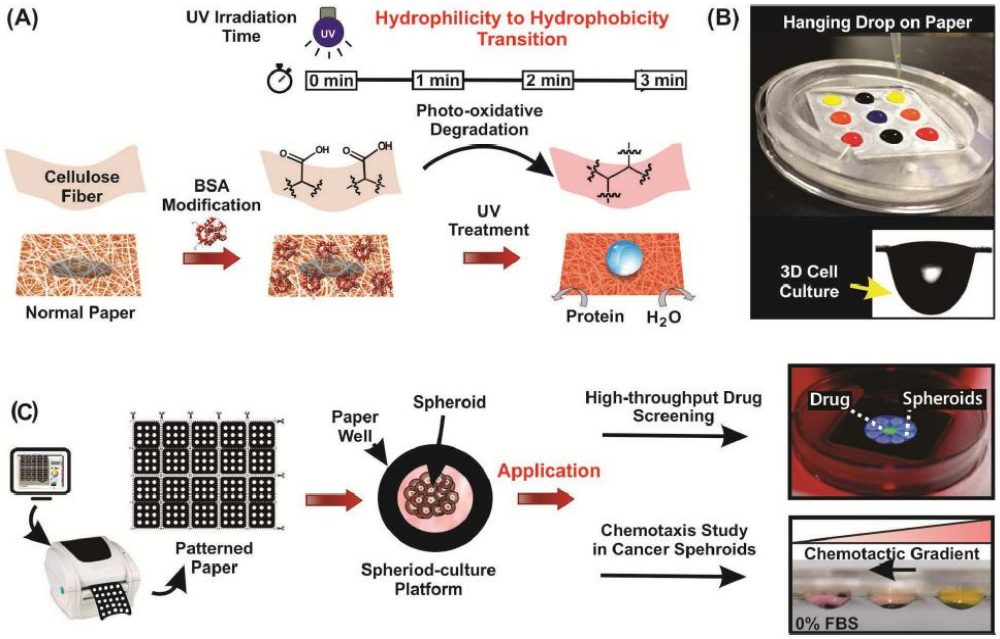

Figure 11. Chemical modification of paper sheets to be used for assembly of heterotypic *in vitro* 3D tumor models. (A) Schematic representation of transition of hydrophilic paper to hydrophobic by photo-oxidative degeneration of protein corona coated cellulose fiber. (B) Restriction of fluid flow across porous paper after surface modification and its application in hanging drop 3D cell culture. (C) Sequence of steps involved in fabrication of Paper Hanging Drop Chips (PHDC), and Networked Paper Hanging Drop Chip (N-PHDC) and its application in for high throughput drug screening and chemotaxis study of cancer spheroids. Adapted from [50].

The effect of the drug on tumor spheroids was assessed by the Live / Dead ™ assay and plotted as the ratio of dead cells to fluorescence intensity, as shown in Figure 12.B

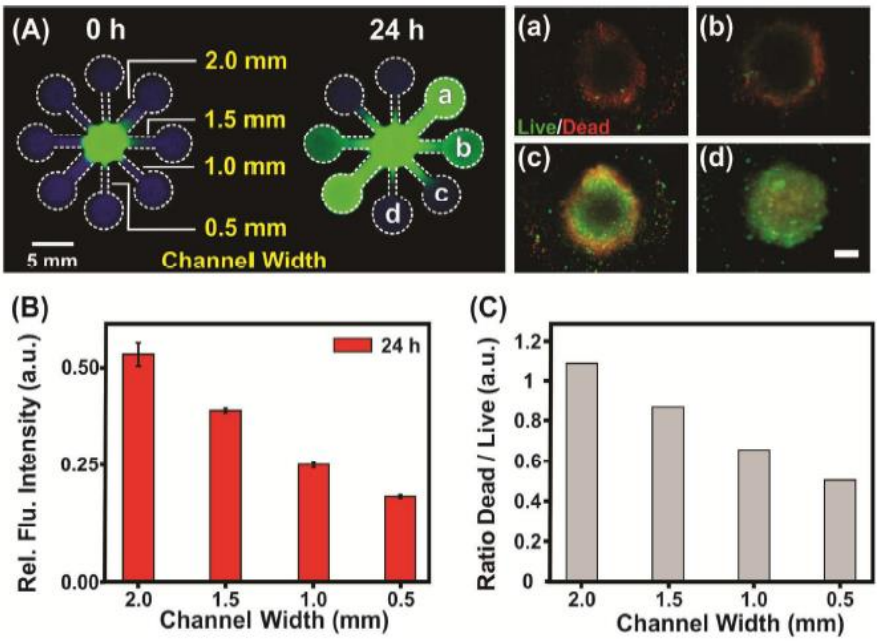

Figure 12. Variable drug dosing in N-PHDC. (A) Single-source, multi-sink N-PHDC for variable dosage drug testing imaged from the top at 0 and 24 hours. (a-d) Live/Dead assay of MCF-7 spheroids after 24 hours of anticancer drug (5-FU) treatment, corresponding to channel widths of 0.5 mm, 1 mm, 1.5 mm, and 2 mm (Scale bar: 100 μm). (B) Plot shows variable dosage corresponding to channel width, quantified using fluorescein dye (green) after 24-hour incubation from individual wells from the top of the N-PHDC (n = 3). (C) Ratio of Fluorescent intensity from dead (red) and live (green) cells in spheroids (a-c) corresponds to the channel width. Adapted from [50].

Interestingly, as the obtained results demonstrate the channel width had a significant influence in the overall therapeutic efficacy of the anti-cancer pharmaceutical performance (Figure 12C). These findings evidence the importance of the vascular network that surrounds human tumors and provides a unique platform for evaluating and modeling this effect *in vitro*.

4. Advanced Microfluidic Chips for 3D Tumor Spheroids Assembly and Screening

Advanced microfluidic platforms offer the unique opportunity to rapidly generate 3D mono and heterotypic tumor spheroids and use the same platform for high throughput screening. In this context, Kwak and co-workers [17], generated breast cancer tumor cell agglomerates (MCF-7 e MDA-MB-231) via alginate micro droplets with diameters between 50 and 150 μm by using a microfluidic system. The microfluidic chip consisted of two intakes, one for the oil solution (which was a surfactant diluted in fluorinated oil) and the other for the aqueous phase which contained a suspension of cells in culture medium, and an outlet for collection of micro- as can be seen in Figure 13. The surface of the microfluidic

channel is hydrophobic, and the yield and diameter of the micro droplets were controlled by changing the channel geometry and rate of speed between the two solutions as seen in Figure 13.

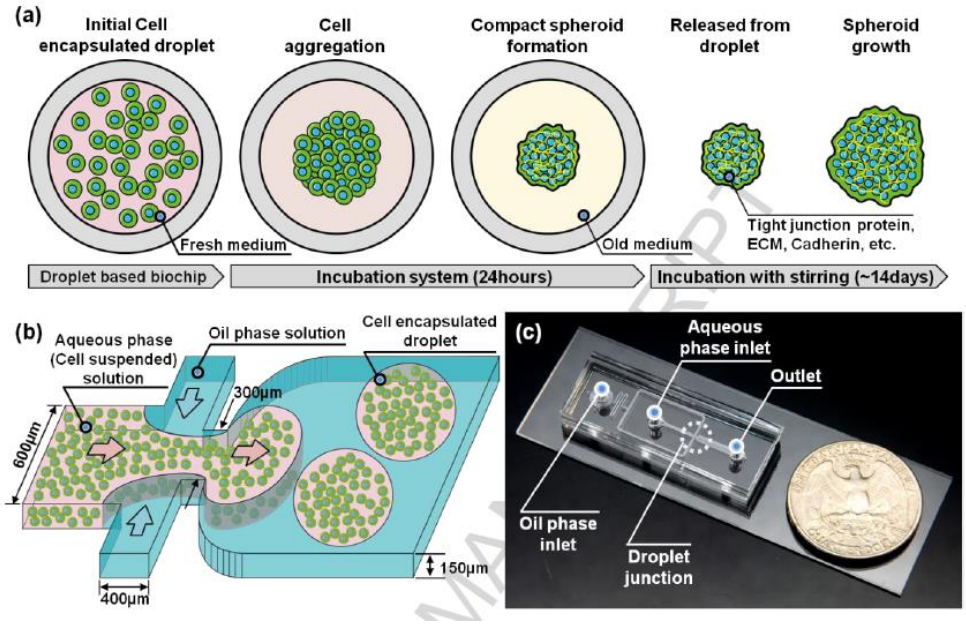

Figure 13. (a) Formation of 3D tumor spheroid model from single cell in micro-droplet. (b) Droplet-based microfluidic system for 3D tumor spheroid model generation and (c) optical image. Adapted from [17].

After 24 h of incubation, the spheroids were withdrawn from within the micro-droplets with the addition of 1H,1H,2H,2H, -perfluoro-1-octanolto the oil solution, which caused the droplets to burst. The authors then centrifuged the mixture and collected the culture medium with 3D spheroids. 3D cell culture was performed in a magnetic stirring cell incubation system. The tumor model was assessed was characterized by labeling the junction protein (ZO-1), adhesion molecules (i.e., E-cadherin) and ECM components (collagen type IV), indicating the presence of these biomarkers. Moreover, anti-cancer drug screening using Doxorubicin as a model drug revealed that at the same Doxorubicin concentration, 23% of cells were dead in 2D monolayer cultures and only 4 % of dead cells were detected in 3D microtissues. These findings could be correlated to cells 3D agglomeration and the presence of extracellular matrix compounds, which serve as a barrier to anti-cancer pharmaceutics diffusion [17].

5. Conclusions and Future Perspectives

Hydrophobized and super-hydrophobic surfaces continue to receive significant interest for tissue engineering and regenerative medicine applications. They have been used for high-throughput screening (HTS) and formation of 3D tumor models. They are very reproducible, versatile, easy to manufacture and allow the development of 3D structures similar *in vivo* tumors (polymer structures, hydrogels or spheroids of 3D cells) where size, shape, cell density and chemical concentrations can be controlled, that traditional methods of spheroid formation can not be. [1], [5], [21], [26], [34], [41], [42].

The versatility of the platform seems to be one of the most promising in terms of real applicability to clinical practice, promoting great technological advances in modern biology and medicine, also allowing the construction of disease models through spheroids in mono or co-culture, useful for *in vitro* studies of new therapies, diagnostic techniques or pharmacological tests [21], [26]. The use of low amounts of biomaterials and encapsulated cells in small spaces makes high-throughput methods an approach that may be essential for the study of rare samples, which is important in miniaturized bioanalytical and biomedical systems, as they decrease sample size can significantly reduce the time required for analysis and associated costs [11], [45].

The use of hydrophobized and super-hydrophobic surfaces seems to be a very useful method for applications in cancer biology, microtissue formation and drug screening.

Acknowledgments

The authors would like to acknowledge the support of the European Research Council for project ATLAS, grant agreement ERC-2014-ADG-669858. The authors also acknowledge the financial support by the Portuguese Foundation for Science and Technology (FCT) through a Post-doctoral grant (SFRH/BPD/119983/2016, Vítor Gaspar) and for the funding of project PANGEIA (PTDC/BTM-SAL/30503/2017).

References

[1] A. I. Neto, P. A. Levkin, and J. F. Mano, "Patterned superhydrophobic surfaces to process and characterize biomaterials and 3D cell culture," *Mater. Horizons*, vol. 5, no. 3, pp. 379–393, 2018.

[2] E. C. Costa, D. de Melo-Diogo, A. F. Moreira, M. P. Carvalho, and I. J. Correia, "Spheroids Formation on Non-Adhesive Surfaces by Liquid Overlay Technique: Considerations and Practical Approaches," *Biotechnol. J.*, vol. 13, no. 1, pp. 1–12, 2018.

[3] A. I. Neto *et al.*, "A novel hanging spherical drop system for the generation of cellular spheroids and high throughput combinatorial drug screening," *Biomater. Sci.*, vol. 3, no. 4, pp. 581–585, 2015.

[4] M. B. Oliveira, A. I. Neto, C. R. Correia, M. I. Rial-Hermida, C. Alvarez-Lorenzo, and J. F. Mano, "Superhydrophobic chips for cell spheroids high-throughput generation and drug screening," *ACS Appl. Mater. Interfaces*, vol. 6, no. 12, pp. 9488–9495, 2014.

[5] X. Li, X. Zhang, S. Zhao, J. Wang, G. Liu, and Y. Du, "Micro-scaffold array chip for upgrading cell-based high-throughput drug testing to 3D using benchtop equipment," *Lab Chip*, vol. 14, no. 3, pp. 471–481, 2014.

[6] G. H. Lee, J. S. Lee, X. Wang, and S. H. Lee, "Bottom-Up Engineering of Well-Defined 3D Microtissues Using Microplatforms and Biomedical Applications," *Adv. Healthc. Mater.*, vol. 5, no. 1, pp. 56–74, 2016.

[7] K. H. Nam, A. S. T. Smith, S. Lone, S. Kwon, and D. H. Kim, "Biomimetic 3D Tissue Models for Advanced High-Throughput Drug Screening," *J. Lab. Autom.*, vol. 20, no. 3, pp. 201–215, 2015.

[8] S. Breslin and L. O'Driscoll, "Three-dimensional cell culture: The missing link in drug discovery," *Drug Discov. Today*, vol. 18, no. 5–6, pp. 240–249, 2013.

[9] F. Pampaloni, E. G. Reynaud, and E. H. K. Stelzer, "The third dimension bridges the gap between cell culture and live tissue," *Nat. Rev. Mol. Cell Biol.*, vol. 8, no. 10, pp. 839–845, 2007.

[10] B. M. Leung, S. C. Lesher-Perez, T. Matsuoka, C. Moraes, and S. Takayama, "Media additives to promote spheroid circularity and compactness in hanging drop platform," *Biomater. Sci.*, vol. 3, no. 2, pp. 336–344, 2015.

[11] M. B. Oliveira and J. F. Mano, "Cell-Based Microarrays Using Superhydrophobic Platforms Patterned with Wettable Regions," *Springer Nat. 2018*, vol. 1771, 2018.

[12] Y. C. Tung, A. Y. Hsiao, S. G. Allen, Y. S. Torisawa, M. Ho, and S. Takayama, "High-throughput 3D spheroid culture and drug testing using a 384 hanging drop array," *Analyst*, vol. 136, no. 3, pp. 473–478, 2011.

[13] S. P. Cavnar, E. Salomonsson, K. E. Luker, G. D. Luker, and S. Takayama, "Transfer, Imaging, and Analysis Plate for Facile Handling of 384 Hanging Drop 3D Tissue

Spheroids," *J. Lab. Autom.*, vol. 19, no. 2, pp. 208–214, 2014.

[14] V. H. B. Ho *et al.*, "Manipulating magnetic 3D spheroids in hanging drops for applications in tissue engineering and drug screening," *Adv. Healthc. Mater.*, vol. 2, no. 11, pp. 1430–1434, 2013.

[15] E. C. Costa, A. F. Moreira, D. de Melo-Diogo, V. M. Gaspar, M. P. Carvalho, and I. J. Correia, "3D tumor spheroids: an overview on the tools and techniques used for their analysis," *Biotechnol. Adv.*, vol. 34, no. 8, pp. 1427–1441, 2016.

[16] Y. Peck and D.-A. Wang, "Three-dimensionally engineered biomimetic tissue models for *in vitro* drug evaluation: delivery, efficacy and toxicity," *Expert Opin. Drug Deliv.*, vol. 10, no. 3, pp. 369–383, 2013.

[17] B. Kwak, Y. Lee, J. Lee, S. Lee, and J. Lim, "Mass fabrication of uniform sized 3D tumor spheroid using high-throughput microfluidic system," *J. Control. Release*, vol. 275, pp. 201–207, 2018.

[18] S. E. Yeon *et al.*, "Application of Concave Microwells to Pancreatic Tumor Spheroids Enabling Anticancer Drug Evaluation in a Clinically Relevant Drug Resistance Model," *PLoS One*, vol. 8, no. 9, pp. 1–12, 2013.

[19] P. Longati *et al.*, "3D pancreatic carcinoma spheroids induce a matrix-rich, chemoresistant phenotype offering a better model for drug testing," *BMC Cancer*, vol. 13, pp. 1–13, 2013.

[20] N. R. Patel, B. Aryasomayajula, A. H. Abouzeid, and V. P. Torchilin, "Cancer cell spheroids for screening of chemotherapeutics and drug-delivery systems," *Ther. Deliv.*, vol. 6, no. 4, pp. 509–520, 2015.

[21] N. M. Oliveira, C. Martins-Cruz, M. B. Oliveira, R. L. Reis, and J. F. Mano, "Coculture of Spheroids/2D Cell Layers Using a Miniaturized Patterned Platform as a Versatile Method to Produce Scaffold-Free Tissue Engineering Building Blocks," *Advanced Biosystems*. p. 1700069, 2017.

[22] M. T. Santini, G. Rainaldi, and P. L. Indovina, "Multicellular spheroids in radiation biology," *Int J Rad Biol*, vol. 75, no. 7, 1999.

[23] M. W. Laschke and M. D. Menger, "Life is 3D: Boosting Spheroid Function for Tissue Engineering," *Trends Biotechnol.*, vol. 35, no. 2, pp. 133–144, 2017.

[24] A. M. S. Costa, M. Alatorre-Meda, N. M. Oliveira, and J. F. Mano, "Biocompatible polymeric microparticles produced by a simple biomimetic approach," *Langmuir*, vol. 30, no. 16, pp. 4535–4539, 2014.

[25] X. Zheng Ting *et al.*, "On-chip investigation of cell – drug interactions ☆," *Adv. Drug Deliv. Rev.*, p. 19, 2013.

[26] G. Ciasca *et al.*, "Recent advances in superhydrophobic surfaces and their relevance to biology and medicine," *Bioinspiration and Biomimetics*, vol. 11, no. 1, p. 11001, 2016.

[27] A. C. Lima and J. F. Mano, "Micro/nano-structured superhydrophobic surfaces in the biomedical field: part II: applications overview," *Nanomedicine*, vol. 10, no. 2, pp.

271–297, 2015.

[28] S. Shin, J. Seo, H. Han, S. Kang, H. Kim, and T. Lee, “Bio-inspired extreme wetting surfaces for biomedical applications,” *Materials (Basel).*, vol. 9, no. 2, 2016.

[29] A. M. S. Costa and J. F. Mano, “Solvent-free strategy yields size and shape-uniform capsules,” *J. Am. Chem. Soc.*, vol. 139, no. 3, pp. 1057–1060, 2017.

[30] W. Barthlott, C. Neinhuis, H. Verlot, and C. L. Schott, “Purity of the sacred lotus , or escape from contamination in biological surfaces,” pp. 1–8, 1997.

[31] H. Zhu, Z. Guo, and W. Liu, “Adhesion behaviors on superhydrophobic surfaces,” *Chem. Commun.*, vol. 50, no. 30, pp. 3900–3913, 2014.

[32] H. K. Webb, R. J. Crawford, and E. P. Ivanova, “Wettability of natural superhydrophobic surfaces,” *Adv. Colloid Interface Sci.*, vol. 210, pp. 58–64, 2014.

[33] B. N. Lourenço *et al.*, “Wettability influences cell behavior on superhydrophobic surfaces with different topographies,” *Biointerphases*, vol. 7, no. 1–4, pp. 1–11, 2012.

[34] N. M. Oliveira, A. I. Neto, W. Song, and J. F. Mano, “Two-dimensional open microfluidic devices by tuning the wettability on patterned superhydrophobic polymeric surface,” *Appl. Phys. Express*, vol. 3, no. 8, 2010.

[35] T. Verho, C. Bower, P. Andrew, S. Franssila, O. Ikkala, and R. H. A. Ras, “Mechanically Durable Superhydrophobic Surfaces,” *Adv. Mater.*, vol. 23, no. 5, pp. 673–678, 2011.

[36] L. Feng, Y. Zhang, J. Xi, Y. Zhu, F. Xia, and L. Jiang, “2008_langmuir_Petal Effect A Superhydrophobic State with High Adhesive Force,” no. 18, pp. 4114–4119, 2008.

[37] M. Nosonovsky and B. Bhushan, “Hierarchical roughness optimization for biomimetic superhydrophobic surfaces,” *Ultramicroscopy*, vol. 107, no. 10–11, pp. 969–979, 2007.

[38] E. Celia, T. Darmanin, E. Taffin de Givenchy, S. Amigoni, and F. Guittard, “Recent advances in designing superhydrophobic surfaces,” *J. Colloid Interface Sci.*, vol. 402, pp. 1–18, 2013.

[39] A. C. Lima, P. Batista, T. A. M. Valente, A. S. Silva, I. J. Correia, and J. F. Mano, “Novel Methodology Based on Biomimetic Superhydrophobic Substrates to Immobilize Cells and Proteins in Hydrogel Spheres for Applications in Bone Regeneration,” *Tissue Eng. Part A*, vol. 19, no. 9–10, pp. 1–38, 2013.

[40] W. Song and C. Lima, “Bioinspired methodology to fabricate hydrogel spheres for multi-applications using superhydrophobic substrates †,” no. C, pp. 5868–5871, 2010.

[41] M. B. Oliveira and J. F. Mano, “On-chip assessment of the protein-release profile from 3D hydrogel arrays,” *Anal. Chem.*, vol. 85, no. 4, pp. 2391–2396, 2013.

[42] A. C. Lima, W. Song, B. Blanco-Fernandez, C. Alvarez-Lorenzo, and J. F. Mano, “Synthesis of temperature-responsive Dextran-MA/PNIPAAm particles for controlled drug delivery using superhydrophobic surfaces,” *Pharm. Res.*, vol. 28, no. 6, pp. 1294–1305, 2011.

[43] A. I. Neto, K. Demir, A. A. Popova, M. B. Oliveira, J. F. Mano, and P. A. Levkin, "3D Cell Culture: Fabrication of Hydrogel Particles of Defined Shapes Using Superhydrophobic-Hydrophilic Micropatterns (Adv. Mater. 35/2016)," *Adv. Mater.*, vol. 28, no. 35, p. 7552, 2016.

[44] C. L. Salgado, M. B. Oliveira, and J. F. Mano, "Combinatorial cell-3D biomaterials cytocompatibility screening for tissue engineering using bioinspired superhydrophobic substrates.," *Integr. Biol. Quant. Biosci. from nano to macro*, vol. 4, no. 3, pp. 318–327, 2012.

[45] A. I. Neto, C. R. Correia, C. A. Custõdio, and J. F. Mano, "Biomimetic miniaturized platform able to sustain arrays of liquid droplets for high-throughput combinatorial tests," *Adv. Funct. Mater.*, vol. 24, no. 32, pp. 5096–5103, 2014.

[46] A. C. Lima, P. Sher, and J. F. Mano, "Production methodologies of polymeric and hydrogel particles for drug delivery applications," *Expert Opin. Drug Deliv.*, vol. 9, no. 2, pp. 231–248, 2012.

[47] K. E. Sung and D. J. Beebe, "Microfluidic 3D models of cancer ☆," *Adv. Drug Deliv. Rev. journa*, pp. 1–11, 2014.

[48] L. P. Ferreira, V. M. Gaspar, and J. F. Mano, "Bioinstructive microparticles for self-assembly of mesenchymal stem Cell-3D tumor spheroids," *Biomaterials*, 2018.

[49] T. Liu, M. Winter, and B. Thierry, "Quasi-spherical microwells on superhydrophobic substrates for long term culture of multicellular spheroids and high throughput assays," *Biomaterials*, vol. 35, no. 23, pp. 6060–6068, 2014.

[50] I. Michael, S. Kumar, J. M. Oh, D. Kim, J. Kim, and Y.-K. Cho, "Surface Engineered Paper Hanging Drop Chip for 3D Spheroid Culture and Analysis.," *ACS Appl. Mater. Interfaces*, p. acsami.8b08778, 2018.

2. Aims

The aim of this thesis was the development 3D tumor-ECM like photo-crosslinkable microgels fabricated via droplet addition in quasi- superhydrophobic surfaces and their use as scaffolds for assembly of *in vitro* 3D heterotypic cancer models capable of recapitulating key aspects of the complex metastatic prostate-to-bone niche found *in vivo*. These platforms ultimately aim to accelerate the discovery of candidate compounds that can be used to target this unique microenvironment. Thus, the specific objectives of this thesis were the following:

- Synthesis and characterization of methacrylated hyaluronic acid (HA-MA);
- Production of quasi-Superhydrophobic Polystyrene Surface (PS);
- Generation of 3D microgels in quasi-hydrophobic surfaces by droplet dispensing and UV-mediated photocrosslinking;
- Encapsulation of PC-3 prostate cancer cells in HA-MA spheroidal microgels and evaluation of cells metabolic activity;
- Synthesis and characterization of Gelatin-Methacryloyl (GelMA);
- Generation tumor ECM mimicking HA-MA/GelMA 3D spheroidal microgels in modified PS surfaces via droplet dispensing and UV-mediated crosslinking;
- Simultaneous encapsulation of PC-3 and human osteoblast cells in HA-MA and Gel-MA spheroidal microgels and metabolic activity evaluation;
- Characterization of micro-tumor size, circularity, morphology and ability to recapitulate key tumor features formation over long periods of culture;
- Analysis of microtumor internal organization and calcium deposition;
- Formation of 3D spheroids of PC-3 and PC-3 + hOB via forced floating;
- Evaluation of cisplatin cytotoxicity in 3D spheroids and 3D tumor ECM like microgels;

3. Materials and Methods

3.1. Materials

Hyaluronic acid sodium salt polymer (MW: 80 – 100 kDa) was obtained from Carbosynth Ltd (Berkshire, United Kingdom). Gelatin Type A from porcine skin, Irgacure 2959, and N,N-dimethylformamide (DMF 99.8 %) reagent solution were acquired from Merk-Sigma (Sintra, Portugal).The regenerated cellulose dialysis membrane with 6-8 kDa MWCO were purchased from (Spectrum Labs, inc). Triethylamine (TEA, 99 %), Glycidyl methacrylate (97%) were acquired from ACROS organics. L-Ascorbic Acid 2-Phosphate was obtained from VWR, Water and Ice Repellent Satellite Coating (WX2100) were acquired from Cytonix and Cisplatin were purchased from Biogen.

Cell culture materials including T-75 and T-175 cell culture treated T-flasks, as well as plates were obtained from Starstedt (Starstedt, Rio de Mouro, Portugal). All of the following reagents cell culture media and supplements namely GIBCO® Dulbecco's Phosphate buffered saline (DPBS), Trypan Blue, Fetal Bovine Serum (FBS; E.U. approved, South America origin), Roswell Park Memorial Institute RPMI-1640 Medium, Dulbecco's Modified Eagle Medium Nutrient Mixture F-12 (DMEM F-12), TrypLE™ Express, GIBCO® Antibiotic/antimycotic solution (ATB) containing 10,000 units/mL of penicillin, 10,000 µg/mL of streptomycin, and 25 µg/mL of Gibco Amphotericin B were purchased from ThermoFisher Scientific (Alfagene, Portugal). Ultra-Low-Adhesion (ULA) round-bottom 96-wells plates were purchased from Corning (Corning, NY, US). Calcein-AM, Propidium Iodide (PI) and β-Glycerol phosphate were all purchased from Thermofisher Scientific Inc (Alfagene, Portugal). Alizarin Red S was obtained from Laborspirit (Loures, Portugal). CellTiter-Glo® were purchased from Promega (Madisson, WI, USA). PC-3, an androgen independent cell line derived from a bone metastasis of a prostate adenocarcinoma, was provided through a partnership with the Portuguese Institute of Oncology (IPO) and primary fetal human osteoblasts were acquired from Cell Applications Inc. (San Diego, CA, US).

3.2. Methods

3.2.1. Synthesis of methacrylated hyaluronic acid (HA-MA)

Methacrylated Hyaluronic acid was synthesized by reacting hyaluronic acid with glycidyl methacrylate under alkaline conditions as previously described in the literature [1]. In brief, Hyaluronic acid (HA) (2.0 g) was dissolved in distilled water (100 mL) in a 500 mL round bottom flask, under magnetic stirring, at room temperature (RT), to yield a 2 % w/v aqueous solution. Additionally, glycidyl methacrylate (35.5 mL) and TEA (25.3 mL) were drop-wised added to 39.2 mL of DMF, in a Schott Flask under magnetic stirring, in a chemical fume hood. Afterwards, the organic DMF phase was added to HA aqueous phase *via* drop-wise addition, and the reaction proceeded for 72 h, at RT protected from light. After this period the modified polymer solution was carefully transferred to a regenerated cellulose dialysis membrane (MWCO 6-8 kDa), and dialyzed against DI water for 5 days, at RT, in a chemical fume hood. The dialysate was exchanged three times a day to assure full sink conditions. The purified solution was then frozen at -80 °C and freeze-dried for 5 days, in the dark. The resulting Methacrylated Hyaluronic acid (HA-MA) polymer as recovered as a white cotton foam.

3.2.2. Synthesis of Gelatin-methacryloyl (GelMA)

Porcine gelatin type A was chemically modified with methacryloyl functional moieties as previously described by Loessner and co-workers, with slight modifications [2]. Initially a 10 % (w/v) gelatin solution was prepared by dissolving gelatin in PBS, under vigorous magnetic stirring, at 50 ºC, overnight, to achieve complete dissolution. Afterward, 0.6 g of methacrylic anhydride per 1 g of dissolved gelatin (very viscous liquid) was added slowly to the mixture for a high degree of methacryloyl functionalization and the reaction was left to proceed for 5 h, at RT, under stirring. Afterward, the solution was transferred into 50 mL tubes and centrifuged at 3500 g for 3 min, at RT, to remove unreacted methacrylic anhydride. The GelMA-containing supernatant was then decanted into another 50 mL tube, and the unreacted methacrylic anhydride deposited on the bottom was discarded. The supernatant was then diluted with 10 mL of pre-heated (37 °C) deionized water and transferred to a regenerated cellulose dialysis membrane (MWCO 6-8 kDa). GelMA was

dialyzed at 50 °C against deionized water for 5 to 7 days in a fume hood and protected from light. The purified methacrylated polymer was then freeze-dried as above mentioned.

3.2.3. Functionalized Biopolymers Spectroscopic Characterization

The inclusion of the acrylate photoreactive moieties in the different biopolymers was initially characterized by Proton nuclear magnetic resonance (^{1}H NMR) spectroscopy. All spectra were acquired on a Bruker Advance III 300 MHz spectrometer. For NMR analysis all samples were dissolved in 500 µL of deuterated water (D_2O) and transferred to 500 MHz NMR glass tubes (Wilmad, Cortenet, France). Samples were acquired with 256 scans, 8 dummy scans and with 18 secs of relaxation delay. The acquired spectra were processed by using the MestReNova v6.0.2 software. ^{1}H NMR data was used to determine HA and Gelatin degree of methacrylation as described in the literature [3], [4].

In addition, the chemically modified ECM-mimetic biopolymers were characterized by attenuated total reflectance Fourier Transformed Infrared spectroscopy (ATR-FTIR). For analysis, powdered samples were place in a Brucker Tensor 27 spectrometer. A total of 256 scans, with a spectral resolution of 4 cm^{-1} were acquired in the spectral window spanning from 4000 to 350 cm^{-1}. The obtained data was processed in OPUS software and plotted in Origin software (v9.1, trial version).

3.2.4. Fluoraldehyde assay for GelMA functionalization characterization

The fluoraldehyde assay that detects primary amines was used to determine the degree of acrylate functionalization (DoF) in gelatin lysine residues as previously described in the literature, with minor modifications [2]. For this purpose, initially, a freshly prepared gelatin stock solution (0.5 mg/mL, in PBS pH =7.4) was used for computing a standard curve (0.02, 0.1, 0.5, 0.75 and 1.0 mg/mL). Before the experiments the fluoraldehyde reagent was warmed to RT. For samples analysis, 300 µL of GelMa samples solutions were mixed with 600 µL of the fluoraldehyde reagent. Control samples were prepared by mixing 300 µL of PBS with 600 µL of the fluoraldehyde reagent under vortex for 1 min. After 5 min of incubation 250 µL of each solution were placed in a 96-well black-clear bottom plate, and the fluorescence intensity at 450 nm using an excitation wavelength of 360 nm was measured by using a plate reader. The average fluorescence intensity was determined to each sample

and the fluorescence intensity of the PBS control was subtracted from the sample and standard solutions to determine the net fluorescence. The DoF was then calculated as DoF = ((0.5 − X)/0.5) × 100 %, where X is gelatin concentration in mg/mL.

3.2.5. Production of quasi Superhydrophobic Polystyrene Surfaces (PS)

The production of polystyrene (PS) quasi superhydrophobic surfaces was performed by using a simple, economical and fast procedure. In brief, circular polystyrene 90 mm petri dish plates were spray coated with the U.V. resistant FluoroThane-MW (WX 2100^{TM}) coating reagent that provides a contact angle ranging from 145° to 150°, i.e. quasi-superhydrophobic [5] as described by the manufacturer (Cytonix, MD, US). The entire petri dish surface was spray coated and left to dry overnight in a chemical safety fume hood, at room temperature. In the following day, the surface was washed with 99 % ethanol and oven dried at 37 °C for 5 days.

3.2.6. In-air production of spheroidal microgels

Spheroidal microgels were produced by using a mechanical electronic repeater pipette (Eppendorf® M4 electronic digital repeater pipette) to dispense biopolymer aqueous solutions (1.25 % to 5 % w/v) onto PS quasi superhydrophobic surfaces. Spheroidal hydrogel droplets of different sizes were formed by dispensing various volumes (1 μL to 5 μL, Figure 5). The droplets were then photocrosslinked by using Irgacure 2959 (1 % w/v) as a photoinitiator and a U.V. curing system (Omnicure® S2000, Excelitas Technologies, US) that was used to irradiate hydrogels for 2 min, at an intensity of 10 mW/cm^2. Through this approach, different ECM-mimetic spheroidal hydrogels formed by HA-MA and HA-MA/GelMA blends were obtained.

3.2.7. Spheroidal microgels morphological characterization

Spherical microgels size and morphological characterization was performed by optical contrast microscopy and optical imaging. For size evaluation different microgel droplets were imaged in a stereomicroscope (Zeiss Stemi 508, Carl Zeiss, Germany), equipped with a 3 MPix color camera, and in a upright optical contrast microscope (Zeiss Primostar, Carl Zeiss, Germany) equipped with an A-Plan 5x/0.12 Ph0 M27 objective.

Macrographs of spheroidal hydrogel particles were also acquired by using a Canon EOS 1200d DLSR camera equipped with a macro lens.

3.2.8. Routine 2D *In vitro* Cell culture

In general, cells were cultured under aseptic conditions in temperature-controlled cell culture incubators at 37 ºC and with a 5% CO_2 atmosphere. For routine cell culture cells were grown in T-75 and T-175 cm^2 cell culture flasks, with cell culture media changes every other day. The human osteoblasts cell line (hOB) was cultured in DMEM-F12 medium supplemented with 10 % (v/v) FBS, 1 % (v/v) ATB and ascorbic acid (50 µg/mL, in PBS pH=7.4). The human prostate cancer cell line (PC-3) was maintained in RPMI 1640 medium (Glucose 2.5 g/L), supplemented with 10 % (v/v) FBS and 1 % (v/v) ATB. All cells were detached from culture flasks by using TrypLE™ Express enzyme detaching reagent upon attaining a confluence of 80-85 %.

3.2.9. Formulation of cell laden spheroidal 3D *in vitro* tumor models

Formulation of monotypic and heterotypic cell laden 3D spheroidal microgels was performed by using quasi superhydrophobic surfaces and U.V. mediated photocrosslinking. Initially, cells were detached as above mentioned and resuspended in equal volumes of HA-MA and GelMA, in order to obtain a homogeneous cell dispersion. After crosslinking for 2 min under U.V. light (λ= 365 nm, 10 mW/cm^2), 3D microgels were washed in DPBS and transferred to Ultra-Low-Adhesion (ULA) round-bottom 96-wells plates. 3D microgels were cultured in 200 µL of culture medium, at 37 °C and in a 5% CO_2 atmosphere. In the case of heterotypic 3D co-cultures, the culture medium was 50% RPMI 1640 and 50% DMEM F12 with 50 µL/mg ascorbic acid and 2.16 mg/mL of β-Glycerol phosphate. These last two compounds were added at day 3 and 7 of culture to mimic the microenvironment found in PC-3 bone metastasis. Production of the 3D tumor model did not follow any previously detailed procedure. Afterward, the cells were trypsinized and counted, pellets with the desired number of cells were formed by centrifugation at 300 g for 5 min, at RT. 3D *in vitro* prostate cancer tumor models' morphology and shape was analyzed overtime via optical contrast microscopy by using an inverted microscope (Primovert, Carl Zeiss, Germany). Images were acquired at specific time points (Days 3, 7 and 14).

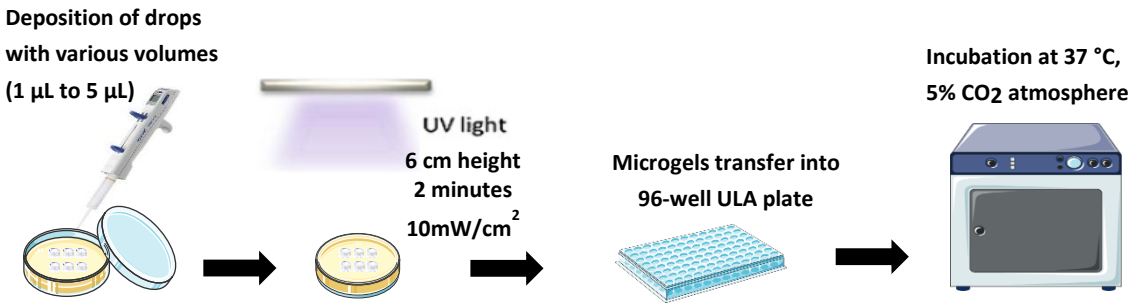

Figure 1. Schematic representation of 3D spheroidal microtumor microgels and their *in vitro* culture.

3.2.10. Cell Viability assays

The cell viability of 3D spheroidal micro-tumors in mono and co-culture were analyzed at 3,7 and 14 days by using: (i) Alamar Blue® Cell Viability Assay and (ii) Live / Dead Assay. Alamar blue® was used to evaluate the metabolical activity of 3D tumor models during monocultures and co-cultures. Both assays were performed according to the manufacturer's guidelines, except for the incubation time of Alamar Blue®, which was performed overnight rather than the standard 2-4 h period. Resazurin reduction to pink colored resorufin was determined by fluorescence measurements (λ_{ex}: 540 nm, λ_{em}: 600 nm). All measurements were performed in a Synergy HTX microplate reader by using a 96-well black-clear flat bottom plate (VWR, CN: CORN3915). To assess cell viability, the microtumors were labeled with Calcein-AM (Cal-AM) (3 µg/mL) and Propidium Iodide (PI) (6 µg/mL) for 45 min at 37 °C. Following incubation, the 3D tumor models were washed 3 times with DPBS and immediately by fluorescence microscopy. Fluorescence micrographs were acquired in an upright Widefield fluorescence microscope (Zeiss Imager M2, Carl Zeiss, Germany), equipped with an Objective EC Plan-Neofluar 5x/0.16 objective and a 3MPix monochromatic camera. All micrographs were acquired and processed in Zeiss Zen SP2 Software (Carl Zeiss, Germany).

3.2.11. 3D *in vitro* tumor calcium deposition evaluation

To detect the calcium deposition, cultured 3D tumor spheroids were stained with Alizarin Red S dye. For this purpose, 3D tumors were initially fixed in 4% formaldehyde overnight, before incubation with 150 µL of Alizarin Red S (40 mM, pH=4.2), for 2 h in the dark, at RT. After incubation, the staining solution was aspirated and 3D tumor was rinsed three times with deionized water. All images were acquired at specific time points (days 7 and 14) by using a Stemi 508 Stereo Microscope.

3.2.12. Cell-specific tracking in 3D Microgels

Cell tracking assays were performed to access internal cellular organization and permanence at a populational level during co-culture within the produced HA-MA / GelMA microgels. For this purpose, the distinct cellular populations of PC-3 and hOB were differentially stained with long-term cell tracking lipophilic dyes DiO and DiD (Thermofisher scientific, Alfagene, Portugal), as per the manufacturer's instructions. Briefly, upon cell trypsinization individual solutions were prepared for a final cellular concentration of 1 million cells per mL of serum free cell culture medium, to which 5 µL of staining agent (per mL of solution) were added. The solutions containing both cells and staining agents were then incubated for 30 min at 37 °C, after which 3x sequential washings, using serum containing medium, were performed. To prevent cell damage, between cycles of washing-centrifugation, cells were allowed to rest for 10 min at 37 °C after each wash.

PC-3 were stained with DiO (blue), and hOB with DiD (red) (Figure 16). These membrane staining are transferable to subsequent cellular generations, with no considerable signal loss being observed up to a period of 14 days of culture. Widefield fluorescence microscopy (Zeiss Imager M2, Carl Zeiss, Germany) analysis of produced microgels, containing PC3 (DiO) and hOB (DiD) stained populations, at days 7 and 14 allowed a qualitative assessment of both localization and aggregation patterns of the different cell populations.

3.2.13. Chemotherapeutic drug cytotoxicity screening in 3D *in vitro* tumor models

3D models of *in vitro* tumors in co-cultures were used as test platforms for evaluation of cisplatin cytotoxicity. On the seventh day of culture, the 3D models were incubated with cisplatin at different concentrations (100 μM, 150 μM, and 200 μM) [6] for 48 h. Cell viability was assessed by quantifying cellular ATP in 3D cell aggregates *in vitro* using a luminescence-based assay (Cell Titer Glo Luminescent viability assay, Promega, Madisson, WI, USA). CellTiter-Glo® assays were performed according to the manufacturer's instructions. After Cisplatin incubation, the medium was removed and 3D tumor models were incubated with a mixture of RPMI 1640/10% FBS / 1% ATB medium and CellTiter-Glo® reagent at a ratio of 1:1. The mixture was then stirred for 5 min and incubated for 25 min at RT. Luminescence was measured on 96-well opaque flat bottom white plates by using a Synergy HTX microplate reader programmed with an integration time of 1 sec.

References

[1] A. Sigen *et al.*, "A facile one-pot synthesis of acrylated hyaluronic acid," *Chem. Commun.*, vol. 54, no. 9, pp. 1081–1084, 2018.

[2] D. Loessner *et al.*, "Functionalization, preparation and use of cell-laden gelatin methacryloyl-based hydrogels as modular tissue culture platforms," *Nat. Protoc.*, vol. 11, no. 4, pp. 727–746, 2016.

[3] M. T. Poldervaart *et al.*, "3D bioprinting of methacrylated hyaluronic acid (MeHA) hydrogel with intrinsic osteogenicity," *PLoS One*, vol. 12, no. 6, pp. 1–15, 2017.

[4] J. W. Nichol, S. T. Koshy, H. Bae, C. M. Hwang, S. Yamanlar, and A. Khademhosseini, "Cell-laden microengineered gelatin methacrylate hydrogels," *Biomaterials*, vol. 31, no. 21, pp. 5536–5544, Jul. 2010.

[5] K. Y. Law, "Definitions for hydrophilicity, hydrophobicity, and superhydrophobicity: Getting the basics right," *J. Phys. Chem. Lett.*, vol. 5, no. 4, pp. 686–688, 2014.

[6] J. Gumulec *et al.*, "Cisplatin-resistant prostate cancer model: Differences in antioxidant system, apoptosis and cell cycle," *Int. J. Oncol.*, vol. 44, no. 3, pp. 923–933, 2014.

4. Results and Discussion

4.1. In-air production of 3D Co-culture Tumor Spheroids for Expedite *In vitro* Drug Screening

Subchapter 4.1.

This subchapter is based on the manuscript entitled

"In-air production of 3D Co-culture Tumor Spheroids for Expedite In vitro Drug Screening"

In-air production of 3D Co-culture Tumor Spheroids for Expedite *In vitro* Drug Screening

Jéssica Antunes [1], Vítor M. Gaspar [1#], Luís Ferreira[1], Maria Monteiro[1], João F. Mano[1#]

[1] Department of Chemistry, CICECO, University of Aveiro, Campus Universitário de Santiago, 3810-193, Aveiro, Portugal

[#]Corresponding authors:
Professor João F. Mano
Department of Chemistry, CICECO – Aveiro Institute of Materials
University of Aveiro, Campus Universitário de Santiago
3810-193, Aveiro, Portugal
E-mail: jmano@ua.pt
Telephone: +351 234370733

Dr. Vítor Gaspar
Department of Chemistry, CICECO – Aveiro Institute of Materials
University of Aveiro, Campus Universitário de Santiago
3810-193, Aveiro, Portugal
E-mail: vm.gaspar@ua.pt
Telephone: +351 234370733

Abstract

Three-dimensional (3D) *in vitro* tumor models are becoming widely used pre-clinical platforms for testing the performance of existing drugs or discovery of novel anti-neoplastic therapeutics. Due to their multicellular compact structure and spatial architecture, *in vitro* 3D tumor models recapitulate major hallmarks of human solid tumors. However, these microphysiologic systems generally lack the existence of tumor-ECM components, a critical aspect that can affect overall therapeutic performance and ultimately the decision of advancing candidate drugs to later stages of the pipeline. Herein, by using easy to assemble quasi super-hydrophobic platforms we fabricated size and shape controlled photocrosslinkable methacrylated hyaluronic acid (HA-MA) and gelatin-methacryloyl (GelMA) spherical microgels. These platforms were used for establishing heterotypic 3D co-culture models of prostate cancer cells (PC-3) and human-derived osteoblasts (hOB) with the aim to mimic prostate cancer-to-bone metastasis cellular heterogeneity and tumor-ECM microenvironment. The produced spheroidal 3D microtumors morphology, size and cell number were easily controlled via digital droplet generation on hydrophobic surfaces and reproducible across numerous conditions. 3D microgels formed by 2.5%HA-MA-5%GelMA and 5%HA-MA-5%GelMA ratios showed the highest calcium deposition after 14 days, thus evidencing osteoblasts viability and the establishment of functional mineralization in the 3D spherical gel matrix. Cisplatin cytotoxicity evaluation showed that 3D microgels are more resistant to platin chemotherapeutics than their mono and heterotypic 3D multicellular spheroid counterparts. Overall, our findings indicate that the produced 3D microgel microenvironments are versatile and robust platforms for *in vitro* screening of therapeutics targeted to prostate-to-bone metastasis microenvironments.

Keywords: Hydrophobized Surfaces, *3*D Prostate Cancer *in vitro* models, Spherical Microgels, Drug Screening

1. Introduction

Prostate cancer (PCa), is the second most commonly diagnosed cancer in men worldwide [1] and despite significant medical advances, prostate cancer is still one of the leading causes of cancer-related deaths in men [2]–[4]. In Portugal, prostate cancer represents about 3.5% of all deaths in the country and more than 10% of cancer-related deaths, recorded in 2010 according to the Portuguese Urology Association [5]. Prostate cancer represents a complex disease normally highly susceptible to androgen regulation, and the establishment of immune-suppressive microenvironments [6]. Ultimately this tumor supportive microenvironment if untreated can, in advanced stages of the disease, leads to cancer cell invasion, migration, and metastasis [6], [7].

Prostate cancer metastasis occurs normally to the growth-factor rich microenvironment of the bone-marrow [8]. Metastasis from prostate cancer cells to the bone is a process involving several steps: i) cancerous cells are released from the primary site; ii) the displacement of cells into the blood or lymph and iii) fixation of tumor cells to bone tissue and development of a tumor at the site of bone metastasis [9]–[11]. Understanding the role of these bone cells (osteoblasts, osteocytes, osteoclasts, hematopoietic cells, mesenchymal cells, and immune cells) and how they interact with tumor cells, is an important aspect for the development of therapies for the metastasis [10]. Throughout the whole process from the primary tumor to its metastatic niche, it is widely accepted that non-malignant cells actively influence the fate of cancer cells [9]. Factors secreted by prostate cancer cells alter the balance between the activity of osteoblasts (bone forming cells) and osteoclasts (bone lysis cells). Both are involved in the progression of prostate cancer metastases because they inhibit these factors and determine the phenotype of bone lesions. Prostate cancer metastases can cause osteoblasts to promote excessive bone formation, to acquire an osteolytic behavior (bone lysis), or trigger a mixed response [11], [12]. Several studies have reported that about 90% of patients with advanced prostate cancer will develop bone metastases [9]–[11]. Presentation of secondary tumors is associated with high levels of morbidity and mortality, in part due to the lack of effective therapies in the clinic. This scenario evidences the urgent need to discover new therapeutic approaches that can realistically impact patient survival rates.

The pre-clinical discovery of new anti-cancer therapeutics using both 2D *in vitro* cell cultures and animal models involves high costs and ethical issues associated with the use of

rodents and has demonstrated a very low correlation with the data that is obtained in clinical trials [13]–[15]. Adding to this, in the pharmaceutics discovery process it is clear that 2D *in vitro* cultures do not represent the 3D spatial environment of a human tumor, nor its ECM or stromal cellular components [13], [16]. To overcome these issues 3D *in vitro* tumor models have been researched in the last two decades as potential alternative testing platforms for new anti-cancer drugs screening [17], [18]. Currently, the most used scaffold-free 3D tumor models are cell-spheroids which are cellular aggregates formed by cancer cells. There are various technologies for 3D spheroids assembly such as those based on ultra-low adhesion cell culture plates (Corning® Costar® Ultra-Low attachment multiwell plates) [19], or micro-molding techniques (MicroTissues® 3D Petri Dish®[20] micro-mold mixed spheroids). Given their tumor-like features, *in vitro* multicellular spheroids have been particularly useful for studying the efficacy of novel chemotherapeutic agents for prostate cancer [21],[22].

However, these scaffold-free models do not include tumor ECM components at their initial stage of assembly. The development of 3D *in vitro* tumor models should take into consideration the inclusion of tumor ECM components, as these trigger key physicochemical responses [23]. In this focus, biomaterials provide an excellent platform to include ECM-like cues, however, such materials must be optimized [13]. Hence, there is a need to develop ECM mimicking biomaterials with suitable mechanical rigidity, 3D architecture, structural organization and cell adhesion, so as to recapitulate in an increasingly reliable form the tumor microenvironment of human tumors [24], [25]. Natural-origin biomaterials (e.g., chitosan, alginate, collagen, hyaluronic acid (HA)), have been exploited for the manufacture of 3D tumor scaffolds (e.g., hydrogel matrixes) as they replicate cancer cells-ECM interactions present in the native tumor microenvironment [25]. However, in hydrogel matrixes the cell number comprising self-forming 3D agglomerates and their shape is highly difficult to control within the gel volume leading to variable drug responses. Cells bioencapsulation in spherically shaped microgels may provide therefore a valuable alternative to address these issues if controllable and cost-effective sphere generating technologies such as hydrophobic surfaces or microfluidic chips are employed.

Superhydrophobic surfaces, have been used in the field of biomedicine, regenerative medicine, and tissue engineering as platforms for biomaterials processing and also for high throughput screening (HTS) and 3D cell niches manufacturing, [26]–[32]. By using

hydrophobized surfaces virtually 100% cell encapsulation is possible and control over spheroids size can be easily attained by adjusting the number of encapsulated cells and the volume of dispensed droplets [27], [33], [34].

In this work we produced a new 3D model of metastatic prostate cancer that mimics prostate cancer bone metastasis cellular heterogeneity and ECM microenvironment. The 3D models are comprised of methacrylated hyaluronic acid and gelatin-methacryloyl (HA-MA and GelMA). Interest in these two biopolymers is related to the fact that GelMA is chemically similar to native tissues ECM [35] and hyaluronic acid is an abundant structural component in the extracellular matrix of prostate cancer [7], [36]. These two methacrylated macromers can be crosslinked by photopolymerization and form a stable network through covalent crosslinking. Cells were encapsulated using quasi-superhydrophobic surfaces for the formation of spherical microgels that were then subjected to photocrosslinking through U.V. light incidence. The produced spheroidal microtumors have a reproducible spherical morphology, it is possible to control the number of encapsulated cells and the size is adjustable with the volume of the drop dispensed on the quasi-superhydrophobic surface. We performed several monoculture assays with different polymer concentrations and cell densities, and the two best formulations were used for cell co-culture with osteoblasts. In addition, the co-cultured models used for cisplatin cytotoxicity screening and the results indicate that 3D co-culture microgels are more resistant to cisplatin than their 3D spheroid counterparts. These findings evidence the importance to develop *in vitro* models that replicate the tissue microenvironments so that the experimental results are reliable and more biologically meaningful.

2. Materials and Methods

2.1. Materials

Hyaluronic acid sodium salt polymer (MW: 80 – 100 kDa) was obtained from Carbosynth Ltd (Berkshire, United Kingdom). Gelatin Type A from porcine skin, Irgacure 2959, and N,N-dimethylformamide (DMF 99.8 %) reagent solution were acquired from Merk-Sigma (Sintra, Portugal).The regenerated cellulose dialysis membrane with 6-8 kDa MWCO were purchased from (Spectrum Labs, inc). Triethylamine (TEA, 99 %), Glycidyl methacrylate (97%) were acquired from ACROS organics. L-Ascorbic Acid 2-Phosphate was obtained from VWR, Water and Ice Repellent Satellite Coating (WX2100) were acquired from Cytonix and Cisplatin were purchased from Biogen.

Cell culture materials including T-75 and T-175 cell culture treated T-flasks, as well as plates, were obtained from Starstedt (Starstedt, Rio de Mouro, Portugal). All of the following reagents cell culture media and supplements namely GIBCO® Dulbecco's Phosphate buffered saline (DPBS), Trypan Blue, Fetal Bovine Serum (FBS; E.U. approved, South America origin), Roswell Park Memorial Institute RPMI-1640 Medium, Dulbecco's Modified Eagle Medium Nutrient Mixture F-12 (DMEM F-12), TrypLE™ Express, GIBCO® Antibiotic/antimycotic solution (ATB) containing 10,000 units/mL of penicillin, 10,000 µg/mL of streptomycin, and 25 µg/mL of Gibco Amphotericin B were purchased from ThermoFisher Scientific (Alfagene, Portugal). Ultra-Low-Adhesion (ULA) round-bottom 96-wells plates were purchased from Corning (Corning, NY, US). Calcein-AM, Propidium Iodide (PI) and β-Glycerol phosphate were all purchased from Thermofisher Scientific Inc (Alfagene, Portugal). Alizarin Red S was obtained from Laborspirit (Loures, Portugal). CellTiter-Glo® were purchased from Promega (Madisson, WI, USA). PC-3, an androgen-independent cell line derived from a bone metastasis of a prostate adenocarcinoma, was provided through a partnership with the Portuguese Institute of Oncology (IPO) and primary fetal human osteoblasts were acquired from Cell Applications Inc. (San Diego, CA, US).

2.2. Methods

2.2.1. Synthesis of methacrylated hyaluronic acid (HA-MA)

Methacrylated Hyaluronic acid was synthesized by reacting hyaluronic acid with glycidyl methacrylate under alkaline conditions as previously described in the literature [37]. In brief, Hyaluronic acid (HA) (2.0 g) was dissolved in distilled water (100 mL) in a 500 mL round bottom flask, under magnetic stirring, at room temperature (RT), to yield a 2 % w/v aqueous solution. Additionally, glycidyl methacrylate (35.5 mL) and TEA (25.3 mL) were drop-wise added to 39.2 mL of DMF, in a Schott Flask under magnetic stirring, in a chemical fume hood. Afterward, the organic DMF phase was added to HA aqueous phase *via* drop-wise addition, and the reaction proceeded for 72 h, at RT protected from light. After this period the modified polymer solution was carefully transferred to a regenerated cellulose dialysis membrane (MWCO 6-8 kDa), and dialyzed against DI water for 5 days, at RT, in a chemical fume hood. The dialysate was exchanged three times a day to assure full sink conditions. The purified solution was then frozen at -80 °C and freeze-dried for 5 days, in the dark. The resulting Methacrylated Hyaluronic acid (HA-MA) polymer as recovered as a white cotton foam.

2.2.2. Synthesis of Gelatin-methacryloyl (GelMA)

Porcine gelatin type A was chemically modified with methacryloyl functional moieties as previously described by Loessner and co-workers, with slight modifications [38]. Initially a 10 % (w/v) gelatin solution was prepared by dissolving gelatin in PBS, under vigorous magnetic stirring, at 50 ºC, overnight, to achieve complete dissolution. Afterward, 0.6 g of methacrylic anhydride per 1 g of dissolved gelatin (very viscous liquid) was added slowly to the mixture for a high degree of methacryloyl functionalization and the reaction was left to proceed for 5 h, at RT, under stirring. Afterward, the solution was transferred into 50 mL tubes and centrifuged at 3500 g for 3 min, at RT, to remove unreacted methacrylic anhydride. The GelMA-containing supernatant was then decanted into another 50 mL tube, and the unreacted methacrylic anhydride deposited on the bottom was discarded. The supernatant was then diluted with 10 mL of pre-heated (37 °C) deionized water and transferred to a regenerated cellulose dialysis membrane (MWCO 6-8 kDa). GelMA was

dialyzed at 50 °C against deionized water for 5 to 7 days in a fume hood and protected from light. The purified methacrylated polymer was then freeze-dried as above mentioned.

2.2.3. Functionalized Biopolymers Spectroscopic Characterization

The inclusion of the acrylate photoreactive moieties in the different biopolymers was innitially characterized by proton nuclear magnetic resonance (^{1}H NMR) spectroscopy. All spectra were acquired on a Bruker Advance III 300 MHz spectrometer. For NMR analysis all samples were dissolved in 500 µL of deuterated water (D_2O) and transferred to 500 MHz NMR glass tubes (Wilmad, Cortenet, France). Samples were acquired with 256 scans, 8 dummy scans and with 18 secs of relaxation delay. The acquired spectra were processed by using the MestReNova v6.0.2 software. ^{1}H NMR data were used to determine HA and Gelatin degree of methacrylation as described in the literature [39], [40].

In addition, the chemically modified ECM-mimetic biopolymers were characterized by attenuated total reflectance Fourier Transformed Infrared spectroscopy (ATR-FTIR). For analysis, powdered samples were placed in a Brucker Tensor 27 spectrometer. A total of 256 scans, with a spectral resolution of 4 cm^{-1} were aquired in the spectral window spanning from 4000 to 350 cm^{-1}. The obtained data was processed in OPUS software and plotted in Origin software (v9.1, trial version).

2.2.4. Fluoraldehyde assay for GelMA functionalization characterization

The fluoraldehyde assay that detects primary amines was used to determine the degree of acrylate functionalization (DoF) in gelatin lysine residues as previously described in the literature, with minor modifications [38]. For this purpose, initially, a freshly prepared gelatin stock solution (0.5 mg/mL, in PBS pH =7.4) was used for computing a standard curve (0.02, 0.1, 0.5, 0.75 and 1.0 mg/mL). Before the experiments the fluoraldehyde reagent was warmed to RT. For samples analysis, 300 µL of GelMa samples solutions were mixed with 600 µL of the fluoraldehyde reagent. Control samples were prepared by mixing 300 µL of PBS with 600 µL of the fluoraldehyde reagent under vortex for 1 min. After 5 min of incubation 250 µL of each solution were placed in a 96-well black-clear bottom plate, and the fluorescence intensity at 450 nm using an excitation wavelength of 360 nm was measured by using a plate reader. The average fluorescence intensity was determined to each sample

and the fluorescence intensity of the PBS control was subtracted from the sample and standard solutions to determine the net fluorescence. The DoF was then calculated as DoF = ((0.5 − X)/0.5) × 100 %, where X is gelatin concentration in mg/mL.

2.2.5. Production of Quasi-Superhydrophobic Polystyrene Surfaces (PS)

The production of polystyrene (PS) quasi superhydrophobic surfaces was performed by using a simple, economical and fast procedure. In brief, circular polystyrene 90 mm petri dish plates were spray coated with the U.V. resistant FluoroThane-MW (WX 2100™) coating reagent that provides a contact angle ranging from 145° to 150°, i.e. quasi-superhydrophobic [41] as described by the manufacturer (Cytonix, MD, US). The entire petri dish surface was spray coated and left to dry overnight in a chemical safety fume hood, at room temperature. In the following day, the surface was washed with 99 % ethanol and oven dried at 37 °C for 5 days.

2.2.6. In-air production of spheroidal 3D microgels

Spheroidal microgels were produced by using a mechanical electronic repeater pipette (Eppendorf® M4 electronic digital repeater pipette) to dispense biopolymer aqueous solutions (1.25 % to 5 % w/v) onto PS quasi superhydrophobic surfaces. Spheroidal hydrogel droplets of different sizes were formed by dispensing various volumes (1 μL to 5 μL, Figure 5). The droplets were then photocrosslinked by using Irgacure 2959 (1 % w/v) as a photoinitiator and a U.V. curing system (Omnicure® S2000, Excelitas Technologies, US) that was used to irradiate hydrogels for 2 min, at an intensity of 10 mW/cm^2. Through this approach, different ECM-mimetic spheroidal hydrogels formed by HA-MA and HA-MA/GelMA blends were obtained.

2.2.7. Spheroidal microgels morphological characterization

Spherical microgels size and morphological characterization was performed by optical contrast microscopy and optical imaging. For size evaluation different microgel droplets were imaged in a stereomicroscope (Zeiss Stemi 508, Carl Zeiss, Germany), equipped with a 3 MPix color camera, and in a upright optical contrast microscope (Zeiss Primostar, Carl Zeiss, Germany) equipped with an A-Plan 5x/0.12 Ph0 M27 objective.

Macrographs of spheroidal hydrogel particles were also acquired by using a Canon EOS 1200d DLSR camera equipped with a macro lens.

2.2.8. Routine 2D *In vitro* Cell culture

In general, cells were cultured under aseptic conditions in temperature-controlled cell culture incubators at 37 ºC and with a 5% CO_2 atmosphere. For routine cell culture cells were grown in T-75 and T-175 cm^2 cell culture flasks, with cell culture media changes every other day. The human osteoblasts cell line (hOB) was cultured in DMEM-F12 medium supplemented with 10 % (v/v) FBS, 1 % (v/v) ATB and ascorbic acid (50 µg/mL, in PBS pH=7.4). The human prostate cancer cell line (PC-3) was maintained in RPMI 1640 medium (Glucose 2.5 g/L), supplemented with 10 % (v/v) FBS and 1 % (v/v) ATB. All cells were detached from culture flasks by using TrypLE™ Express enzyme detaching reagent upon attaining a confluence of 80-85 %.

2.2.9. Formulation of cell laden spheroidal 3D *in vitro* tumor models

Formulation of monotypic and heterotypic cell laden 3D spheroidal microgels was performed by using quasi superhydrophobic surfaces and U.V. mediated photocrosslinking. Initially, cells were detached as above mentioned and resuspended in equal volumes of HA-MA and GelMA, in order to obtain a homogeneous cell dispersion. After crosslinking for 2 min under U.V. light (λ= 365 nm, 10 mW/cm^2), 3D microgels were washed in DPBS and transferred to Ultra-Low-Adhesion (ULA) round-bottom 96-wells plates. 3D microgels were cultured in 200 µL of culture medium, at 37 °C and in a 5% CO_2 atmosphere. In the case of heterotypic 3D co-cultures, the culture medium was 50% RPMI 1640 and 50% DMEM F12 with 50 µL/mg ascorbic acid and 2.16 mg/mL of β-Glycerol phosphate. These last two compounds were added at day 3 and 7 of culture to mimic the microenvironment found in PC-3 bone metastasis. Production of the 3D tumor model did not follow any previously detailed procedure. Afterward, the cells were trypsinized and counted, pellets with the desired number of cells were formed by centrifugation at 300 g for 5 min, at RT. 3D *in vitro* prostate cancer tumor models' morphology and shape was analyzed overtime via optical contrast microscopy by using an inverted microscope (Primovert, Carl Zeiss, Germany). Images were acquired at specific time points (Days 3, 7 and 14).

2.2.10. Cell Viability assays

The cell viability of 3D spheroidal micro-tumors in mono and co-culture were analyzed at 3,7 and 14 days by using: (i) Alamar Blue® Cell Viability Assay and (ii) Live / Dead Assay. Alamar blue® was used to evaluate the metabolical activity of 3D tumor models during monocultures and co-cultures. Both assays were performed according to the manufacturer's guidelines, except for the incubation time of Alamar Blue®, which was performed overnight rather than the standard 2-4 h period. Resazurin reduction to pink colored resorufin was determined by fluorescence measurements (λ_{ex}: 540 nm, λ_{em}: 600 nm). All measurements were performed in a Synergy HTX microplate reader by using a 96-well black-clear flat bottom plate (VWR, CN: CORN3915). To assess cell viability, the microtumors were labeled with Calcein-AM (Cal-AM) (3 μg/mL) and Propidium Iodide (PI) (6 μg/mL) for 45 min at 37 °C. Following incubation, the 3D tumor models were washed 3 times with DPBS and immediately by fluorescence microscopy. Fluorescence micrographs were acquired in an upright Widefield fluorescence microscope (Zeiss Imager M2, Carl Zeiss, Germany), equipped with an Objective EC Plan-Neofluar 5x/0.16 objective and a 3MPix monochromatic camera. All micrographs were acquired and processed in Zeiss Zen SP2 Software (Carl Zeiss, Germany).

2.2.11. 3D *in vitro* tumor calcium deposition evaluation

To detect the calcium deposition, cultured 3D tumor spheroids were stained with Alizarin Red S dye. For this purpose, 3D tumors were initially fixed in 4% formaldehyde overnight, before incubation with 150 μL of Alizarin Red S (40 mM, pH=4.2), for 2 h in the dark, at RT. After incubation, the staining solution was aspirated and 3D tumor was rinsed three times with deionized water. All images were acquired at specific time points (days 7 and 14) by using a Stemi 508 Stereo Microscope.

2.2.12. Cell-specific Tracking in 3D microgels

Cell tracking assays were performed to access internal cellular organization and permanence at a populational level during co-culture within the produced HA-MA / GelMA microgels. For this purpose, the distinct cellular populations of PC-3 and hOB were

differentially stained with long-term cell tracking lipophilic dyes DiO and DiD (Thermofisher scientific, Alfagene, Portugal), as per the manufacturer's instructions. Briefly, upon cell trypsinization individual solutions were prepared for a final cellular concentration of 1 million cells per mL of serum free cell culture medium, to which 5 µL of staining agent (per mL of solution) were added. The solutions containing both cells and staining agents were then incubated for 30 min at 37 °C, after which 3x sequential washings, using serum containing medium, were performed. To prevent cell damage, between cycles of washing-centrifugation, cells were allowed to rest for 10 min at 37 °C after each wash.

PC-3 were stained with DiO (blue), and hOB with DiD (red) (Figure 16). These membrane staining are transferable to subsequent cellular generations, with no considerable signal loss being observed up to a period of 14 days of culture. Widefield fluorescence microscopy (Zeiss Imager M2, Carl Zeiss, Germany) analysis of produced microgels, containing PC3 (DiO) and hOB (DiD) stained populations, at days 7 and 14 allowed a qualitative assessment of both localization and aggregation patterns of the different cell populations.

2.2.13. Chemotherapeutic drug cytotoxicity screening in 3D *in vitro* tumor models

3D models of *in vitro* tumors in co-cultures were used as test platforms for evaluation of cisplatin cytotoxicity. On the seventh day of culture, the 3D models were incubated with cisplatin at different concentrations (100 µM, 150 µM, and 200 µM) [42] for 48 h. Cell viability was assessed by quantifying cellular ATP in 3D cell aggregates *in vitro* using a luminescence-based assay (Cell Titer Glo Luminescent viability assay, Promega, Madisson, WI, USA). CellTiter-Glo® assays were performed according to the manufacturer's instructions. After Cisplatin incubation, the medium was removed and 3D tumor models were incubated with a mixture of RPMI 1640/10% FBS / 1% ATB medium and CellTiter-Glo® reagent at a ratio of 1:1. The mixture was then stirred for 5 min and incubated for 25 min at RT. Luminescence was measured on 96-well opaque flat bottom white plates by using a Synergy HTX microplate reader programmed with an integration time of 1 sec.

3. Results and Discussion

The body of knowledge regarding the involvement of the tumor microenvironment as a barrier or promoter of cancer progression is constantly being expanded [43]. Being a complex multifactorial quasi organ, the tumor microenvironment is composed by both cellular and extracellular matrix components that are modulated and modulate disease progression. In this context, the microenvironment of secondary metastasis sites becomes equally important, especially for the study and testing of novel anti-metastatic therapeutics, and as such requires robust models that are capable of mimicking it. During the establishment of secondary prostate cancer tumors into the bone microenvironment migrating cancer cells modify the resident bone-marrow microenvironment. As recently reviewed by Park and coworkers 2018 [44], migrating prostate cancer cells of advanced stage III and IV tumors preferentially target the highly vascularized microenvironment of the red-marrow. These metastatic cells are attracted not only by the anatomical characteristics that defined these tissues but also due to chemoattractant gradients [45]. For example, increased expression of C-X-C chemokine receptor type 4 (CXCR4) receptor by migrating prostate cancer cells is believed to allow these cells to home into the C-X-C motif chemokine ligand 12 (CXCL12) reach microenvironment of bone-marrow in a similar fashion to the behavior exhibited by bone-marrow derived mesenchymal stem cells [44].

Upon establishment in the bone-marrow prostate cancer cells can enter a state of dormancy, in order to evade the immune system. Moreover, cancer cells also immediately upon invasion begin promoting altered phenotypes on bone-marrow resident cells, ultimately modifying the surrounding microenvironment to a pro-tumoral, mostly osteoblastic, landscape [44]. As a consequence of these communications and phenotypic alteration, uncontrolled bone-formation takes place [46]. In this context, HA and collagen are reported as to major components of ECM present in the process of the metastatic niche ECM [46]. Hyaluronic acid (HA) is a non-thrombogenic and non-immunogenic anionic biopolymer, that consists of D-N-acetylglucosamine and D-glucuronic acid repeating units, covalently linked through alternating β-1,4 and β-1,3 glycosidic bonds [47], [48]. This polysaccharide is well-recognized as a major ECM component in a variety of tissues, is a highly expressed in bone ECM and is associated with prostate tumor growth [7], [36], [49], [50]. It is produced by hyaluronan synthases and secreted into the extracellular space as a constituent of the extracellular matrix (ECM) [47], [51],[52].

HA is highly expressed by motile PCa epithelial cells and associated stromal cells, being concentrated within the tumor-associated stromal ECM, making it an integral component of the microenvironment of bone metastatic cancer cell [51], [53]. HA can be degraded by hyaluronidase, so an HA-rich environment can be partially degraded, creating a permissive pathway for the migration of tumor cells [47],[53].

Gelatin is a biocompatible material which is widely used as a scaffold to promote cell fate processes in 3D constructs, either alone or in combination [54]. It can be obtained by partially hydrolyzing collagen which comprises approximately 95% of the organic matrix of bone [10], [48]. Gelatin contains peptide sequences as binding sites (e.g., Arg-Gly-Asp sequence) for integrins and protease sensitive sites for matrix metalloproteinases (MMPs), being chemically similar to native tissues ECM [54]. This cationic biomaterial degrades due to its matrix metalloproteinase (MMP) sensitive protein sequences, which are essential to allow for the deposition of newly formed ECM. Therefore, hyaluronic acid-gelatin hydrogels may mimic the ECM of native tissues. However, these biomaterials when used singularly to generate 3D microgel models, demonstrate several disadvantages, such as the non-adhesive nature of HA and its low stability, and gelatin hydrogels exhibit mechanical weakness and rapid degradation [55]. To improve the physical and biological properties of these macromers they were chemically modified with methacryloyl chemical groups.

3.1. Spectroscopic Characterization of methacrylated hyaluronic acid (HA-MA)

Hyaluronic acid consists of two saccharide rings as a repeating unit that gives it biodegradable and biocompatible properties. The polymer can be chemically modified or methacrylated (MA) to facilitate crosslinking upon exposure to UV light [48]. Herein, we modified HA with the methacrylate group through a reaction with glycidyl methacrylate, as reported in the literature [37], to obtain methacrylated hyaluronic acid. The ^{1}H NMR spectra (Figure 1) and FTIR (Figure 2) are shown and allowed the confirmation of the substitution.

In the ^{1}H NMR spectrum of methacrylated hyaluronic acid, two new peaks with a chemical shift of 5.8 and 6.2 ppm were obtained. These peaks are characteristic of methacrylate vinyl groups (Figure 1, Peak 1) [43].

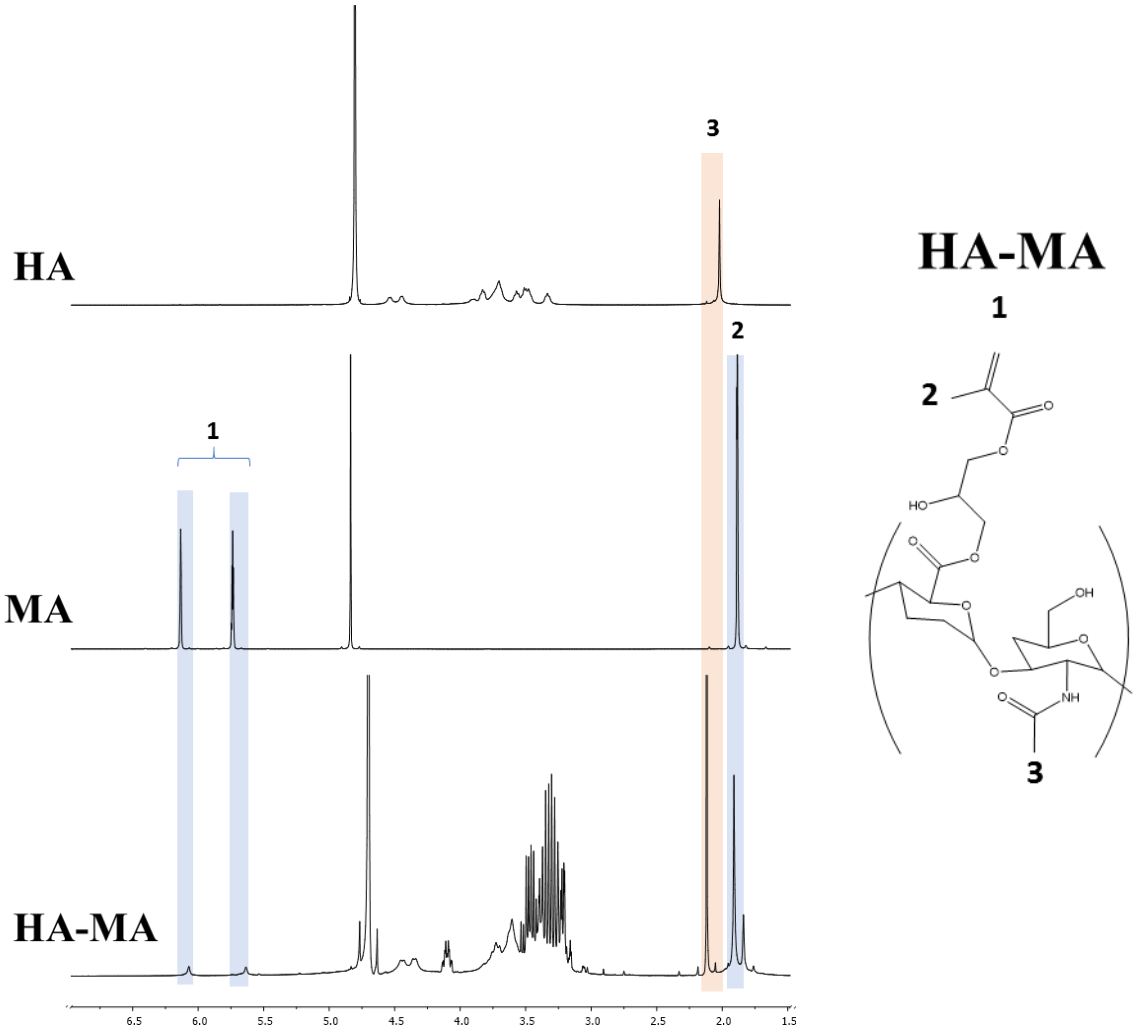

Figure 1. ^{1}H NMR spectra of methacrylated HA. The new peaks were observed at approximately 5.8 and 6.2 ppm, these correspond to methyl groups of methacrylated moieties included in HA polymeric backbone. These peaks were not present in the unmodified HA. The peaks 2 and 3 located at approximately 1.8 and 2.1 ppm respectively, are the methyl group signals.

Following chemical modification of HA polymeric backbone the degree of substitution was calculated as described in the literature by the integrated intensity of the double bond protons to those of the HA polymeric backbone [37]. The synthesized HA derivative had a 35% degree of methacrylation, indicating that a significant amount of HA monomers is modified with photo-crosslinkable groups. It is important to emphasize that the multiplicity of peaks observed between δ 3.0 ppm and δ 3.8 ppm are attributed to the high degree of HA methacrylation as also observed in other recent reports [37].

In addition, HA methacrylation was also evaluated by using ATR-FTIR spectroscopy (Figure 2).

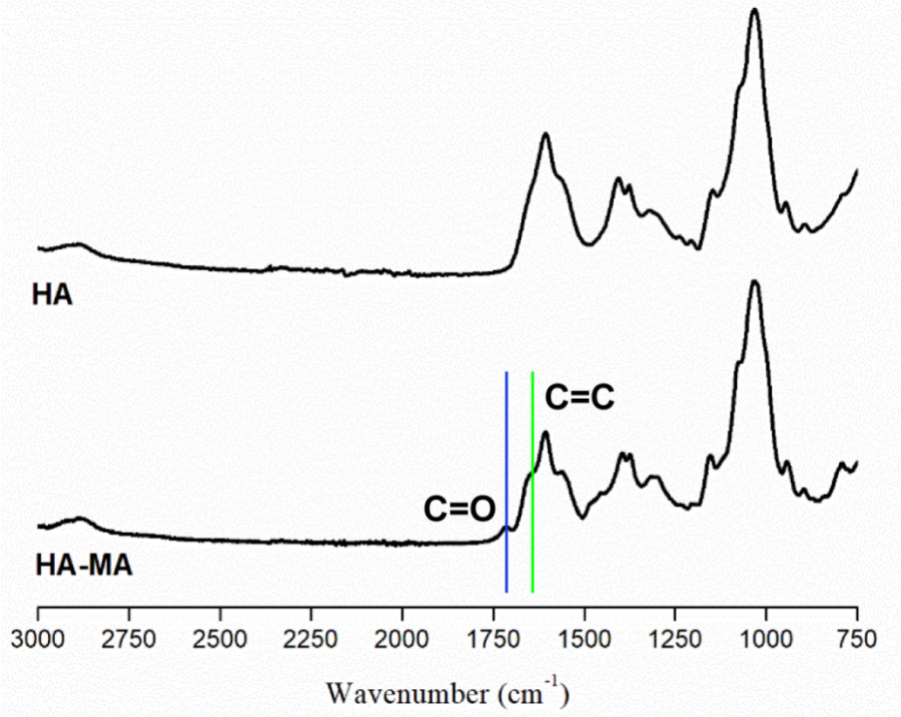

Figure 2. Absorbance FTIR spectra of HA and methacrylated HA derivative.

ATR-FTIR spectroscopy demonstrated the existence of a new peak at ~1730 cm^{-1} which can be assigned to the C=O bond and also the existence of a second new peak at 1643 cm^{-1} that is assigned to the C=C bond (Figure 2). These findings further corroborate the successful functionalization of HA polymeric backbone with methacrylate moieties.

3.2. Spectroscopic Characterization of gelatin-methacryloyl (Gel-MA)

Although gelatin can form physically crosslinked hydrogels through temperature-induced physical gelation, a high concentration of gelatin is often needed for this process. To improve hydrogel stiffness, a number of crosslinking strategies have been adopted, including the use of chemical modification to support photo-crosslinking (e.g., methacrylic anhydride (MA), that is currently the most widely used to gelatin modification) [38]. Gelatin has abundant amino, hydroxyl, and carboxyl groups that can be used for modification. Therefore gelatin-methacryloyl was synthesized through the reaction of the amino and hydroxyl groups in gelatin molecules with methacrylic anhydride. The ^{1}H NMR spectra of gelatin (Gel) and Gel-MA macromers is shown in Figure 3. As the results indicate the MA modification of lysine residues could be confirmed by the decrease in lysine protons signal at δ = 3.31 ppm, indicating the conjugation of lysine with MA. In addition, the

increases in the methacrylate vinyl group signal at δ = 5.7 ppm and δ = 5.9 and the methyl group signal at δ = 2.2 ppm reinforce the occurrence of the linkage between MA and gelatin.

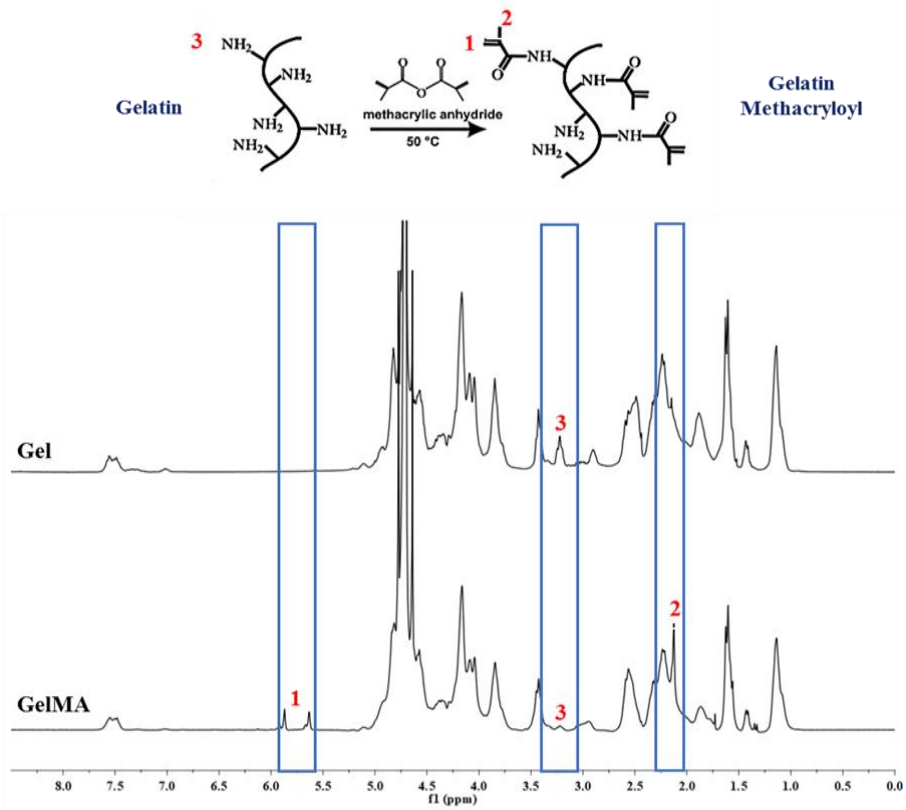

Figure 3. Schematics of gelatin methacrylate substitution. ^{1}H NMR spectra were recorded for unsubstituted gelatin and GelMA. The MA modification of lysine residues can be confirmed by the decrease in the lysine signal at δ = 3.31 ppm (peak labeled with number 3), and the increases in the methacrylate vinyl group signal at δ = 5.7 ppm and δ = 5.9 ppm (peaks labelled with number 1) and the methyl group signal at δ = 2.2 ppm (peak labelled with number 2).

3.3. Fluoraldehyde assay for GelMA functionalization characterization

To estimate the degree of functionalization of the gelatin the fluoraldehyde assay was performed. To this end, after measuring the fluorescence of each standard gelatin solution, a calibration curve was established which correlates the fluorescence with the concentration of gelatin in the solution (Figure 4). From the calibration curve obtained, and the average absorbance read for the Gel-MA sample, the respective gelatin concentration was calculated. In this way, the fluorescence intensity of the Gel-MA sample corresponding to a gelatin concentration of 0.0524 mg/mL on the calibration curve and the residual amine concentration was determined. The degree of functionalization (DoF) was then calculated as DoF = (0.5 – 0.0524)/0.5 × 100%, thus DoF obtained for synthetized Gel-MA was 89.53%.

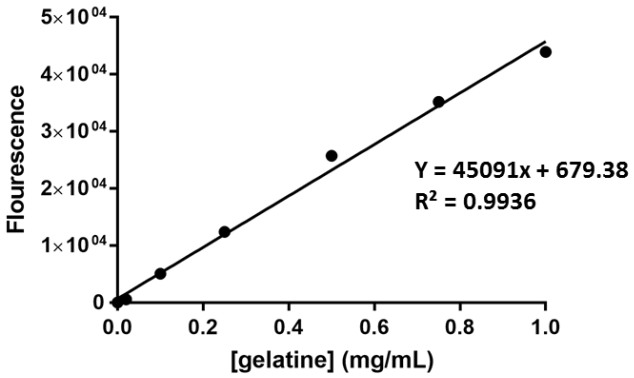

Figure 4. The degree of methacrylate substitution was determined for the GelMA formulations via fluoraldehyde assay: linear calibration curve based on the standard gelatin solutions was constructed. The fluorescence intensity of the GelMA sample corresponding to a gelatin concentration of X mg/ml (X= 0,0524 mg/mL) on the calibration curve and the residual amine concentration was determined. The degree of functionalization (DoF) was then calculated as DoF = (0.5 − X)/0.5 × 100%, thus DoF obtained for synthetized GelMA was 89.53%.

3.4. Spheroidal microgels morphological characterization

As previously demonstrated, *in vivo* microtissues with sizes superior to 100-200 µm lack oxygenation and have a poor nutrient aport in their core [56]. In the context of solid tumors, such characteristics are also common in the poorly vascularized environment of expanding tumor mass at initial stages. In order to access which conditions of micro-tumor production would allow an ideal size, for recapitulation of such physiological conditions, distinct volumes of HA-MA droplets were dispensed with a repeater pipette on quasi-superhydrophobic surfaces. We started by analyzing particle diameter with HA-MA microgel formulations, testing multi-volume droplets (1µL, 2µL, 3µL, and 5µL) to determine the most appropriate size to recapitulate a microtumor. To verify the spherical shape and the diameter of the particles, they were analyzed using a stereomicroscope and an inverted optical microscope. The obtained results demonstrate that all 3D microgel formulations have a well-defined spherical shape.

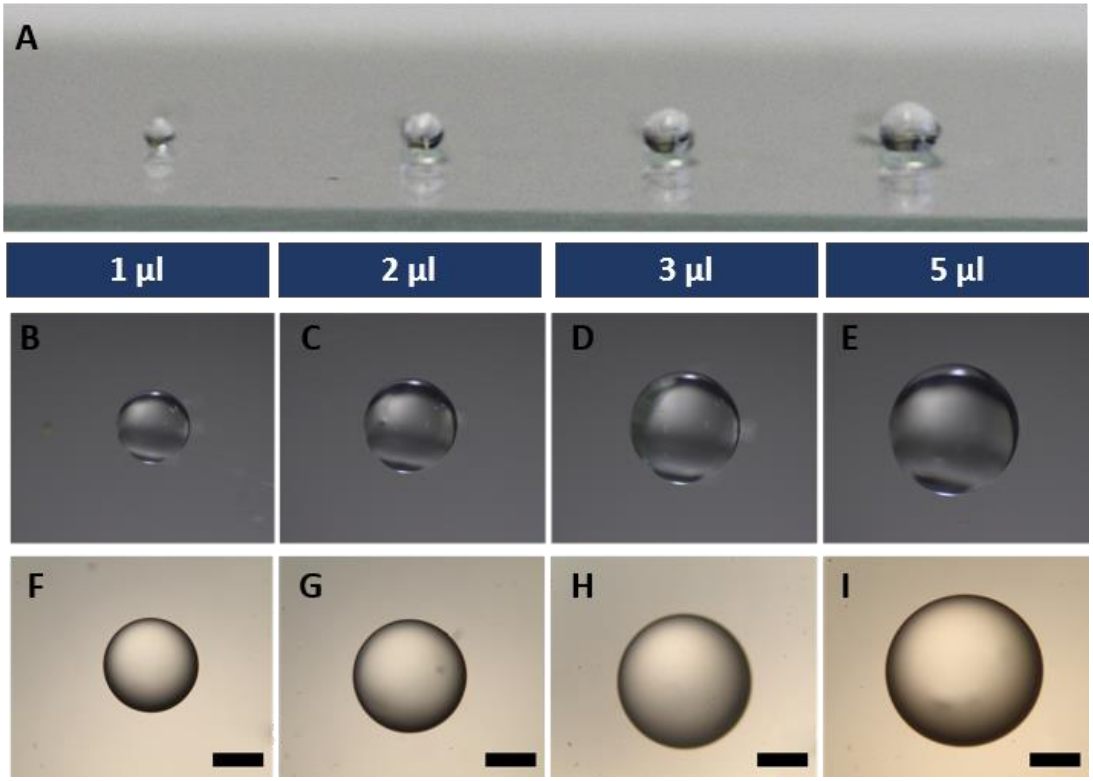

Figure 5. Morphological characterization of 3D microgels formed by 10% HA. A) Enlarged photograph of variation of droplet size with deposited volume (side view); B) Particle with a volume of 1µL seen in stereomicroscope (Zeiss Stemi 508); C) Particle with a volume of 2µL seen in stereomicroscope; D) Particle with a volume of 3µL seen in stereomicroscope; E) Particle with a volume of 5µL seen in stereomicroscope. F) 1 µL particle seen in an inverted microscope (Primvert Car Zeiss, Germany); G) 2 µL particle seen in the inverted microscope; H) 3µL particle seen in inverted microscope; I) 5µL particle seen in inverted microscope. Scale bar is 500 µm.

Moreover, as demonstrated in Figure 6 the particle size varied with the increase of the deposited droplet volume. The particles of 1µl, 2µL, 3µL, and 5µL presented a mean diameter of (821.9 ± 41.42µm), (1090.8 ± 44.64µm), (1348.7 ± 51.96µm) and (1834.1 ± 26.31µm), respectively.

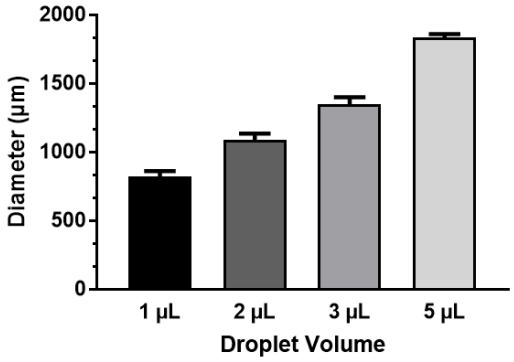

Figure 6. Variation of particle diameters with increasing droplet volume. Measurement of the diameter of the various particle sizes was performed in the ImageJ software. Data is presented as mean ± s.d, *n*= 12.

The volume of 1µL was chosen given their preferred mean size of ~821 µm. It is important to mention that this is an innovative approach that easily allows the obtention of spherical microgel constructs compatible with HTS and already established protocols for downstream spheroid analysis. To the best of our knowledge, this is the first report of quasi-superhydrophobic surfaces use for the assembly of HA-MA / Gel-MA microgels containing co-cultured PC-3 and hOB populations.

3.5. HA-MA 3D Microgels for monotypic tumor spheroids assembly

HA has been reported to play significant roles in cellular proliferation, angiogenesis and cell-receptor interactions [47],[53]. Therefore, HA-based materials have been widely used for *in vitro* study of novel therapeutics targeting bone metastatic prostate cancer cells [51]. However, when this biomaterial is used singularly to generate 3D models, may demonstrate some disadvantages mainly because the non-adhesive nature of HA limits its use when 3D cell proliferation and bioactivity is required [48].

Initially, to optimize the cell density of 3D microgel encapsulated cells and verify if PC-3 cells adhere to this biopolymer we begun by producing HA particles with a low cell density (4000 PC-3 cells per particle (per uL) and a high cell density (20 000 PC-3 cells/µL. As visualized in Figure 7 A1, A4 and A7, 3D microgels formed at the lowest HA were distroyed in culture. For this reason, the concentration of HA 2.5% was no longer used. From the optical images, it is clear that a higher cell density and cells compaction was observed for the bioencapsulation of 20000 cells in 3D microgels volume.

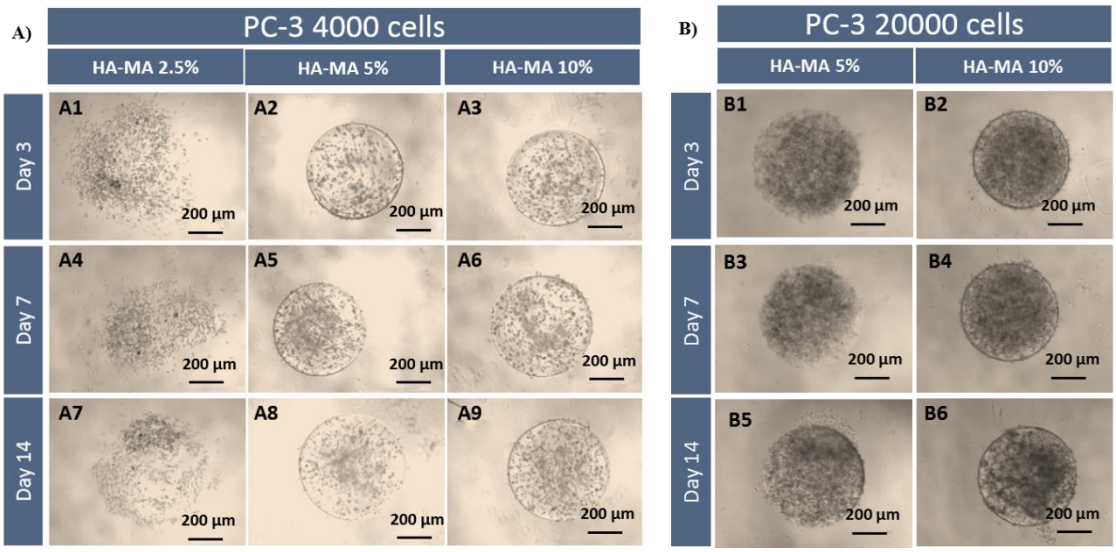

Figure 7. Follow up of PC-3 cancer cells encapsulation in 3D HA microgels along time. A) Optical micrographs of cell laden 3D microgels formed by different HA-MA concentrations. B) Optical micrographs of HA 5% and HA 10%. 3D microgels encapsulating 20 000 PC-3 cells per particle.

Metabolic activity and cell dead were then verified by AlamarBlue (Figure 8 A and C) and LiveDead (Figure 8 B), respectively. The obtained results indicate that even with an increase in cell number per particle, the metabolic activity decreases over time. We hypothesize that this result is a consequence of HA non-adhesive nature that prevents its use in applications where it is necessary to maintain cells metabolic activity and proliferation, such as those of tumor mimicking *in vitro* models. As observed between day 3 and 7 only a small loss in cell viability. However, when PC-3 3D HA microgels were cultured for extended periods of time (14 days) a significant loss in metabolical activity was observed. This was further corroborated by the increased number of dead cells in Live-dead assay (Figure 8 B). Despite this decrease in viability, no necrotic core formation was observable in all 3D microgel models. Instead, a generalized cell death seemed to occur, perhaps a result of cells incapacity to adhere and effectively spread. Such observations are concordant with previous reports, where cells cultured within HA scaffolds seem to loose the ability to acquire a physiological three-dimensional conformation and die [48].

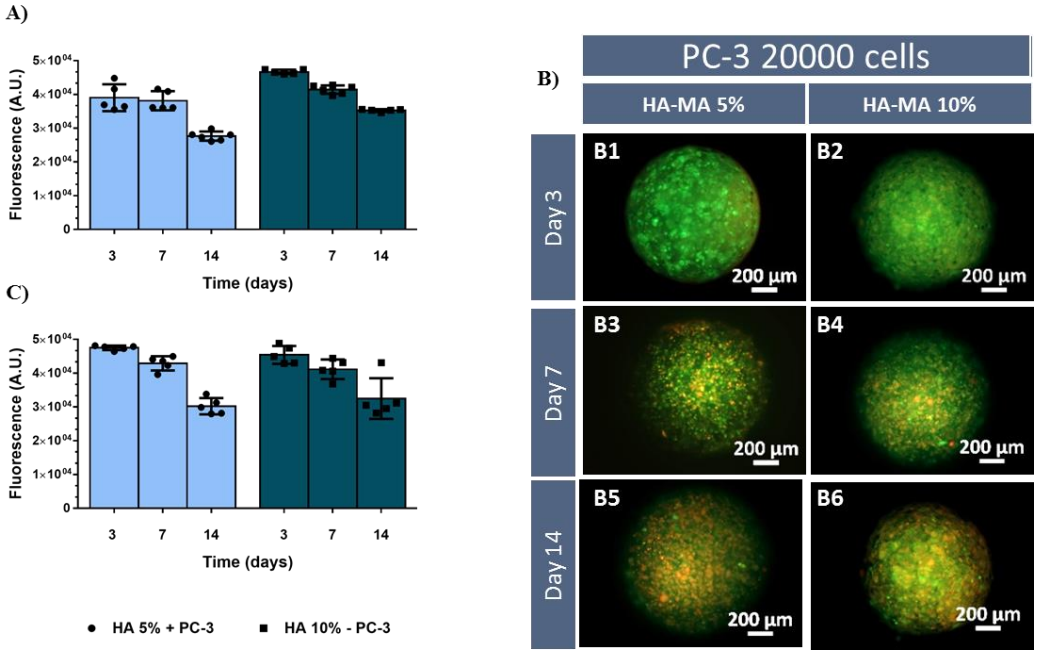

Figure 8. Assessment of PC-3 cells viability in 3D HA microgels along time. A and C) AlamarBlue metabolic analysis of particles with 4000 and 20000 cells per particle, respectively. B) Live Dead analysis of higher cell density particles (20000 cells per particle). Green channel – Calcein-AM, Red channel: PI.

3.5.1. HA-MA/Gel-MA 3D microgels for monotypic tumor models assembly

Contrarily to HA, gelatin is a well-established natural scaffold containing extensive collagen fragments to which cells can adhere through integrins and is known for its well reported biocompatibility and ECM-mimicking properties. As such, the use of GelMA for microgels formation was hypothesized to not only improve cell adhesion properties of the microgel matrix but also to provide crucial collagen I motifs that mimic those of native bone tissue. Gelatin addition was performed in a (1:1) volume ratio to HA-MA. Initially, HA-MA and Gel-MA microgels were manufactured through U.V. photocrosslinking, alloying the generation of 3D microgels for studying cell-cell and cell-biomaterial interactions in a controlled manner.

To verify if the addition of GelMA affected the diameter of 3D microgels, various formulations were fabricated. Figure 9 (A and B) shows the variations of particles diameter according to the variation of GelMA amounts. As optical micrographs demonstrate, particle diameters remain constant regardless of the type of formulation used, hence it becomes clear that droplet volume is the most important parameter to control 3D microgel spheres diameter upon manufacture in quasi-superhydrophobic platforms.

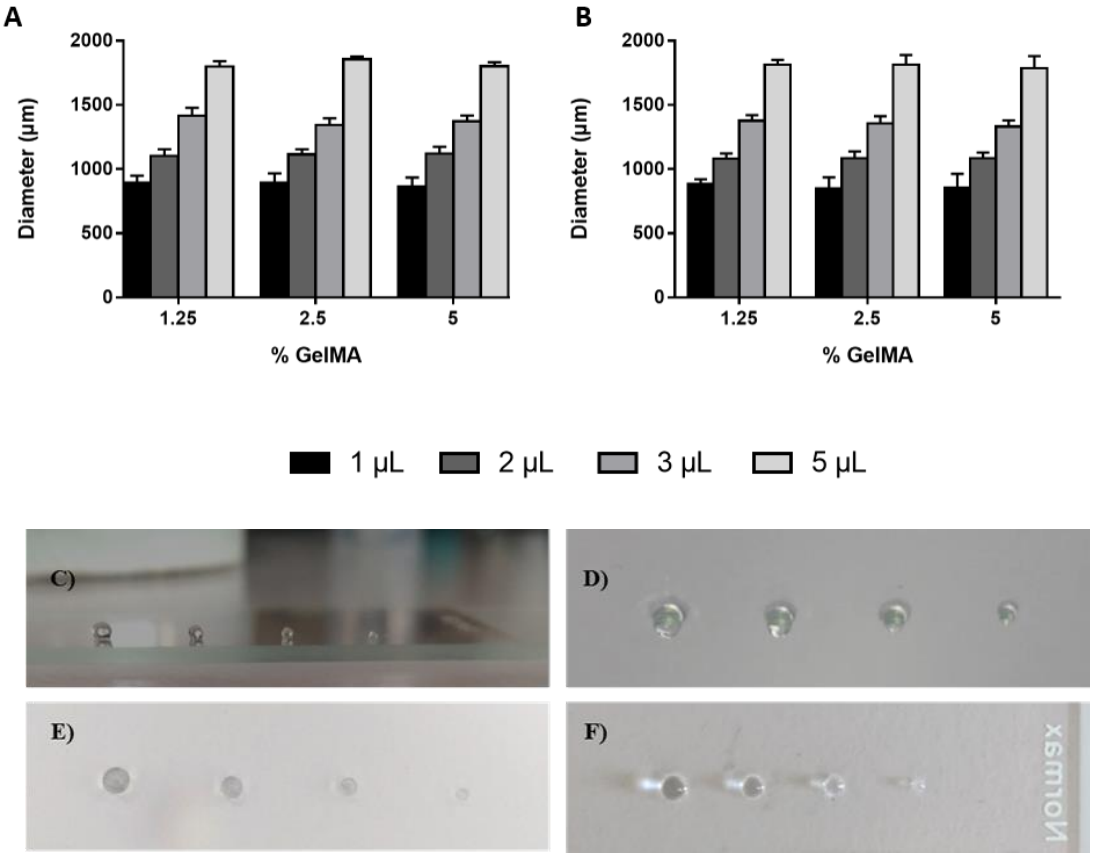

Figure 9. HA-MA/GelMA 3D microgels size and morphological characterization. A) Variation of the HA-MA 2.5% particles with several concentrations of Gel-MA. B) Variation of the HA-MA 5% particles with several concentrations of Gel-MA. C) Side view of 2.5% HA particles with Gel-MA. D) Side view of 5% HA particles with Gel-MA. E) Top view of HA particles 2.5%. F) Top view of HA particles 5%.

HA-MA/Gel-MA 3D microgels formed with 1 µL droplets presented sub-millimeter sizes similar to those generally obtained for scaffold-free *in vitro* 3D tumor spheroids. Therefore, in all following assays, 1 µL volumes were used to produce 3D tumor microgel models to promote a closer cell-cell contact in microgels 3D volume. To fully characterize this new ECM-mimetic matrix for *in vitro* tumor models assembly various cell densities per microgel were (Figure 10 I to VI).

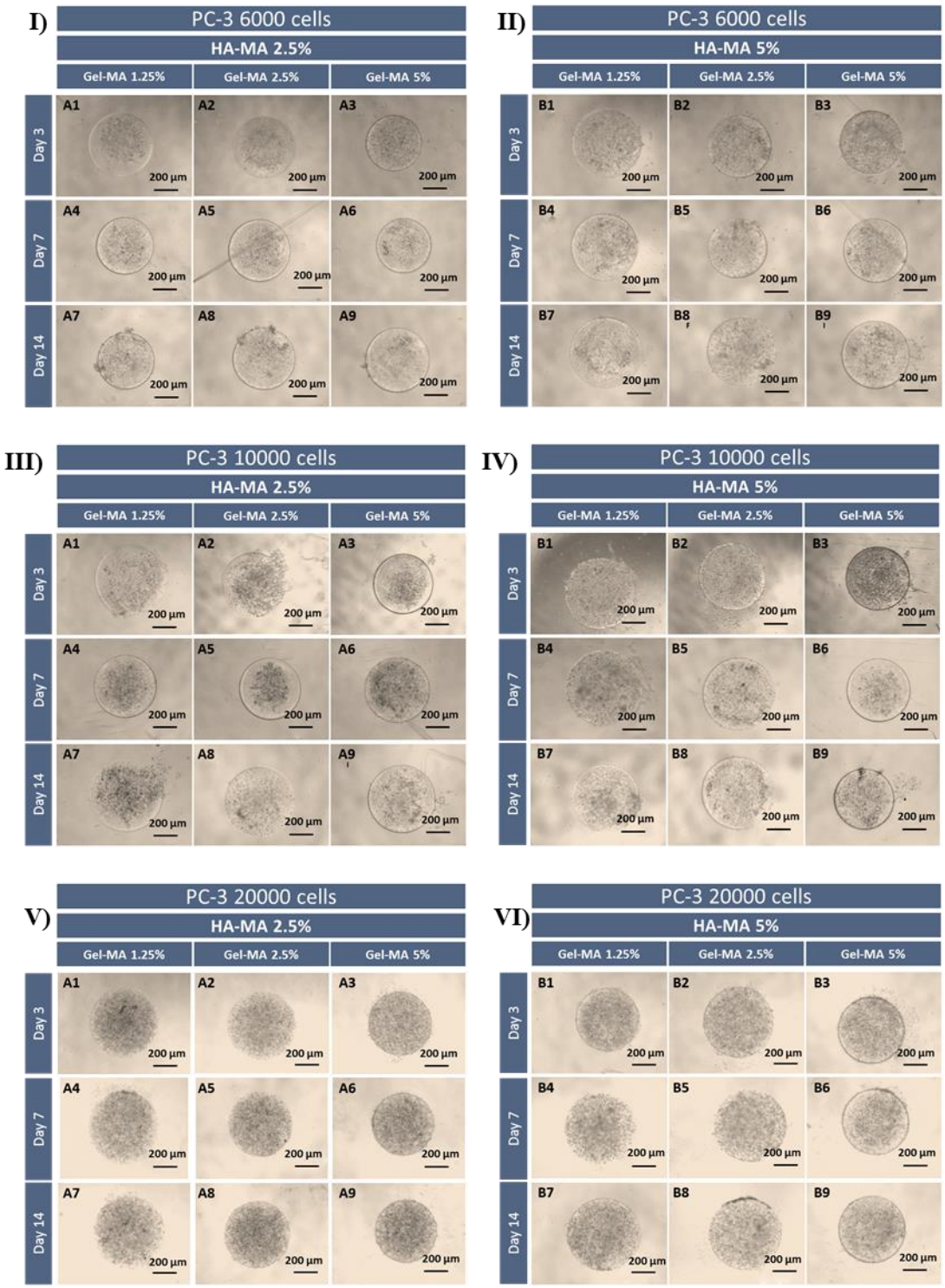

Figure 10. Optical micrographs of 3D HA-MA/GelMA microgels bioencapsulating PC-3 cells along time. I and II) 2.5% and 5% HA-MA 3D microgels with 6000 PC-3 / µL, respetively. III and IV) 2.5% and 5% HA-MA particles with 10000 PC-3 / µL, respectively. 2.5% HA-MA and 5% HA-MA particles with 20000 PC-3 / µL, respectively.

Metabolic activity and cell dead were verified by AlamarBlue (Figures 11 A to F) and Live/Dead (Figures 12 I to VI) respectively. With the addition of gelatin, the metabolic

activity increased over time in all 3D microgels with the various cell densities tested, a desirable result since these cultures better mimic the proliferative nature of PC-3 metastasis in bone. Moreover, this increase in cells metabolic activity was corroborated by Live/Dead analysis since no significant death was observed at 14 days.

Among all the conditions, the 3D microgels with 20000 encapsulated cells were those that presented the highest metabolic activity, therefore, these conditions were chosen for the posterior establishment of heterotypic 3D microgel PC-3 osteoblast tumor models.

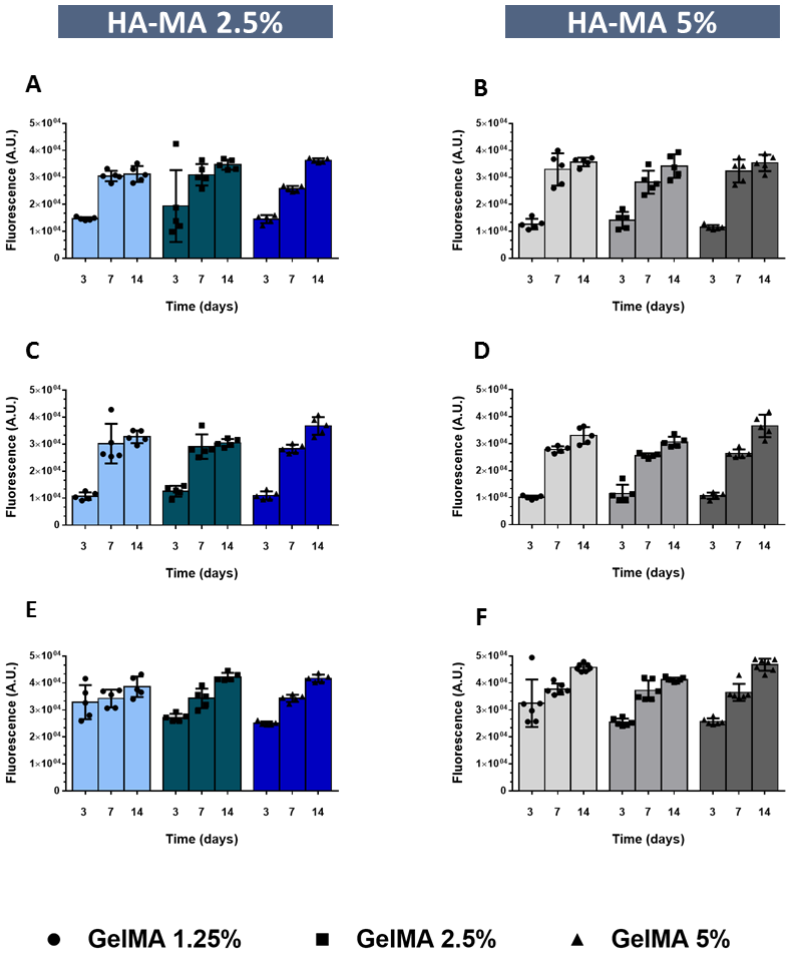

Figure 11. Metabolic activity analysis of 3D microgel monocultures formed by various concentrations of gelatin and cells, at 3,7 and 14 days. A and B) 2.5% HA-MA and 5% HA-MA particles with 6000 PC-3 / µL, respetively. C and D) 2.5% HA-MA and 5% HA-MA particles with 10000 PC-3 / µL, respectively. E and F) 2.5% HA-MA and 5% HA-MA particles with 20000 PC-3 / µL, respectively. Data is presented as mean ± s.d., *n*=3.

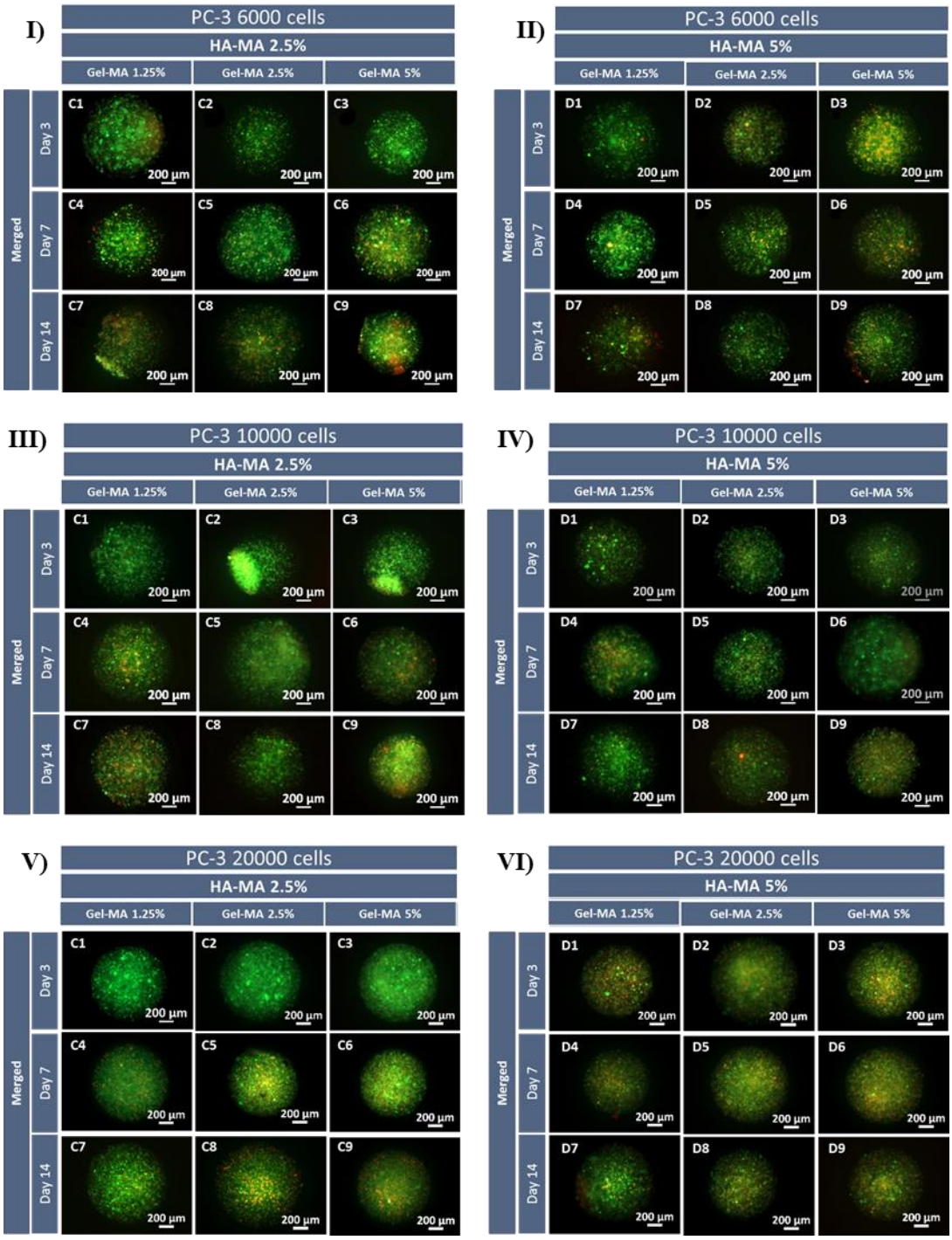

Figure 12. Fluorescece micrographs of LiveDead assays performed at 3,7 and 14 days of PC-3 cutlure in different 3D microgels. I and II) 2.5% HA-MA and 5% HA-MA particles with 6000 PC-3 / µL, respetively. III and IV) 2.5% HA-MA and 5% HA-MA particles with 10000 PC-3 / µL, respectively. V and VI) 2.5% HA-MA and 5% HA-MA particles with 20000 PC-3 / µL, respectively.

3.6. HA-MA/Gel-MA 3D microgels for heterotypic tumor models assembly

As previously discussed, metastasis of prostate cancer cells to the bone microenvironment is a process involving several sequencial steps: 1) cancerous cells are released from the primary site after suffereing a process of EMT; 2) after which the invading cancer cells enter into the blood or lymphatic circulatory system and either by chance or natural tropism migrate into mestastic sites (seed and soil), 3) where upon exit of the vasculature these circulating cancer cells invade and colonized the growth-factor rich bone microenvironment, establishing a secondary tumor site. Throughout the whole process from the primary tumor to metastasis, it is widely accepted that non-malignant cells actively influence the fate of cancer cells [9]. Understanding the role of the bone cells that compose this new microenvironment (osteoblasts, osteocytes, osteoclasts, hematopoietic cells, mesenchymal cells, and immune cells) in the attraction, establishment and consequent interaction with the secondary tumor site, is a crucial starting point for the development of novel therapies targeting metastasis [10]. Factors secreted by prostate cancer cells alter the balance between the activity of osteoblasts (bone forming cells) and osteoclasts (bone lysis cells). Both are involved in the progression of prostate cancer metastases because they inhibit these factors and determine the phenotype of bone lesions. Prostate cancer metastases cause osteoblasts (excessive bone formation), osteolytic (bone lysis), or mixed bone response [11], [12].

For the formation of 3D bone tumor metastasis models PC-3 were co-encapsulate with osteoblast cells in 3D microgels at a 1:1 ratio [11]. This ratio was selected from previous literature reports that indicate it to be a suitable representation of prostate-bone models. Figure 13 A and B shows optical images of the established 3D heterotypic microgel models containing the tumor ECM-mimicking components (HA-MA and GelMA).

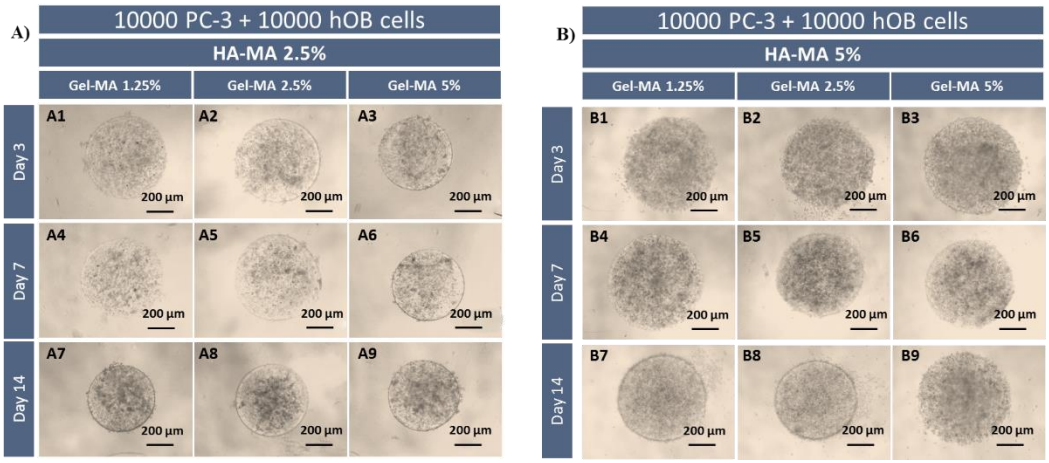

Figure 13. Optical images of 3D tumor models of HA-MA and Gel-MA with PC-3 and human osteoblasts. A) Co-culture of HA-MA 2.5% and Gel-MA with 1: 1 ratio of PC-3 and human osteoblasts. B) Co-culture of HA-MA 5% and Gel-MA with 1: 1 ratio of PC-3 and human osteoblasts.

Metabolic assays (Figure 14) demonstrated an increased metabolic activity over time, which would be expected in all concentrations, as osteoblasts are associated with the proliferation of prostate cancer cells as before mentioned. However, the metabolic activity at 14 days in the HA-MA 2.5% Gel-MA 5% and HA-MA 5% Gel-MA 5% conditions is slightly higher than on the other conditions tested and for this reason, these conditions were selected for testing of drug. Live/Dead analysis (Figure 15) evidences some cell death at later culture stages in HA-MA 2.5% /GelMA 5% formulation at 14 days, however, the number of dead cells is much lower than that of live cells.

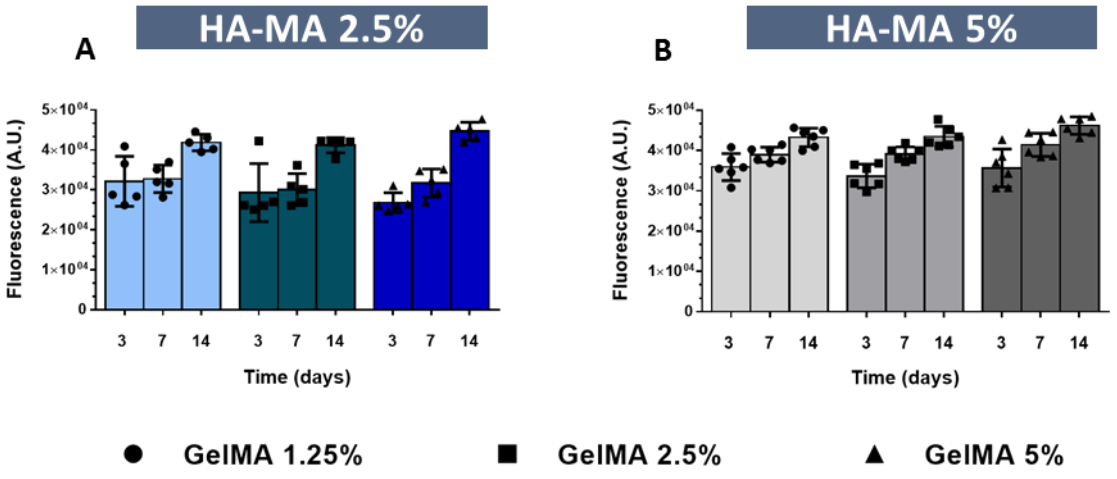

Figure 14. Metabolic activity of 3D heterotypic PC-3/hOB microgel models. A) Co-culture of HA-MA 2.5% and Gel-MA with 10000 PC-3 and 10000 human osteoblasts. B) Co-culture of HA-MA 5% and Gel-MA with 10000 PC-3 and 10000 human osteoblasts. Data are presented as mean ± s.d., *n*=3.

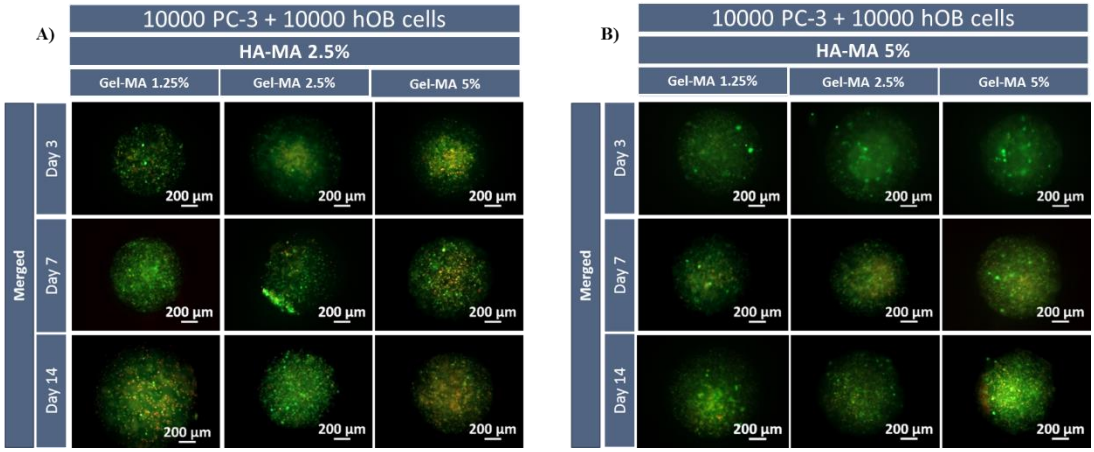

Figure 15. Pictures of LiveDead at 3,7 and 14 days of cocultures. A) Co-culture of HA-MA 2.5% and Gel-MA with 1: 1 ratio of PC-3 and human osteoblasts. B) Co-culture of HA-MA 5% and Gel-MA with 1: 1 ratio of PC-3 and human osteoblasts.

3.7. 3D microgel heterotypic *in vitro* tumor models' mineralization

Matrix mineralization consists of the deposition of bone tissue components such as extracellular calcium deposits. The presence of calcium in 3D PC-3:hOB co-culture microgels was determined by using the Alizarin Red S assay which provides a red coloration if calcium deposits are detected. The obtained results clearly demonstrate that in time calcium deposits are more evident. Interestingly, a higher calcium deposition was obtained for 3D microgels assembled with higher gelatin concentration, (Figure 16). These important results demonstrate the effect of osteoblasts when in closed culture with PC-3, as previously discussed and evidence the bioactivity of bone forming cells upon bioencapsulation in the fabricated 3D ECM-mimetic microgels.

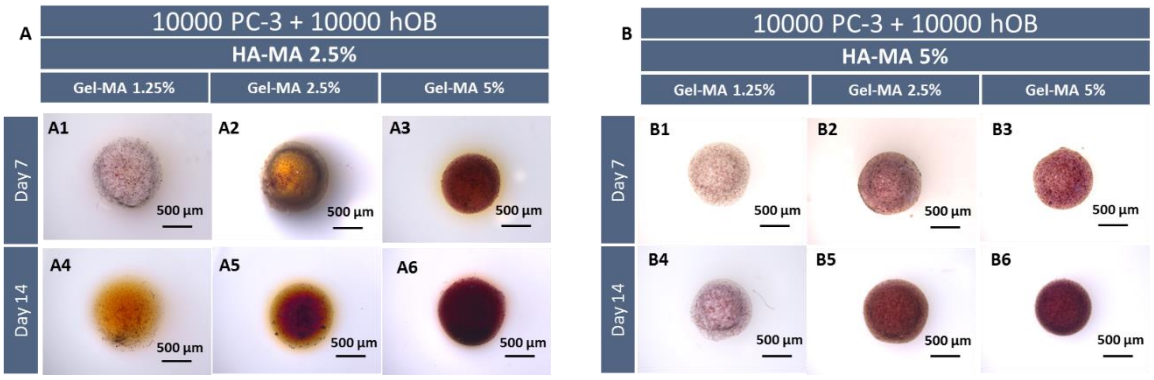

Figure 16. Images of calcium quantification in cocultures over time. A) Co-culture of HA-MA 2.5% and Gel-MA with 1: 1 ratio of PC-3 and human osteoblasts. B) Co-culture of HA-MA 5% and Gel-MA with 1: 1 ratio of PC-3 and human osteoblasts. Scale bar is 500 µm.

3.8. Cell-specific tracking in 3D microgels

In order to further understand the organization and behavior of co-cultured cells within the 3D microgel matrix, we labeled PC-3 with DiO and osteoblasts with DiD cell tracking fluorophores and analyzed the localization and aggregation patterns of the different cell populations at 7 and 14 days of cultures (Figure 17). Interestingly the signaling of PC-3 (blue) was always higher than that of hOB cells.

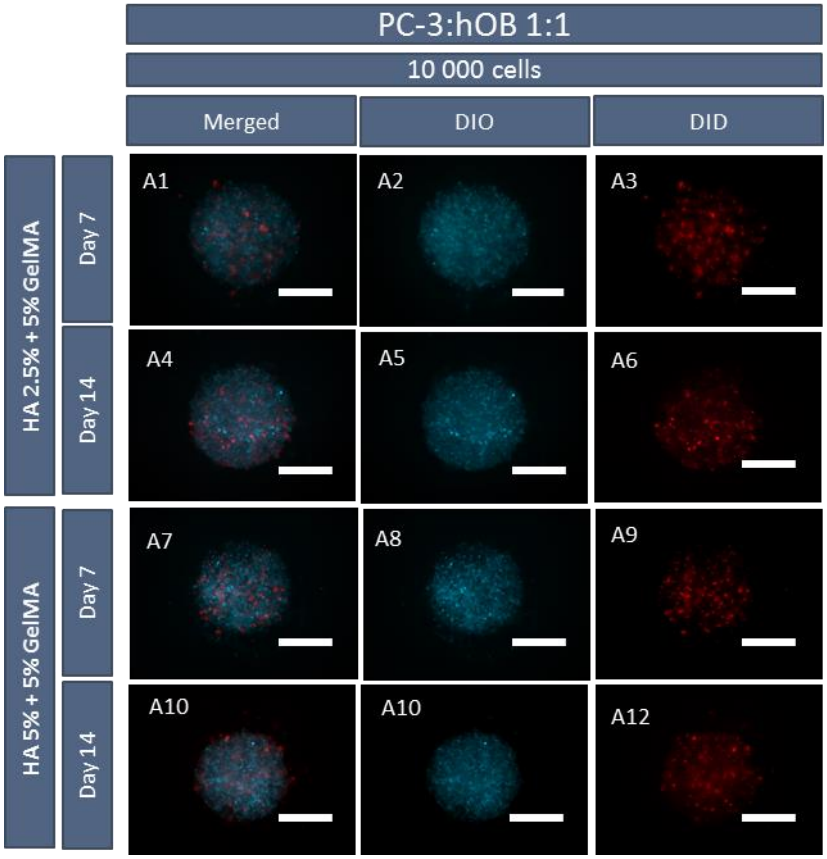

Figure 17. Widefield fluorescence micrographs of cell-specific tracking in different 3D microgels at 7 and 14 days. PC-3 were stained with DiO (blue), and hOB with DiD (red). Scale bar is 200 µm.

Such results could be attributed to the higher cell proliferation rate of PC-3 cells when compared to that of human osteoblasts and is an important factor that must be taken into consideration in drug screening assays. Moreover, cell-specific tracking assays demonstrate that no preferential spatial organization of PC-3 nor hOB occurs. Taking this data into consideration the formed 3D microgels were then used for the evaluation of cisplatin cytotoxic potential.

3.9. Anti-cancer drug screening in 3D microgel *in vitro* tumor models

As the formulations 2.5% HA-MA-5% Gel-MA and 5% HA-MA - 5% Gel-MA were those where a higher calcium deposition was observed they were selected for drug screening assays. Before, performing the drug screening assays, scaffold-free monotypic and heterotypic 3D tumor spheroids were established via forced floating techniques (Supplementary Figure S1) and were used as controls to evaluate the influence of tumor ECM mimetic microgel matrix. The size, morphology and shape of control 3D spheroids were monitored over 5, 7 and 14 days. It is clearly observable that monotypic and heterotypic 3D spheroids have different sizes and morphologies (Supplementary figure S1). The size in both cultures increases over time, however the spheroids with hOB are significantly more compact and exhibit a necrotic nucleus, a feature that is not visible in monotypic 3D spheroids. This clearly demonstrates the effect of PC-3 and hOB cell-cell interactions, evidencing its importance in the recapitulation of prostate-bone metastasis *in vitro*.

In these studies, 3D microgel co-cultures were subjected to various concentrations of cisplatin (100 µM, to 200 µM) an anti-cancer pharmaceutical clinically approved for the treatment of bone cancer [42]. As the results of Figure 18 a demonstrate, the increase in cisplatin dose led to a direct decrease in cell viability (Figure 18 a).

The evaluation of cisplatin cytotoxicity in heterotypic co-cultures showed that HA-MA 2.5% - GelMA 5% microgels have slightly higher drug resistance than HA-MA 5% - GelMA 5% such could be correlated with higher cells bioactivity in these microgels. In fact, as previously demonstrated, at day 7 and 14, 3D microgels of HA-MA 2.5% / GelMA 5% present higher calcium deposition. Interestingly, 3D microgels present slightly higher resistance to cisplatin activity when compared to their 3D spheroid counterparts.

Such evidences the importance of evaluating different ECM-like hydrogel formulations during drug screening so a final decision over a particular treatment performance can be inferred.

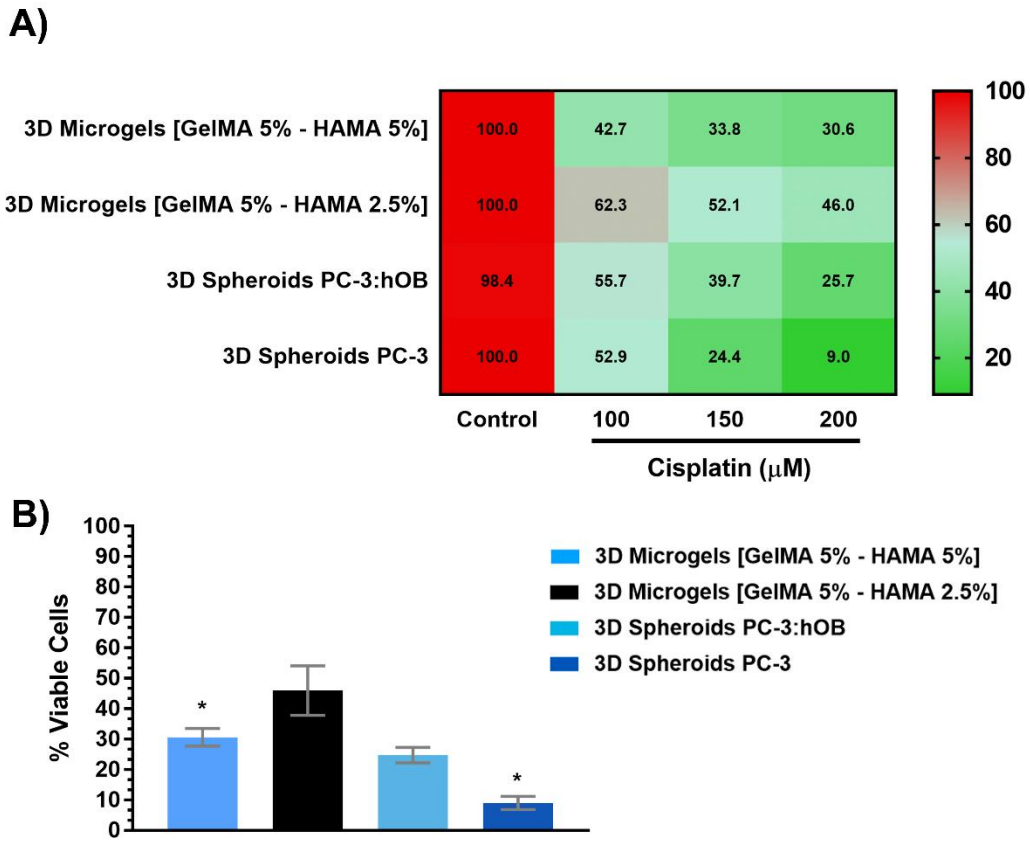

Figure 18. Cisplatin cytotoxicity evaluation. A) Dose dependent heat map of cell viability following administration of various cisplatin concentrations. Data is represented as mean, *n*=3. B) 3D cell titer glow cell viability analysis of 3D models incubated with the highest cisplatin concentration (200 μM). Data is presented as mean ± s.e.m., *n*=3.

The obtained results indicate that HA-MA 2.5% /GelMA 5% 3D spherical microgels have potential to be used for screening of candidate anti-cancer therapeutics that target prostate-to-bone metastatic niches. The versatility of these systems in terms of the inclusion of ECM-mimicking biomaterials as well as diverse cell cultures such as immune system cells or tissue resident mesenchymal stem cells increases the applicability potential of these platforms. It is important to emphasize that the ease of manufacture of these platforms and photo-crosslinkable 3D spherical microgels may contribute for their widespread use.

4.Conclusions

Through the use of a quasi superhydrophobic surface it was possible to produce a 3D disease model of prostate cancer in mono and co-culture. The *in vitro* generated micro-tumor exhibits tumor-associated characteristics in vivo, such as matrix deposition, resulting from cell-cell and cell-ECM interaction. The addition of osteoblasts to the cultures allowed the metabolic activity of the cells to increase and that calcium deposition was higher, the greater the % Gel-MA. This result evidences the interaction between PC-3 and osteoblasts, to promote the bioactivity of bone-forming cells. The evaluation of cisplatin cytotoxicity in heterotypic co-cultures showed that HA-MA 2.5% - GelMA 5% microgels have slightly higher drug resistance than HA-MA 5% -GelMA 5% may be correlated with the fact that this condition was also the one with the highest calcium deposition.

The current microtumor may be improved in the future with regards to the inclusion of new assays or other cell types, so that *in vitro* assays replicate the tumor microenvironment better and better.

Acknowledgments

The authors would like to thank Professor Carmen Jerónimo and Professor Rui Henrique from IPO Porto Research Center (CI-IPOP), Portuguese Oncology Institute of Porto (IPO Porto) for kindly providing the prostate cancer PC-3 cell line. The authors would like to acknowledge the support of the European Research Council for project ATLAS, grant agreement ERC-2014-ADG-669858. The authors also acknowledge the financial support by the Portuguese Foundation for Science and Technology (FCT) through a Post-doctoral grant (SFRH/BPD/119983/2016, Vítor Gaspar) and the funding for project Hidralazine (PTDC/MEC-ONC/29030/2017).

References

[1] "World Cancer Research Fund," *World Cancer Research Fund*. [Online]. Available: https://www.wcrf.org/dietandcancer/cancer-trends/prostate-cancer-statistics.

[2] S. Jayakumar, A. Kunwar, S. K. Sandur, B. N. Pandey, and R. C. Chaubey, "Differential response of DU145 and PC3 prostate cancer cells to ionizing radiation: Role of reactive oxygen species, GSH and Nrf2 in radiosensitivity," *Biochim. Biophys. Acta - Gen. Subj.*, vol. 1840, no. 1, pp. 485–494, 2014.

[3] R. Siegel, "Cáncer Statistics," *Ca Cáncer J.*, vol. 67, no. 1, pp. 7–30, 2017.

[4] E. J. Sousa *et al.*, "Enoxacin inhibits growth of prostate cancer cells and effectively restores microRNA processing," *Epigenetics*, vol. 8, no. 5, pp. 548–558, 2013.

[5] A. P. de Urulogia, "No Title." [Online]. Available: http://www.apurologia.pt/frameset.htm?http://www.apurologia.pt/doencas.htm.

[6] K. D. Foust and B. K. Kaspar, "Mechanisms involved in the progression of androgen-independent prostate cancers: it is not only the cancer cell's fault," vol. 8, no. 24, pp. 4017–4018, 2010.

[7] D. Nikitovic, M. Tzardi, A. Berdiaki, A. Tsatsakis, and G. N. Tzanakakis, "Cancer microenviroment and inflammation: Role of hyaluronan," *Front. Immunol.*, vol. 6, no. MAR, pp. 1–7, 2015.

[8] D. M. Betsch, S. Gray, and S. E. Zed, "A case of metastatic prostate cancer and immune thrombocytopenia," *Curr. Oncol.*, vol. 24, no. 5, pp. e434–e436, 2017.

[9] Z. Erlangung *et al.*, "The prostatic tumour stroma : Design and validation of a 3D in vitro angiogenesis co-culture model." 2016.

[10] A. M. Sitarski, H. Fairfield, C. Falank, and M. R. Reagan, "3D Tissue Engineered in Vitro Models of Cancer in Bone," *ACS Biomater. Sci. Eng.*, p. acsbiomaterials.7b00097, 2017.

[11] A. Shiirevnyamba *et al.*, "Enhancement of osteoclastogenic activity in osteolytic prostate cancer cells by physical contact with osteoblasts," *Br. J. Cancer*, vol. 104, no. 3, pp. 505–513, 2011.

[12] C. J. Logothetis and S. H. Lin, "Osteoblasts in prostate cancer metastasis to bone," *Nat. Rev. Cancer*, vol. 5, no. 1, pp. 21–28, 2005.

[13] M. R. Carvalho, D. Lima, R. L. Reis, V. M. Correlo, and J. M. Oliveira, "Evaluating Biomaterial- and Microfluidic-Based 3D Tumor Models," *Trends Biotechnol.*, vol. 33, no. 11, pp. 667–678, 2015.

[14] B. A. Ruggeri, F. Camp, and S. Miknyoczki, "Animal models of disease: Pre-clinical animal models of cancer and their applications and utility in drug discovery," *Biochem. Pharmacol.*, vol. 87, no. 1, pp. 150–161, 2014.

[15] R. H. Shoemaker, "The NCI60 human tumour cell line anticancer drug screen," *Nat. Rev. Cancer*, vol. 6, pp. 813–823, 2006.

[16] M. Alemany-Ribes and C. E. Semino, “Bioengineering 3D environments for cancer models,” *Adv. Drug Deliv. Rev.*, vol. 79, pp. 40–49, 2014.

[17] L. P. Ferreira, V. M. Gaspar, and J. F. Mano, “Bioinstructive microparticles for self-assembly of mesenchymal stem Cell-3D tumor spheroids,” *Biomaterials*, 2018.

[18] L. P. Ferreira, V. M. Gaspar, and J. F. Mano, “Design of Spherically Structured 3D In vitro Tumor Models -Advances and Prospects,” *Acta Biomater.*, 2018.

[19] C. C. Ultra-Low, “No Title.” [Online]. Available: https://www.sigmaaldrich.com/catalog/product/sigma/cls3471?lang=pt&region=PT.

[20] 3D Petri Dish, “No Title.” [Online]. Available: https://www.sigmaaldrich.com/catalog/product/sigma/cls3471?lang=pt&region=PT.

[21] P. Orlandi *et al.*, “Idarubicin and idarubicinol effects on breast cancer multicellular spheroids.,” *J. Chemother.*, vol. 17, no. 6, pp. 663–667, 2005.

[22] J. J. Richardson, J. Cui, M. Björnmalm, J. A. Braunger, H. Ejima, and F. Caruso, “Innovation in Layer-by-Layer Assembly,” *Chem. Rev.*, vol. 116, no. 23, pp. 14828–14867, 2016.

[23] P. K. Chaudhuri, B. C. Low, and C. T. Lim, “Mechanobiology of Tumor Growth,” *Chem. Rev.*, vol. 118, no. 14, pp. 6499–6515, 2018.

[24] X. Cui, Y. Hartanto, and H. Zhang, “Advances in multicellular spheroids formation,” *J. R. Soc. Interface*, vol. 14, no. 127, p. 20160877, 2017.

[25] Z. Liu and G. Vunjak-Novakovic, “Modeling tumor microenvironments using custom-designed biomaterial scaffolds,” *Curr. Opin. Chem. Eng.*, vol. 11, pp. 94–105, 2016.

[26] A. I. Neto, P. A. Levkin, and J. F. Mano, “Patterned superhydrophobic surfaces to process and characterize biomaterials and 3D cell culture,” *Mater. Horizons*, vol. 5, no. 3, pp. 379–393, 2018.

[27] N. M. Oliveira, C. Martins-Cruz, M. B. Oliveira, R. L. Reis, and J. F. Mano, “Coculture of Spheroids/2D Cell Layers Using a Miniaturized Patterned Platform as a Versatile Method to Produce Scaffold-Free Tissue Engineering Building Blocks,” *Advanced Biosystems*. p. 1700069, 2017.

[28] G. Ciasca *et al.*, “Recent advances in superhydrophobic surfaces and their relevance to biology and medicine,” *Bioinspiration and Biomimetics*, vol. 11, no. 1, p. 11001, 2016.

[29] X. Li, X. Zhang, S. Zhao, J. Wang, G. Liu, and Y. Du, “Micro-scaffold array chip for upgrading cell-based high-throughput drug testing to 3D using benchtop equipment,” *Lab Chip*, vol. 14, no. 3, pp. 471–481, 2014.

[30] N. M. Oliveira, A. I. Neto, W. Song, and J. F. Mano, “Two-dimensional open microfluidic devices by tuning the wettability on patterned superhydrophobic polymeric surface,” *Appl. Phys. Express*, vol. 3, no. 8, 2010.

[31] M. B. Oliveira and J. F. Mano, “On-chip assessment of the protein-release profile

from 3D hydrogel arrays," *Anal. Chem.*, vol. 85, no. 4, pp. 2391–2396, 2013.

[32] A. C. Lima, W. Song, B. Blanco-Fernandez, C. Alvarez-Lorenzo, and J. F. Mano, "Synthesis of temperature-responsive Dextran-MA/PNIPAAm particles for controlled drug delivery using superhydrophobic surfaces," *Pharm. Res.*, vol. 28, no. 6, pp. 1294–1305, 2011.

[33] B. Kwak, Y. Lee, J. Lee, S. Lee, and J. Lim, "Mass fabrication of uniform sized 3D tumor spheroid using high-throughput microfluidic system," *J. Control. Release*, vol. 275, pp. 201–207, 2018.

[34] A. M. S. Costa, M. Alatorre-Meda, N. M. Oliveira, and J. F. Mano, "Biocompatible polymeric microparticles produced by a simple biomimetic approach," *Langmuir*, vol. 30, no. 16, pp. 4535–4539, 2014.

[35] K. Yue *et al.*, "Synthesis, properties, and biomedical applications of gelatin methacryloyl (GelMA) hydrogels," *Biomaterials*, vol. 73, pp. 254–271, 2016.

[36] B. P. Toole, T. N. Wight, and M. I. Tammi, "Hyaluronan-cell interactions in cancer and vascular disease," *J. Biol. Chem.*, vol. 277, no. 7, pp. 4593–4596, 2002.

[37] A. Sigen *et al.*, "A facile one-pot synthesis of acrylated hyaluronic acid," *Chem. Commun.*, vol. 54, no. 9, pp. 1081–1084, 2018.

[38] D. Loessner *et al.*, "Functionalization, preparation and use of cell-laden gelatin methacryloyl-based hydrogels as modular tissue culture platforms," *Nat. Protoc.*, vol. 11, no. 4, pp. 727–746, 2016.

[39] M. T. Poldervaart *et al.*, "3D bioprinting of methacrylated hyaluronic acid (MeHA) hydrogel with intrinsic osteogenicity," *PLoS One*, vol. 12, no. 6, pp. 1–15, 2017.

[40] J. W. Nichol, S. T. Koshy, H. Bae, C. M. Hwang, S. Yamanlar, and A. Khademhosseini, "Cell-laden microengineered gelatin methacrylate hydrogels," *Biomaterials*, vol. 31, no. 21, pp. 5536–5544, Jul. 2010.

[41] K. Y. Law, "Definitions for hydrophilicity, hydrophobicity, and superhydrophobicity: Getting the basics right," *J. Phys. Chem. Lett.*, vol. 5, no. 4, pp. 686–688, 2014.

[42] J. Gumulec *et al.*, "Cisplatin-resistant prostate cancer model: Differences in antioxidant system, apoptosis and cell cycle," *Int. J. Oncol.*, vol. 44, no. 3, pp. 923–933, 2014.

[43] A. Weeks, D. Morrison, J. G. Alauzun, M. A. Brook, L. Jones, and H. Sheardown, "Photocrosslinkable hyaluronic acid as an internal wetting agent in model conventional and silicone hydrogel contact lenses," *J. Biomed. Mater. Res.*, vol. 100A, no. 8, pp. 1972–1982, 2012.

[44] S. H. Park, E. T. Keller, and Y. Shiozawa, "Bone Marrow Microenvironment as a Regulator and Therapeutic Target for Prostate Cancer Bone Metastasis," *Calcif. Tissue Int.*, 2017.

[45] A. E. Karnoub *et al.*, "Mesenchymal stem cells within tumour stroma promote breast cancer metastasis," vol. 449, pp. 557–565, 2007.

[46] Y. Kimura, A. Matsugaki, A. Sekita, and T. Nakano, “Alteration of osteoblast arrangement via direct attack by cancer cells : New insights into bone metastasis,” *Nat. Publ. Gr.*, 2017.

[47] M. A. Serban and A. Skardal, “Hyaluronan chemistries for three-dimensional matrix applications,” *Matrix Biol.*, 2018.

[48] G. Camci-Unal, D. Cuttica, N. Annabi, D. Demarchi, and A. Khademhosseini, “Synthesis and characterization of hybrid hyaluronic acid-gelatin hydrogels,” *Biomacromolecules*, vol. 14, no. 4, pp. 1085–1092, 2013.

[49] L. Zou *et al.*, “Effect of hyaluronan on osteogenic differentiation of porcine bone marrow stromal cells in vitro,” *J. Orthop. Res.*, vol. 26, no. 5, pp. 713–720, 2008.

[50] C. Qu, K. Rilla, R. Tammi, M. Tammi, H. Kröger, and M. J. Lammi, “Extensive CD44-dependent hyaluronan coats on human bone marrow-derived mesenchymal stem cells produced by hyaluronan synthases HAS1, HAS2 and HAS3,” *Int. J. Biochem. Cell Biol.*, vol. 48, no. 1, pp. 45–54, 2014.

[51] L. A. Gurski, A. K. Jha, C. Zhang, X. Jia, and M. C. Farach-Carson, “Hyaluronic acid-based hydrogels as 3D matrices for in vitro evaluation of chemotherapeutic drugs using poorly adherent prostate cancer cells,” *Biomaterials*, vol. 30, no. 30, pp. 6076–6085, 2009.

[52] B. J. Engel *et al.*, “Multilayered, Hyaluronic Acid-Based Hydrogel Formulations Suitable for Automated 3D High Throughput Drug Screening of Cancer-Stromal Cell Cocultures,” *Adv. Healthc. Mater.*, vol. 4, no. 11, pp. 1664–1674, 2015.

[53] X. Xu, L. A. Gurski, C. Zhang, D. A. Harrington, M. C. Farach-Carson, and X. Jia, “Recreating the tumor microenvironment in a bilayer, hyaluronic acid hydrogel construct for the growth of prostate cancer spheroids,” *Biomaterials*, vol. 33, no. 35, pp. 9049–9060, 2012.

[54] T. Greene and C. C. Lin, “Modular Cross-Linking of Gelatin-Based Thiol-Norbornene Hydrogels for in Vitro 3D Culture of Hepatocellular Carcinoma Cells,” *ACS Biomater. Sci. Eng.*, vol. 1, no. 12, pp. 1314–1323, 2015.

[55] X. Li, J. Zhang, N. Kawazoe, and G. Chen, “Fabrication of Highly Crosslinked Gelatin Hydrogel and Its Influence on Chondrocyte Proliferation and Phenotype,” *Polymers (Basel).*, vol. 9, no. 309, 2017.

[56] W. Y. Leong *et al.*, “In Vitro Growth of Human Keratinocytes and Oral Cancer Cells into Microtissues : An Aerosol-Based Microencapsulation Technique,” *J. Bioeng.*, vol. 4, no. 43, 2017.

5. Conclusions and Future Perspectives

There is no doubt that the interactions between the cellular and tumor components of stroma ECM act as regulators in the aspects of cancer progression or not. However, the exact nature of these complex interactions is not fully understood. Thus, it is extremely important to develop new models of *in vitro* disease that replicate the environment *in vivo*.

A 3D model of metastatic prostate cancer was developed containing extracellular matrix compounds (hyaluronic acid and gelatin) cancerous human cells (PC-3), one of the key populations of ECM cells (the osteoblasts). The inclusion of the cells in biomaterials, led to a closer approximation of these models to the reality of tumors *in vivo*.

3D microgels present slightly higher resistance to cisplatin activity when compared to their 3D spheroid counterparts.

In the future, the versatile method used in this work can be employed to the culture of other cell lines and with other ECM-mimetic biopolymers. Microtumors can also be coated via layer by layer with ECM components or with other types of chemical functionalization technologies. In all these hypotheses, the screening of drugs is a possibility, thus contributing to the advancement of new therapies or discovery of new anti-neoplastic drugs.

6. Annexes

Supplementary Information

In-air production of 3D Co-culture Tumor Spheroids for Expedite *In vitro* Drug Screening

Jéssica Antunes [1], Vítor M. Gaspar [1#], Luís Ferreira[1], Maria Monteiro[1], João F. Mano[1#]

[1] Department of Chemistry, CICECO, University of Aveiro, Campus Universitário de Santiago, 3810-193, Aveiro, Portugal

[#]Corresponding authors:
Professor João F. Mano
Department of Chemistry, CICECO – Aveiro Institute of Materials
University of Aveiro, Campus Universitário de Santiago
3810-193, Aveiro, Portugal
E-mail: jmano@ua.pt
Telephone: +351 234370733

Dr. Vítor Gaspar
Department of Chemistry, CICECO – Aveiro Institute of Materials
University of Aveiro, Campus Universitário de Santiago
3810-193, Aveiro, Portugal
E-mail: vm.gaspar@ua.pt
Telephone: +351 234370733

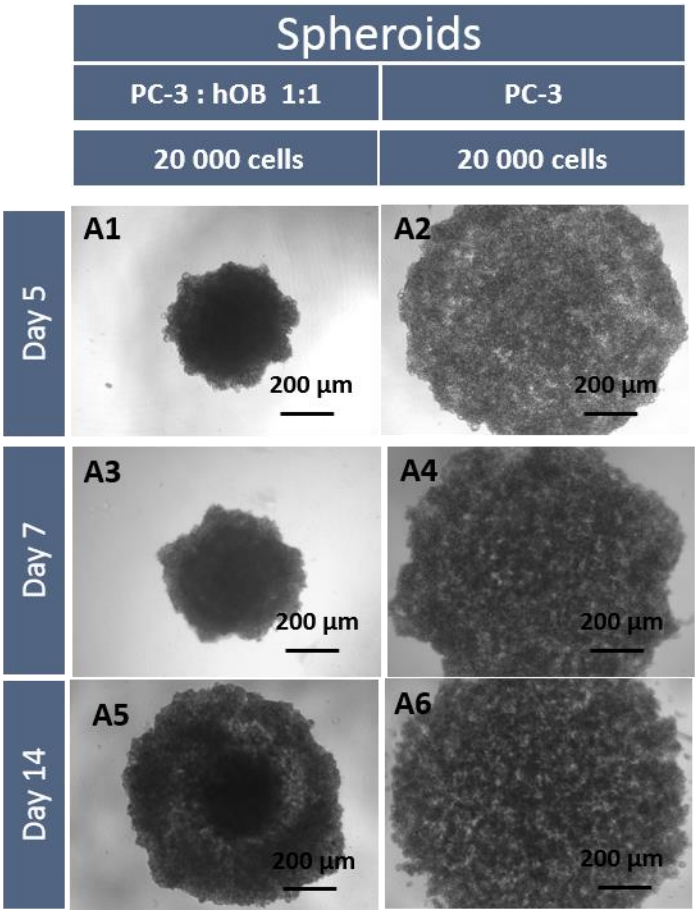

Supplementary Figure S1. Optical contrast micrographs of 3D monotypic and heterotypic tumor spheroids size and morphology at 5, 7 and 14 days of culture. 3D heterotypic tumor spheroids were assembled at 1:1 ratio of PC-3 to hOB cells.